LEVEL II

①

DTIC
SELECTED
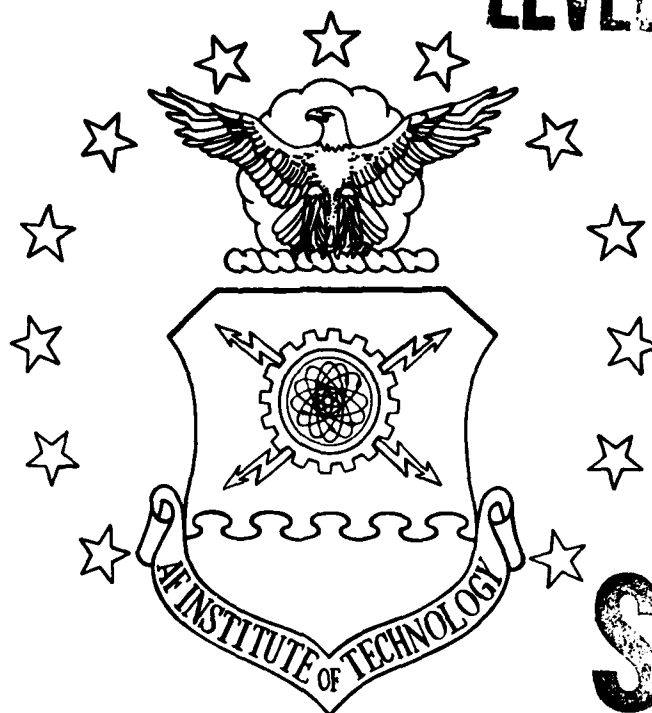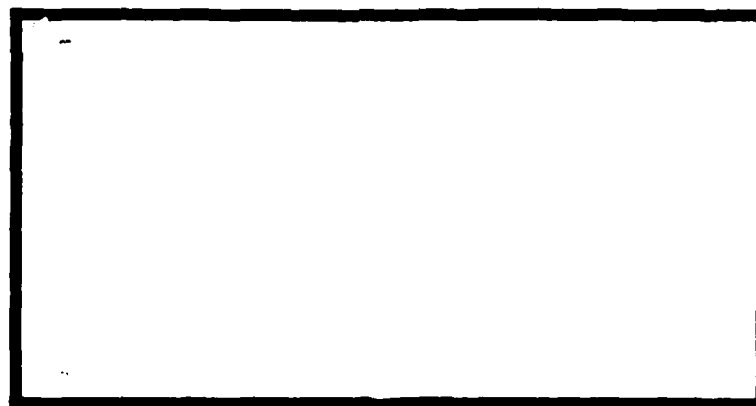FEB 1 9 1982

E

UNITED STATES AIR FORCE
AIR UNIVERSITY
AIR FORCE INSTITUTE OF TECHNOLOGY
Wright-Patterson Air Force Base,Ohio

82 02

COMPUTER ASSISTED VELOCITY

AND TURBULENCE MEASUREMENTS IN A PLANE

FREE JET AT HIGH SUBSONIC VELOCITIES

THESIS

AFIT/GAE/AA/81D-17   Michael J. Kirchner

Captain   USAF

COMPUTER ASSISTED VELOCITY

AND TURBULENCE MEASUREMENTS IN A PLANE

FREE JET AT HIGH SUBSONIC VELOCITIES

THESIS

Presented to the Faculty of the School of Engineering

of the Air Force Institute of Technology

Air University

in Partial Fulfillment of the

Requirements for the Degree of

Master of Science

by

Michael J. Kirchner, B.S.

Captain   USAF

Graduate Aeronautical Engineering

December 1981

Preface

Turbulence is a most interesting natural phenomenon. Mathematical solutions are difficult to handle, even with computers, due to the closure problem. Experimental measurements of turbulence are difficult because they are based on statistical averages, which require large numbers of samples to be meaningful.

In this study, I have tried to take advantage of the strides that have been made in compact, efficient computers to measure and analyze the quantities defining turbulent flow fields. These on-line computers allow the accumulation of data much more rapidly and efficiently than ever possible before.

I wish to thank my sponsor, Dr. Richard B. Rivir, of the Air Force Wright Aeronautical Laboratory for all his support. I also wish to thank my thesis advisors, Dr. Harold E. Wright, Dr. James E. Hitchcock, and Maj. Martin M. Wallace, for continuing support and guidance. Mr. William Baker and Mr. Harold Cannon provided valuable assistance in setting up laboratory equipment. Also, I want to thank Maj. John Vonada for all his help in mastering the intricacies of hot wires. Finally, I would like to thank Teresa, Brandon, and Marilyn for letting me spend so much time away from home to complete this project.

<div align="right">Michael J. Kirchner</div>

<div align="center">ii</div>

Contents

Contents

List of Figures

List of Tables

List of Symbols

Symbol		Units
g	gravitational constant	ft/sec^2
M	Mach number	
Pa	atmospheric pressure	in. Hg
Po	total pressure	in. Hg
R	universal gas constant	ft-lbf/lbm-R
T	time delay	microseconds
To	total temperature	deg R
t	time	microseconds
U	mean velocity in X direction	fps
Uloc	local mean velocity	fps
Ucen	mean velocity at test plane centerline	fps
u´	fluctuating velocity, X direction	fps
V	mean velocity in Y direction	fps
v´	fluctuating velocity, Y direction	fps
W	mean velocity in Z direction	fps
w´	fluctuating velocity, Z direction	fps
X	coordinate axis in primary flow direction	cm
Y	orthogonal horizontal coordinate axis	cm
Yo	half width of jet exit nozzle	cm
Z	vertical coordinate axis	cm
γ	ratio of specific heats	
λ_t	time microscale	microseconds
λ_L	spatial microscale	cm
Λ_t	time integral scale	microseconds
Λ_L	spatial integral scale	cm

Abstract

Methods and results of an experimental study of turbulence
parameters for a plane free jet at high subsonic velocities,
using hot wire anemometer signals outputing directly to an
on-line computer controlled data acquistion system are
reported. The apparatus studied had a nozzle exit, 1 x 10 cm,
designed for two-dimensional flow.

Two measurement planes at 25 and 50 jet widths downstream
were chosen to provide measurements to compare with existing
data for the facility. Nozzle exit velocities of $M=0.4$ and
$M=0.6$ were chosen for the same reason.

The techniques for employing hot wire anemometry coupled
with a computer controlled data acquisition system are
described. A comparison of data obtained with the computer is
made to data previously obtained by more traditional methods. A
comparison of linearized and non-linearized anemometer output
is made. A new calibration technique, also utilizing the data
aquisition system to greatly decrease the sensor calibration
time, was also developed.

The turbulence parameters compared are mean velocity,
turbulence intensities, micro-scale, and integral scale of
turbulence. The computer determined parameters compared
favorably in all cases with the already available data.

COMPUTER ASSISTED VELOCITY

AND TURBULENCE MEASUREMENTS IN A PLANE

FREE JET AT HIGH SUBSONIC VELOCITIES

I. Introduction

Measurement of the parameters which characterize turbulent flows has always been a time-consuming task, due to the large amounts of data required to get statisically meaningful results. Since turbulence is a universal phenomenon, present in the flow of every viscous fluid, determination of these turbulence parameters in a near real-time manner is essential to increased understanding of the behavior of turbulent flows.

Background

The approach to this research was to develop procedures for direct computer determination of turbulence parameters, using an established free jet facility to generate the flow field of interest, and constant temperature hot wire and hot film anemometry for taking measurements. The flow of the free jet chosen is classical in nature, and is comparable to free jets already documented (Ref. 1:7 and 8:7). Its flow field has been thoroughly investigated previously with the use of hot wire anemometers by Shepard (Ref. 10). The computer software and interface equipment developed are a beginning to the continued investigation into any turbulent flow using a computer controlled data acquisition system to take measurements throughout the flow field.

1

Objectives

This research has four major objectives.

1. Update sensor calibration techniques for single and X-wire hot film and hot wire sensors through the use of a computer controlled data acquisition system.

2. Develop computer software and related hardware interface equipment to enable processing of data directly from hot wire and hot film sensors through the data acquisition system.

3. Compare the results of turbulence parameters computed using the non-linear, or bridge, output of the anemometer with results computed using analog linearized output.

4. As a result of efficient application of the first two objectives, reduce the run time required for sensor calibration and data acquisition, hence reducing the risk of sensor breakage and aging.

This report is divided into six major areas. First is a description of the apparatus used to generate the flow field, followed by a description of the instrumentation, including the automatic data acquisition system, used to take measurements. The next section outlines the procedures used to take and analyze the data. The fourth section is a discussion of the results, while the final two sections present conclusions and recommendations.

2

II. Test Apparatus

The two-dimensional flow field of interest was generated by a 1 x 10 cm free jet issuing into still air. A flow field schematic is illustrated in Fig. 1, showing the planes of primary interest for measurements, and the coordinate system used. At the nozzle exit plane, the issuing jet has a top hat velocity and temperature profile, both spatially and in time, to within 1/2% (Ref. 10:3), well within the electronic noise level of the instrumentation. Nozzle exit velocities of Mach 0.4 and 0.6 at test planes of 25 and 50 jet widths (25 and 50 cm) downstream were chosen to provide a range of data, and to compare with previously gathered data (Ref. 10). At 25 cm, similarity has not yet been completely established, while by 50 cm, similarity has been freely established. Also, at 25 cm the turbulence is not yet isotropic, while the 50 cm test plane is well within the isotropic region. Exit velocities of 137 mps and 198 mps were used as representing Mach 0.4 and Mach 0.6.

Parameters of Interest

The parameters used to describe turbulent flow fields are generally standard, and are the same as used by Shepard (Ref. 10). They include mean velocity, turbulence intensity, the microscales of turbulence, and the integral scales. Symbols and definitions are contained in Table I. For this study, the air flow was assumed to be an ideal gas, and nozzle exit velocities were computed assuming compressible flow.

3

Fig. 1. Flow field schematic

POTENTIAL CORE

MIXING REGION

TURBULENT REGION

PRIMARY JET

1 cm

25 cm

50 cm

PLAN VIEW

X

Z

Y

10 cm

1 cm

NOZZLE WALLS

4
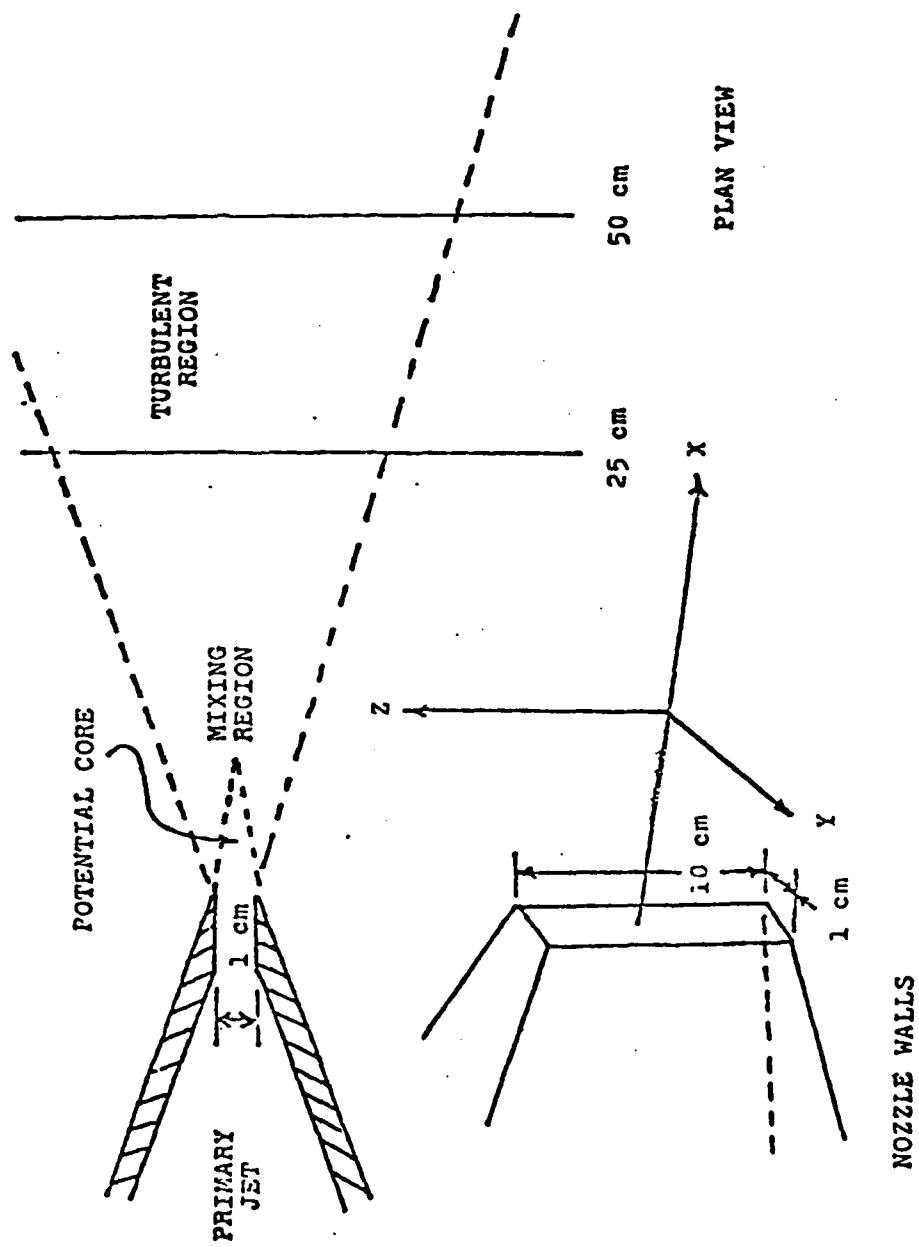
Table I

Selected Parameters Used to Characterize the Flow Field

Symbol	Description
$\bar{U}$	Mean streamwise velocity in X direction
$\bar{V}$	Mean velocity in Y direction (width)
$\bar{W}$	Mean velocity in Z direction (height)
u'	Fluctuating velocity in X direction
v'	Fluctuating velocity in Y direction
w'	Fluctuating velocity in Z direction
$u'/\bar{U}$	X direction component of turbulence intensity
$v'/\bar{U}$	Y direction component of turbulence intensity
$w'/\bar{U}$	Z direction component of turbulence intensity
λ_t	Time microscale of turbulence
λ_L	Spatial microscale
Λ_t	Time intergal scale of turbulence
Λ_L	Spatial integral scale

Experimental Apparatus

The free jet used in this study was designed to be used
for a broad range of research conditions. Therefore, many of
its design features were not utilized here. Figure 2 is a
cross-section schematic of the free jet facility.

The current limit on the amount of compressed air readily
available limited the flow to velocities of approximately
Mach=0.6. However, this was considered sufficient to validate
techniques and procedures, and to provide enough data for
comparisons. The flow was established by use of a 27 cm
diameter calming chamber, 2.13 m in length. A replaceable
paper filter system was located 1 m downstream of the inlet to
the calming chamber. This filter removed foreign particles from
the flow, helping to alleviate some of the problem of sensor
breakage. A multi-layered steel mesh provided support for the
filter.

The nozzle has an area contraction ratio of 50:1, which
insures an extremely low turbulence flow and a very thin
boundary layer at the nozzle exit plane. The 1 x 10 cm nozzle
achieves two-dimensional flow over the range of interest, with
$V<U$ and $W<<U$, where U is the local streamwise mean flow
velocity, in the X axis direction, V is the velocity in the Y
direction, and W is in the Z axis direction. The measurements
of parameters of interest were taken along the X axis, and
parallel to the Y axis at the 25 and 50 cm locations.

6

A. AIR SUPPLY INLET

B. ORIFICE

C. TURBULENT MIXING REGION

D. STAINLESS STEEL MESH FILTER SUPPORT
   WITH REPLACEABLE PAPER FILTER
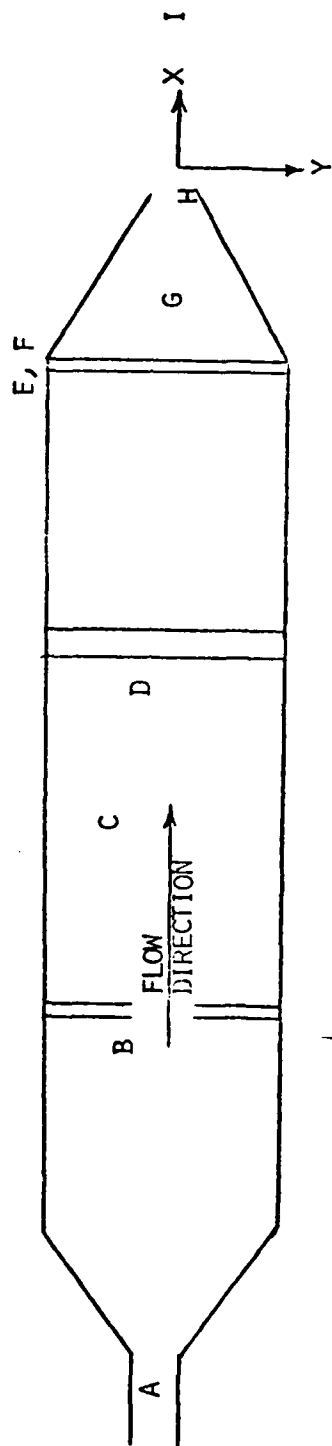
E. PRESSURE MONITORING STATION

F. TEMPERATURE MONITORING STATION

G. 50:1 NOZZLE

H. NOZZLE EXIT PLANE

I. DOWNSTREAM TEST REGION

Figure 2   Schematic of Experimental Apparatus

7

III.   Instrumentation

A Hewlett-Packard (HP) 3052A Automatic Data Acquisition System was used to read and process electronic signals from a Thermo-systems, Inc. (TSI) anemometer system utilizing hot wire and hot film sensors, and their associated equipment. Figure 3 is a schematic showing the instrumentation setup, and also a flow diagram of how the sensor signals are processed.

Data Acquisition System

The HP 3052A Data Acquisition System consists of a 9845B Progammable Desktop Computer/Controller, a 3495A Scanner, a 3455A Digital Voltmeter (DVM), two 9885 Flexible Disk Drives, and a 9872S Graphics Plotter. A 3437A System Voltmeter is also installed as part of the system, but was not used in this study.

Computer

The 9845B is a desktop computer system designed with a built-in cathode ray tube display, thermal printer, two tape drives, and an extended keyboard (Ref. 6:3-6). The cathode ray tube, or CRT, display is the primary means of communicating with the computer, and is used to edit programs, view data or graphical information, and to display error messages. An eighty character thermal line printer for hard copy output of any CRT display is built into the front of the computer. Also in the front of the computer are two magnetic cassette cartridge tape drives, used to store programs and data for use in the

8
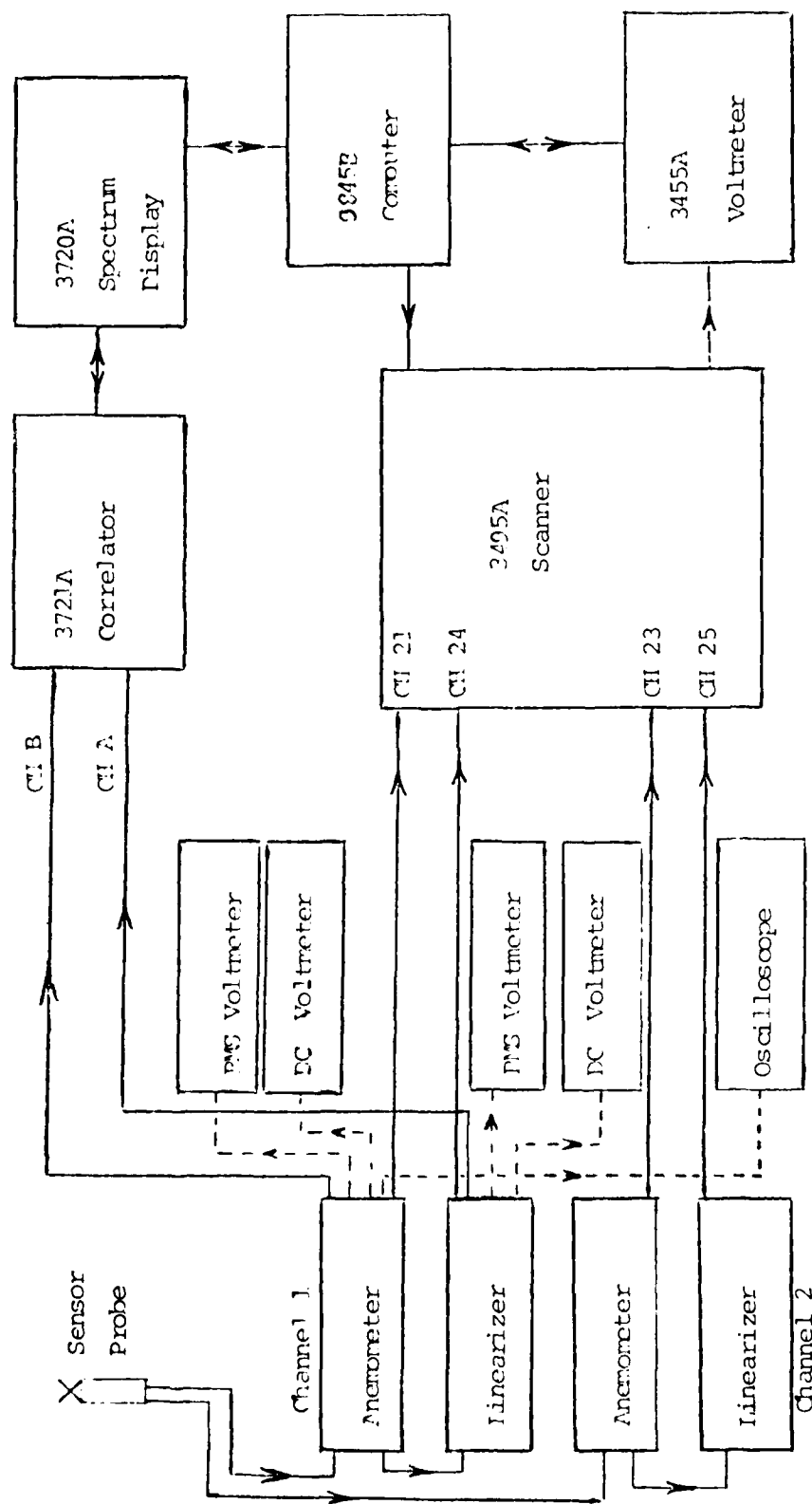
Figure 3 Instrumentation Schematic

computer. Each cassette tape can hold up to 216,832 bytes of
information. The computer is equipped with a Graphics Read Only
Memory, or ROM, allowing program execution of plotting
commands, an I/O ROM, which expands the computer's capability
for execution of input and output functions, and a Mass Storage
ROM, which permits the use of the flexible disk drive system.
The main working area of the computer is a total of 318,026
bytes of read/write, or Random Access, Memory (RAM).

Flexible Disk Drives

Two flexible disk drives are connected to the computer to
expand program and data storage capabilities. One of the disk
drives is a Master unit, the other a Slave. Each unit operates
independently of the other in storage and retrieval of data.
Each flexible disk used with the disk drive can store up to
499,200 bytes of information. The disk drives are an average of
25 times faster in operation than the computer's internal tape
drives, and the flexible disks themselves are generally less
suseptible to wear than are the cassette tapes.

Plotter

The plotter can produce four color graphical output,
either interactively, or under program control.

Digital Voltmeter

As a part of the data acquisition system, the digital
voltmeter makes AC voltage measurements with five digit
resolution, and DC voltage measurements with either five or six
digit resolution, as programmed by the user. The voltmeter
employs an automatic calibration (AUTO CAL) feature which

10

automatically corrects for possible gain and offset errors in the analog circuitry to provide maximum accuracy. In the DC modes employed in this study, the voltmeter reading is accurate to within .01%, with a maximum reading rate of 24 readings per second. In the AC mode, voltage accuracy is within .2%, with a reading rate of 1.3 readings per second (Ref. 4:2-4).

Scanner

For this study, the scanner was configured with a 20 Channel Low Thermal relay assembly. This is a 20-to-1 multiplexer, allowing 20 signals (up to 42 volts maximum) to be monitered by one measurement instrument, in this case, the digital voltmeter. Signals are multiplexed to the common terminals one-at-a-time in a break-before-make sequence. With switching time between channels of 1 msec maximum, the scanner is capable of switching speeds up to 1000 channels per second, far faster than the voltmeter is capable of reading (Ref. 5:2).

Anemometers and Linearizers

Two TSI Model 1050 anemometers processed signals from the hot film and hot wire sensors during calibration and data collection. The anemometers were operated in the constant temperature mode, with electrical circuits optimized for maximum frequency response. Output from the anemometers consisted of a DC voltage, corresponding to mean velocity, and an AC voltage, corresponding to fluctuating velocity. These voltages were then fed directly to the data acquisition system as non-linear bridge output, and also to two TSI Model 1052 Analog Linearizers, which linearized the signals throughout the

11

velocity range of interest. These linearized signals were then fed to the data acquisition system for processing and comparison with the non-linearized signals.

Sensors

Hot film sensors were selected for the majority of this study because they were readily available, and much sturdier than the hot wire sensors available. As one of the objectives of this study was to develop procedures for the direct transfer of anemometer signals to the data acquisition system, sturdiness was a highly desirable attribute. The sensors were required to be exposed to flow conditions for extended periods of time, both during calibration, and during the collection of data. Because of this the use of hot film sensors was considered an acceptable trade-off with the better frequency response of the more fragile hot wire sensors. Single wire TSI Model 1214-20 .002 in. diameter hot film sensors were used for most of the measurements. These sensors were orientated with the sensor axis parallel to the Z axis. A single wire TSI Model 1214-T1.5 .00015 in. diameter hot wire sensor was used as a final check to compare the differences in results due to its increased frequency response.

Data for turbulence intensities in the Y and Z planes was taken with a TSI Model 1241-10 .001 in. diameter X-film sensor. This probe consists of two orthogonal film sensors separated by .012 cm. Each sensor was connected to a separate anemometer, and the sensor signals were processed in both the linearized and non-linearized form by the computer. Measurements of U, u',

12

V, and v' were made with the sensor wires parallel to the X-Y plane, while measurements of U, u', W, and w' were made with the sensor wires parallel to the X-Z plane.

Correlator

A HP Model 3721A Correlator was used to calculate the autocorrelation function, needed to determine the integral scales and microscales of turbulence. The two channel capability of the correlator was used to process the real-time linearized and non-linearized signals as near as possible to each other in time. The autocorrelation functions calculated by the correlator were passed to the computer for further processing through a HP Model 3720A Spectrum Display, and a hardware interface box designed and built by Mr. Gregg Tibbs of the Air Force Propulsion Laboratory. This interface was necessary because the data transfer rate of the spectrum display unit is incompatible with the data acquisition system, a common problem with instrumentation interconnection. The computer software to control the correlator and to transfer data to the computer was developed in conjuction with Mr. Greg Tibbs and Maj. John Vonada (Ref. 14).

Voltmeters

Two Digitec Model 268 DC Millivoltmeters were used during calibration and data collection. One was used to moniter the non-linearized bridge output of the anemometer, the other monitered the linearized signal.

Two HP Model 3400A RMS voltmeters were used to moniter the AC component of the anemometer signals, which is proportional

to fluctuating velocity. These voltmeters were used in the same manner as described for the DC voltmeters.

Manometers

A 60 in. mercury manometer was used to measure the total pressure in the calming chamber of the free jet. Two manometers were used to measure calibrator calming chamber pressure during sensor calibration. A 20 in. water micro-manometer was used to measure pressures from 0 to 2.5 in. of water. A 120 in. U-tube water manometer was used to measure pressures from 2.5 in. of water up to 115 in. of water, corresponding to a velocity of approximately 650 ft per sec.

Cathotometer

A Gaertner Scientific Co. cathotometer was used during data acquisition to position the sensors to within .001 in. of desired location in all three coordinate directions.

Oscilloscope

A Ballantine Model 1066S Oscilloscope was used in maximizing the frequency response of the anemometer circuits during sensor calibration.

Transducers

Two Validyne Model DP15 transducers were used during sensor calibration to convert pressures into proportional voltages. A .5 psi transducer was used to measure pressures up to 2.5 in. of water, or velocities up to approximately 125 ft per sec. Pressures above 2.5 in. of water were measured with a 25 psi transducer. Two Validyne Model CD23 Power and Display units were used to moniter the transducer output and to pass

14

the transducer output directly to the data acquisition system.

Calibrator

A TSI Model 1025 Calibrator was used to calibrate both single and X-wire hot film and hot wire sensors throughout the velocity range of interest.

IV. Experimental Procedure

Sensor Calibration

One of the objectives of this study was to simplify and automate the time-consuming task of sensor calibration. General calibration instructions are provided by TSI (Ref. 12:2.2-2.9). To accomplish this, sensors were calibrated using the calibrator, with the anemometer bridge output fed directly to the data acquisition system. Pressures in the calibrator stilling chamber were converted to voltages using a .5 psi and a 25 psi transducer, and these voltages were fed to the data acqusition system. The computer then calculated the velocity using the compressible flow equation for average velocity

$$U=(2*g*R*To*(\gamma/(\gamma-1))*(1-(Pa/Po)^{(\gamma-1)/\gamma}))^{.5} \qquad (1)$$

after converting transducer voltages back to pressures. This voltage and velocity data was then used to calculate the fourth order coefficients to be set in the four potentiometers on the TSI 1052 Linearizers. The computer program to calculate these coefficients was based on a BASIC program provided by TSI (Ref 13:42-54). These coefficients were set in the linearizer, and the calibration was run again to check the accuracy of the linearized output. A least squares program was then used to calculate a fourth order curve fitting the non-linear bridge output, and a linear curve fitting the linearized output. All of the calibration data and the resulting curve-fit coefficients are stored on floppy disk for future reference and

16

for use during data manipulation. Storing and using the coefficients of the curve saves both computer time and storage space when compared to using a computer-stored table of the calibration values.

X-wire sensors were calibrated in the same manner as single wire sensors, except that the wires were each orientated 45 degrees to the mean streamwise velocity. Each wire was calibrated individually, coefficients calculated, and data stored in the same manner as the single wire sensors. Typical output from the sensor calibration program is given in Appendix A.

Control of Test Conditions

Since the nozzle exit velocities under consideration in this study were well within the compressible flow regime, Equation 1 was used to determine the pressure required in the free jet calming chamber to provide the required velocity. Velocity in the calming chamber itself was negligible, so that chamber temperature and pressure represented total conditions. Constant pressure in the calming chamber was maintained by adjusting the compressed air by-pass, which was vented to the atmosphere, until steady flow was obtained at the desired pressure, with the compressor running continuously.

Measurement Techniques

The sensor probe support was attached to the three dimensional traversing mechanism of the cathotometer. The nozzle centerline and test planes had been previously set by plumb bob and theodolite, and were referenced to the

17

cathotometer. Each time the probe was mounted on the traversing mechanism, it was referenced to the centerline of the nozzle. Measurement points were determined, in general by attempting to cover the same range investigated by Shepard. To reduce the possibility of flow effects from the probe supports and to reduce vibration, the sensors were mounted on a 90 degree elbow facing the streamwise flow direction.

As the primary objective of this study was to evaluate the feasibility and suitability of using the data acquisition system to process anemometer data, the sturdier hot film sensors were used in place of the more fragile hot wire sensors for the majority of measurements. Hot wire sensors were used to take measurements at the 25 cm and 50 cm test planes at M=0.4 for comparison purposes. Attempts to obtain hot wire data at M=0.6 met with failure, as the sensors were immediately destroyed upon insertion into the flow field. The single wire sensors were used to measure the velocities, obtain turbulence intensities, the microscale, and the integral scale of turbulence. The X-wire sensors were used to calculate the turbulence intensity components in the X, Y, and Z directions.

Measurements of Velocities and Turbulence Intensities

Voltages needed to calculate velocities and turbulence intensities at each measurement station were input directly to the computer through the scanner and the digital voltmeter of the data acquisition system. When using single wire sensors, one scanner channel was connected directly to the anemometer bridge output, while a second channel was dedicated to the

18

linearizer output. At each data point, the computer controller directed sequential access to each channel, first reading DC voltage, followed by the RMS voltage for each channel. For the X-wire sensors, four scanner channels were used, one for each bridge output and one for each linearizer output. The DC and RMS voltages for each output channel at each data point were stored on floppy disk for subsequent manipulation and for permanent storage. DC voltages were converted to mean velocities by the computer, using the stored sensor calibration curve, and non-dimensionalized by the centerline velocity, Ucen. RMS voltages were converted to fluctuating velocities by evaluating the slope of the calibration curve at the corresponding DC voltage and multiplying by the RMS voltage (Ref 15:142). Turbulence intensities were then determined by dividing the fluctuating velocities by Ucen.

Calculation of Microscale and Integral Scale

The microscale and integral scale of turbulence were determined from the autocorrelation function calculated by the correlator. In this study, both correlator channels were used. The linearized anemometer signal was fed to one channel, while the bridge output went to the other channel. The linearized signal was evaluated first, through variation of the time scale, to obtain a correlation function suitable for calculating micro and integral scales. This curve was then transfered to the computer and stored. The second correlator channel, the bridge output, was then manually selected and processed in the same way. This method kept the evaluation of

19

the two signals as close together as possible.

The time microscale is the average time for the smallest eddies to pass the sensor. The time microscale was determined by fitting an osculatory parabola to the first portion of the autocorrelation curve as outlined by Hinze (Ref 7:34-42) and Freathy (Ref 3:22-24). The microscale is then found from

$$\lambda t = T/(1-R(T)/R(0))^{.5} = T/.316 \qquad (2)$$

where R(0) is the value of the autocorrelation curve at time zero, R(T) is defined as .9 of R(0), and T represents the time corresponding to R(T) on the time axis.

To transform from the time domain to the spatial domain, Taylor's hypothesis

$$\frac{\partial}{\partial t} = U \frac{\partial}{\partial x} \qquad (3)$$

was utilized to determine an approximation of the physical size of the eddies. The spatial microscale is presented only to show trends, fully recognizing the limitations of Taylor's hypothesis (Ref 7:30,40-42).

The time integral scale is defined as the area under the autocorrelation curve to the point where it first crosses the abscissa. The time integral scale is the longest time scale of the turbulent fluctuations. The area under the autocorrelation curve was numerically evaluated by the computer using Simpson's rule. Taylor's hypothesis was again invoked to obtain a spatial

20

integral scale. The spatial integral scale is an approximation
of the size of the largest eddies in the flow (Ref 2:39).

V. Results and Discussion of Results

Primary measurements were made at 25 cm and 50 cm downstream of the nozzle exit. These test planes were chosen in order to compare data taken with the automatic data acquisition system to that previously obtained through other methods. Data was collected employing both hot film and hot wire sensors across the flow field. Results are presented for only half of the jet width out the Y axis, as the flow field is symmetrical, and this is the manner chosen by Shepard to present his data. All data collected in this study, and the computer programs used for data collection and manipulation, are maintained on floppy disk in the Department of Aeronautical and Astronautical Engineering, Air Force Institute of Technology, Wright-Patterson Air Force Base, Ohio 45433.

Presentation of Results

The experimental results of this study are presented in this section and in Appendices A, B, and C. Appendix A contains typical results from the sensor calibration program. Appendix B contains comparisons of data collected at a jet velocity of $M=0.4$. Appendix C contains comparisons of data collected at a jet exit velocity of $M=0.6$.

Data for the graphs presented in Appendices B and C has been nondimensionalized. Quantities on the ordinate were divided by a velocity, normally the jet centerline velocity. Quantities on the abscissa were divided by the half width of the jet, Yo. This method was chosen since it allows easier comparison with the data previously presented by Shepard,

22

although the scaling itself results in some smoothing of the data. Also, the lines drawn between data points on the graphs in Appendices B and C are only to assist in following the data set, and do not represent any actual values.

Calibration. The procedures and techniques developed and employed in this study yielded excellent results for all types of sensors across a broad range of velocities. For this study, the mean velocities in the flow field ranged from near zero velocity to over 600 ft per second. Three other students have used and referenced the computer programs and techniques developed here to calibrate sensors. Two of these were investigating flow fields of intermediate velocity, in the range of 200 to 450 ft per second. The third was an investigation of much slower velocities, with maximum velocities less than 35 ft per second. In all cases, sensors could be quickly and accurately calibrated, with the data points used and the resulting curve fit coefficients immediately available from the computer's internal thermal printer. Figures 11,12, and 13 of Appendix A present typical results of the calibration program.

One area of interest was noted during these calibration runs. When attempting to calibrate at very low velocities, below approximately 10 ft per second, the .5 psi transducer used to measure pressures was not stable enough to provide good voltages to the data acquisition system. This resulted in incorrect velocity calculations at those points. It appeared that the transducer may have been reacting as much to slight

23

temperature variations in the room, as to the very small
pressures it was trying to measure. This problem could be
easily avoided by taking the zero flow reference point as the
first point in the calibration, then taking the second reading
at a velocity slightly above 10 ft per second. This corresponds
to a transducer reading of approximately 0.1 volt, and seems to
be in a more stable range for transducer operation. After the
second point, calibration points could be taken in any higher
range, and a smooth fourth order curve fit to them.

TSI recommends at least 20 calibration data points be
taken if the sensor circuits are to be linearized (Ref. 12:18),
and 20 points provided smooth accurate curves for the
non-linearized case as well, without the requirement for
weighting data points. Equal voltage increments gave the best
data point spacing, keeping in mind the above restriction on
the very low velocity points. In all cases, the sensor was
required to be exposed to the flow during calibration for a
shorter period of time than was usually possible with previous
calibration techniques. Also, the sensor was available for
immediate use and feedback, without first having to resort to
laborious hand graphing of the calibration curve.

Data Acquisition. The data collected with the use of the
automatic data acquisition system shows very close correlation
with the data collected and presented by Shepard. Turbulence
intensity profiles calculated from the single wire sensor data
were generally within approximately 3% of the profiles
presented by Shepard, and in all cases, confirmed the trends

24

shown by Shepard. Typical results for turbulence intensity profiles are shown in Figs. 4, 16 and 27 of Appendix B, and 37 and 45 of Appendix C.

Time microscale profiles also follow Shepard's data very closely, especially around the center of the flow field. At 25 cm at M=0.4, this study found that the microscale tended to rise a little faster than predicted by Shepard, as the sensor was moved across the flow field, but the trend still followed Shepard's data. The same trend to a slightly faster rise in the time microscale is also present at 50 cm. at M=0.4. However, at M=0.6, the data from this study points to a smaller increase than Shepard's data indicates. The trends are identical to those presented by Shepard, though, in all cases. Since the microscale is the measurement most dependent on sensor diameter, the data obtained with the hot wire sensor is most applicable here. Figure 21 shows the data for the microscale at M=0.4 taken at 25 cm with the .00015 in. diameter 11.5 sensor. Again, the data follows Shepard's very closely at the center of the flow, but rises slightly more rapidly as the sensor is moved out from the center of the jet. Compared with the data presented for the hot film sensor, there is almost no difference between the microscale calculations. At 50 cm, the trends are the same, but here the points calculated from the hot wire data increase slightly faster than do those points calculated from the hot film signals, indicating some increased frequency response. Closer to the center of the flow field, hot wire and hot film data agree almost exactly. Typical output for

TURBULENCE INTENSITY PROFILES

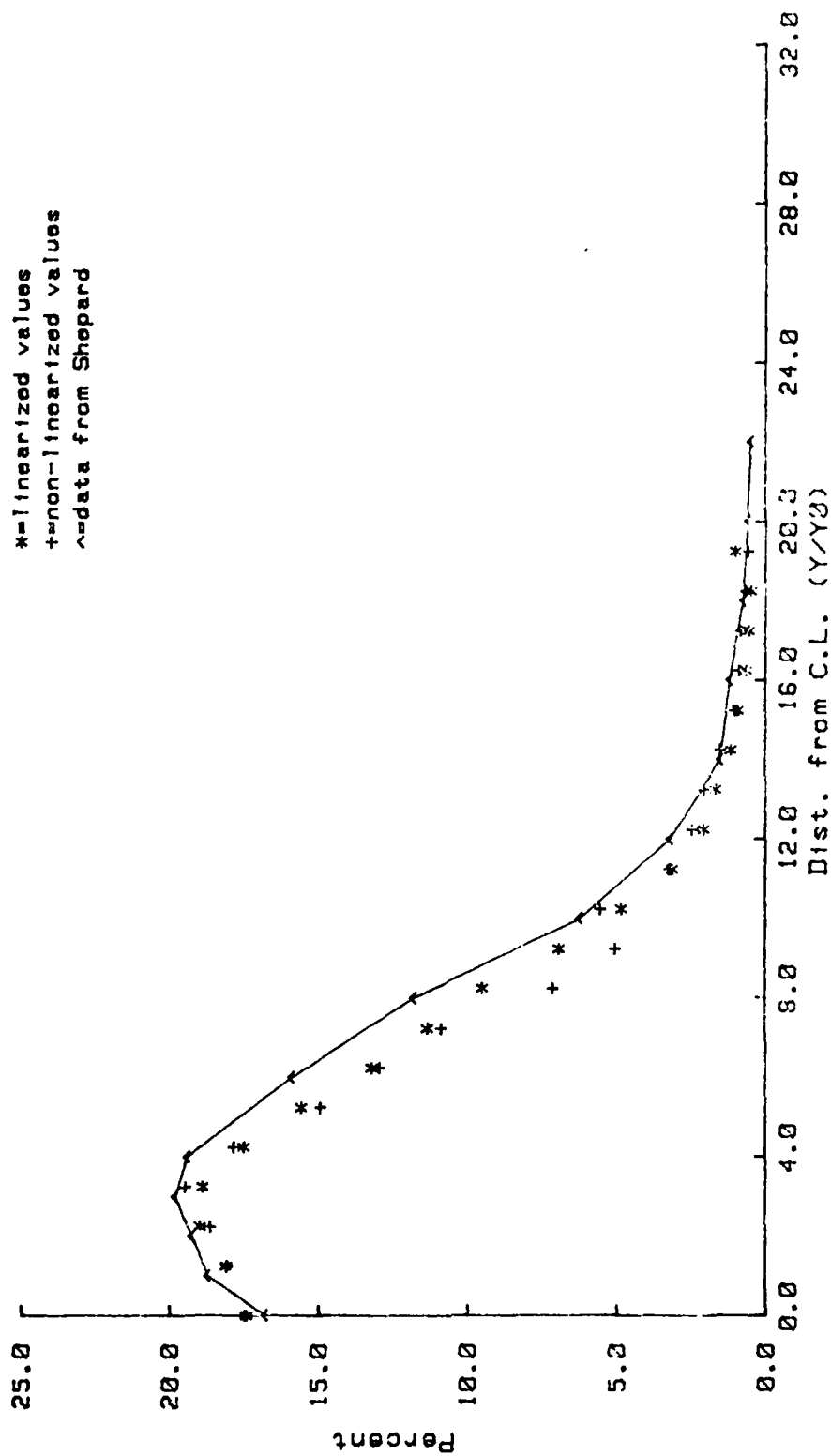*=linearized values
+=non-linearized values
^=data from Shepard

Fig. 4. Turbulence Intensity at 25 cm, N=0.4

the time microscale calculations are found in Figs. 5, 17, 21, 28 and 32 of Appendix B, and 39 and 46 of Appendix C.

The transformation from time microscale to the spatial microscale using Taylor's hypothesis yielded results very close to those shown by Shepard at 25 cm. Typical results are shown in Figs. 6, 18 and 22 of Appendix B, and 40 of Appendix C. At 50 cm, however, the data shows a tendency to start at lower values in the center of the flow, then to steadily rise before starting to decrease as the sensor is moved out of the mixing region. This tendency was noted for all runs. Also, the spatial microscale reached higher values than Shepard's data had predicted at the edge of the mixing region, and showed wider variations after passing the edge of the mixing region. Typical results for the spatial microscales are shown in Figs. 29 and 33 of Appendix B, and 47 of Appendix C. Very little additional smoothing is indicated for the spatial scales compared to the data collected by Shepard. Some of the scatter here can be attributed to the use of Taylor's hypothesis, with very small numbers (the time microscales) being multiplied by relatively large numbers (the velocities). This can cause magnification of small variations in either time or velocity.

Time integral scale profiles are presented in Fig. 7, 19, 23, 30, and 34 of Appendix B, and 41 and 48 of Appendix C. At 25 cm, the data from this study matches Shepard's data with only very slight variations. At 50 cm, however, the integral scales fall slightly below those presented by Shepard, and level off at a somewhat lower value. Again, these results were
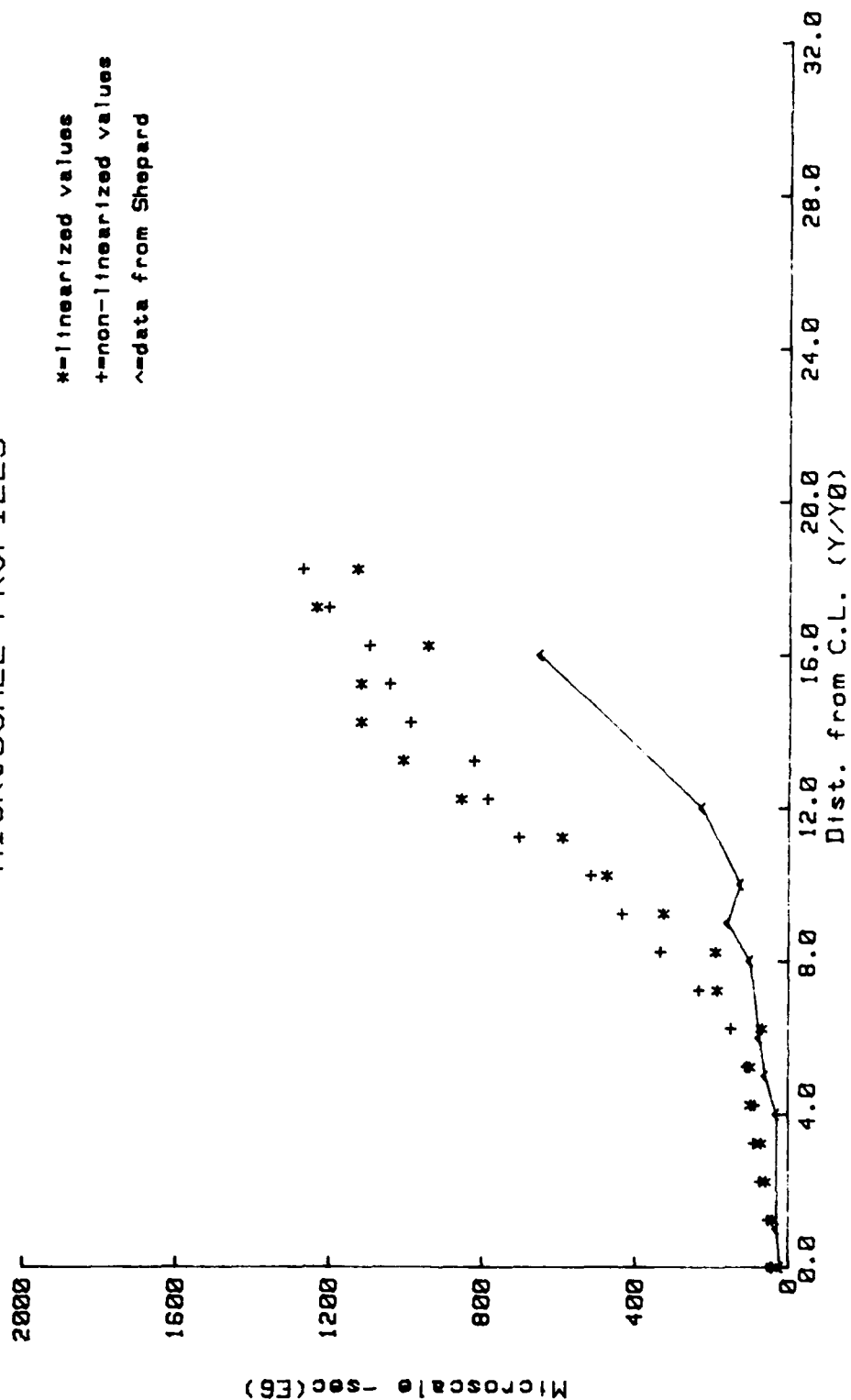
27

MICROSCALE PROFILES

*=linearized values

+=non-linearized values

^=data from Shepard

Microscale -sec(E6)

Dist. from C.L. (Y/YO)

Fig. 5. Time Microscale at 25 cm, M=0.4

MICROSCALE PROFILES

*=linearized values
+=non-linearized values
^=data from Shepard

Microscale -cm

Dist. from C.L. (Y/Y0)

Fig. 6. Spatial Microscale at 25 cm, H=0.4

INTEGRAL SCALE PROFILES

*=linearized values

+=non-linearized values

^=data from Shepard

Integral scale -sec(E6)

Dist. from C.L. (Y/YØ)
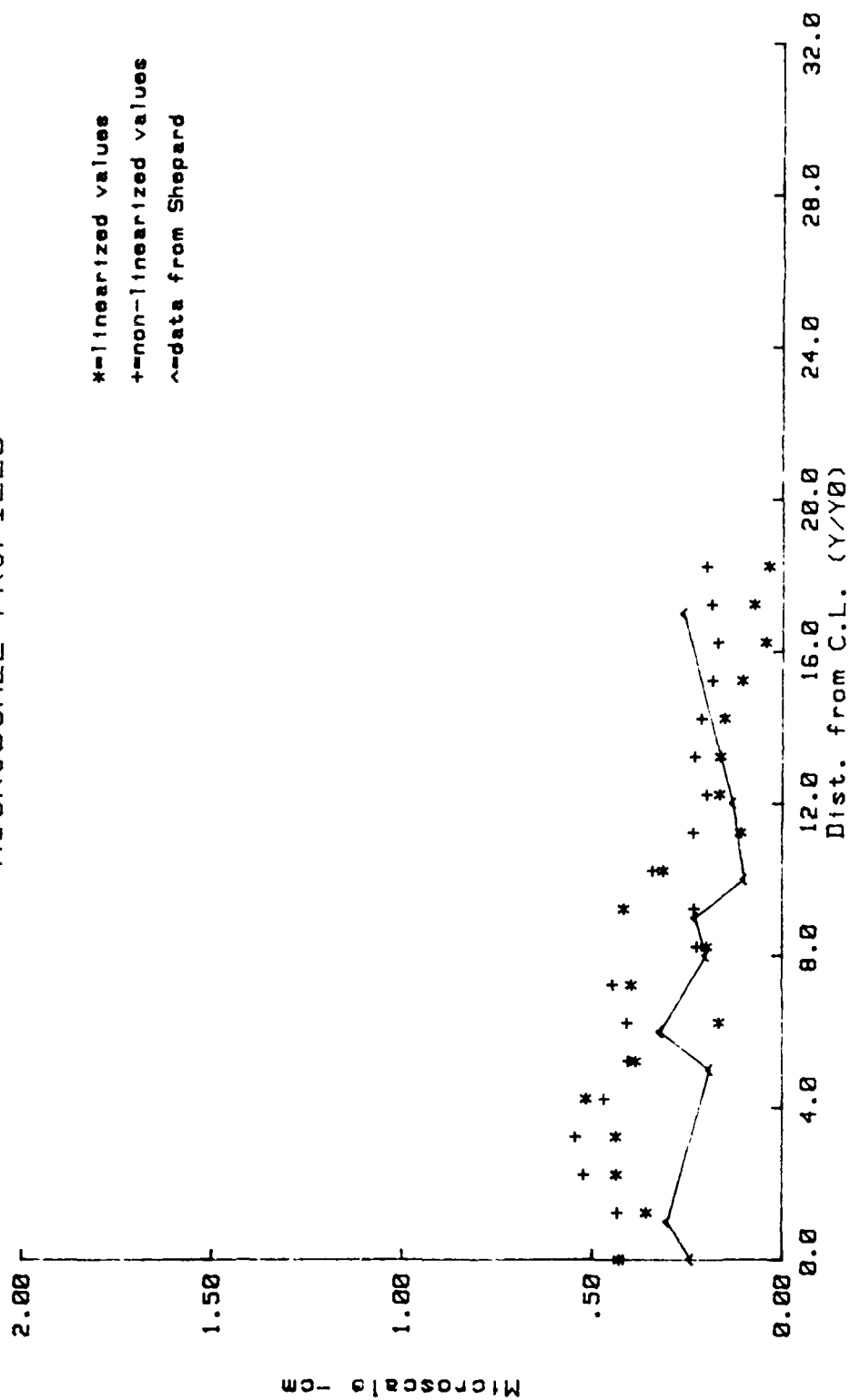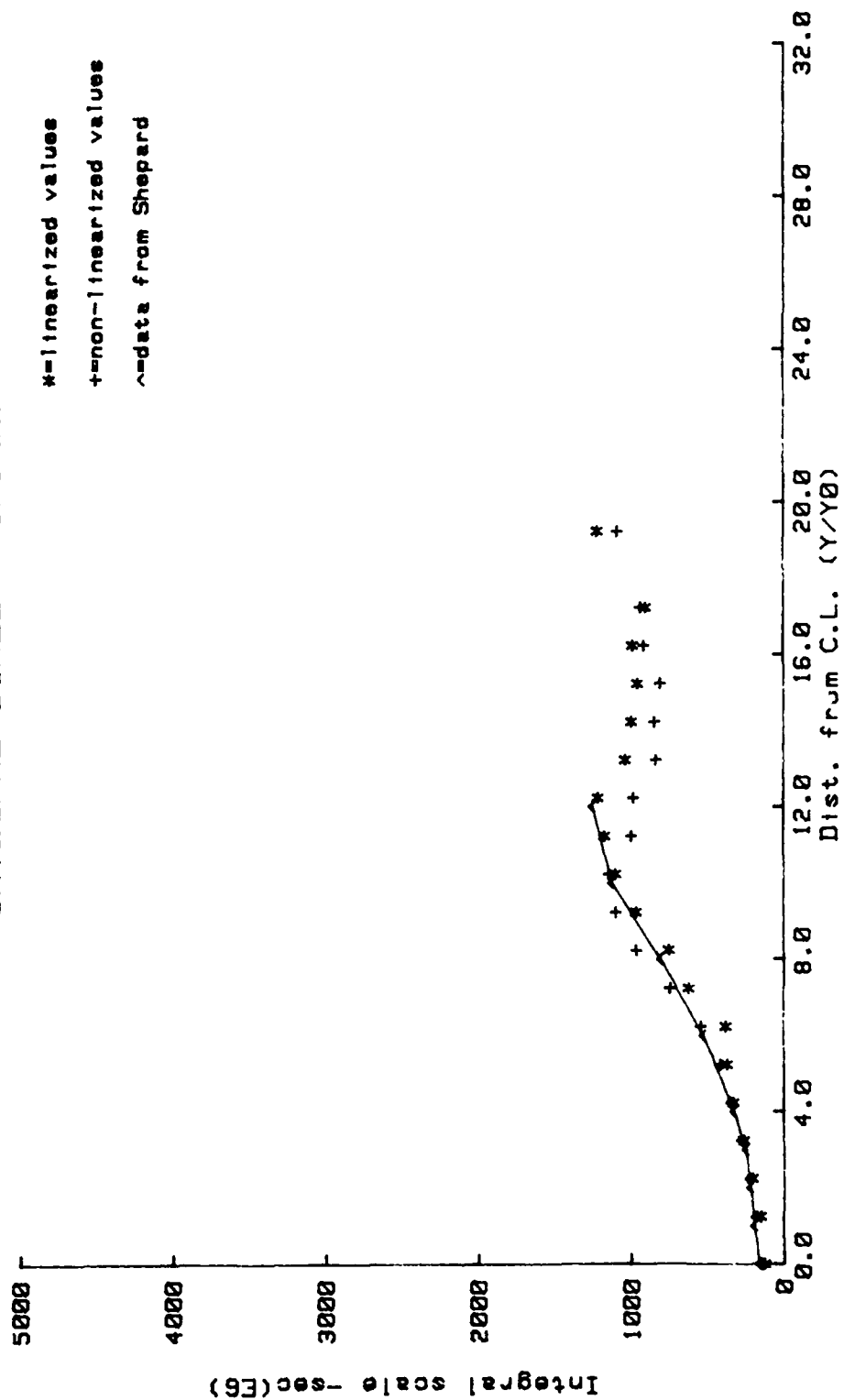
Fig. 7. Time Integral Scale at 25 cm, M=0.4

consistent for all runs.

The transformation from time integral scale to spatial integral scale also followed Shepard's data very closely at the 25 cm data plane. These results are shown on Fig. 8, 20 and 24 of Appendix B, and 42 of Appendix C. At the 50 cm data plane the results show a fairly rapid increase, followed by a fairly rapid decrease after passing the edge of the mixing region. Shepard's data predicts this kind of trend for M=0.4, but indicates a much more gradual, almost constant integral scale at M=0.6. Results at the 50 cm plane are found in Figs. 31 and 35 of Appendix B, and 49 of Appendix C. Again, additional data points show no tendency to increase the smoothness of the curves.

Comparison of Linearized and Non-linearized Signals. Figures 15 and 26 of Appendix B, and 37 and 44 of Appendix C, show results of mean velocity profiles calculated from both the bridge output and the linearizer output for the single wire sensors. At 25 cm, the difference between ratios calculated from the non-linearized output varies only slightly from that shown by the linearized signals. At 50 cm the variation is slightly greater, but no real trends are indicated, with some linearized values being lower than the non-linearized values at the same point, and vice-versa.

Turbulence intensity profiles tend to show more variation between the linearized calculations and the non-linear ones, especially in the range of turbulence intensities above 10%. This result is predicted by TSI (Ref. 11:3). The linearized
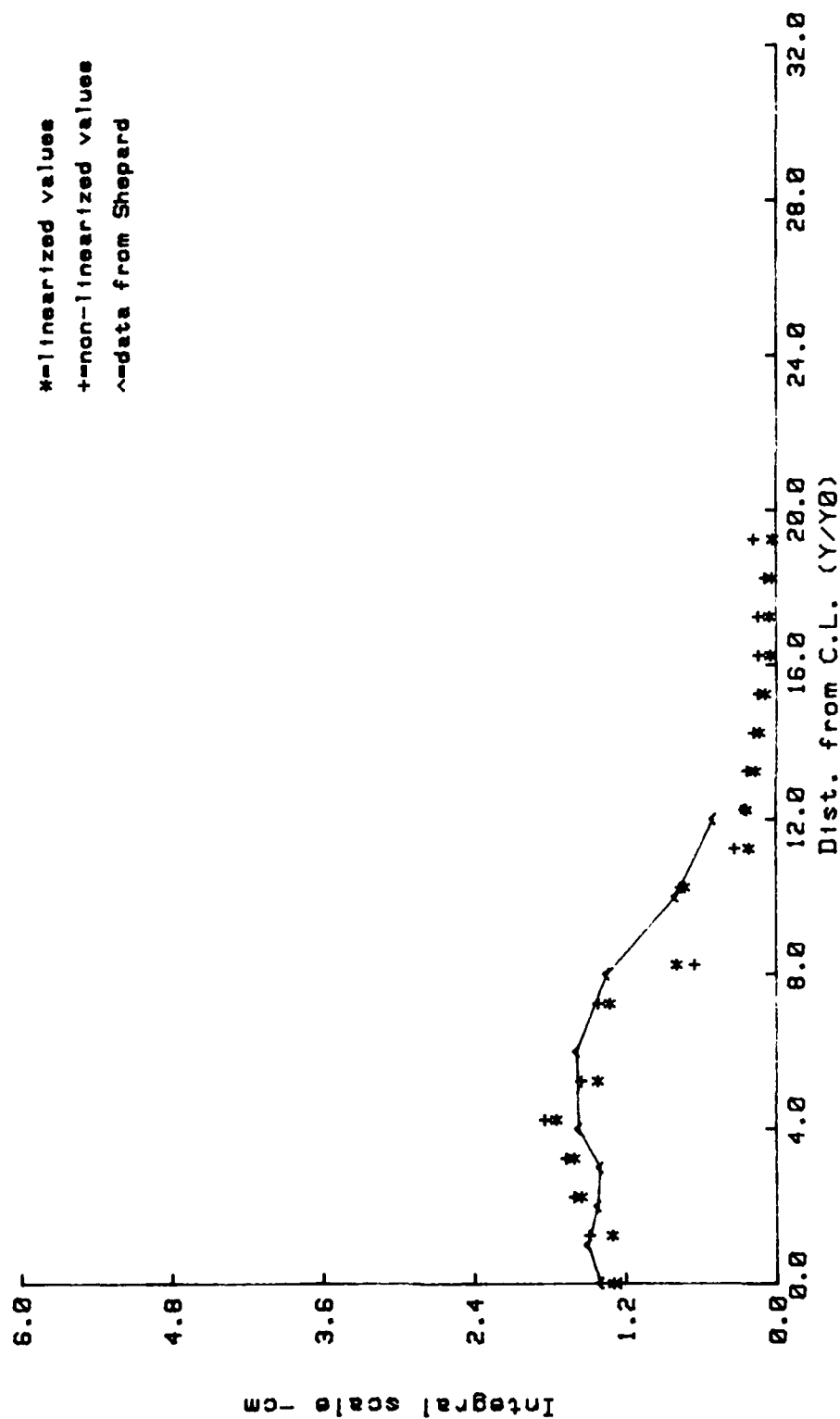
INTEGRAL SCALE PROFILES

*=linearized values
+=non-linearized values
^=data from Shepard

Fig. 9. Spatial Integral Scale at 25 cm, M=0.4

32

calculations show much smoother tendencies, while the non-linearized calculations show considerable fluctuation. This trend is especially noticable in the turbulence intensities plotted from signals from the X-wire sensors. These plots are presented in Figs. 25 and 36 of Appendix B, and 43 and 50 of Appendix C. Here, the linearized calculations present a relatively smoothly decreasing curve, while the non-linear effect is multiplied, resulting in a highly fluctuating curve from the non-linearized signals.

The turbulence parameters calculated from the correlator data, the time microscale and the time integral scale, do not show this dependency on linearization. On both scales, the linearized signals and the non-linearized signals lie very close, with no clear trends favoring one over the other. Since these parameters are frequency dependent, this would indicate that correlation over longer time periods tends to smooth the resulting data by eliminating frequency differences between the linearized and the non-linearized signals. When transforming to the spatial scales, the difference between the linearized result and the non-linearized result tend to increase somewhat as the sensor is moved outside the mixing region. Small differences in the calculated local velocities outside the mixing region tend to magnify differences in calculations using Taylor's hypothesis.

VI. Conclusions

Experimental measurement of turbulence parameters is of great interest in the study of fluid flows, since the great majority of these flows are turbulent. Hot wire and hot film anemometry has been found to be an excellent instrument for the study of turbulence. However, to really get meaningful results, many data points throughout each flow field must be investigated. Therefore, the integration of an automatic data acquisition system into the collection, analysis, and interpretation of turbulence parameters was developed. The following conclusions are drawn from the results of this study:

1. The automatic data acquisition system provides for real-time, on-line determination of turbulence parameters using information provided by hot wire anemometry. Results can be available for analysis and evaluation much more rapidly than possible with the present system.

2. The automatic data acquisition system also provides for fast, accurate calibration of hot wire and hot film sensors. The resulting calibration curves can be used either with the data acquisition system to analyze data, or they can be used when taking data manually.

3. Use of the automatic data acquisition system decreased the time the sensors had to be exposed to the flow field, which materially reduces sensor aging, or accumulation of dirt, and random sensor breakage.

4. Comparison of turbulence parameters calculated from linearized hot wire and hot film sensors with those calculated

from the non-linearized signals show linearization to be an
effective tool for use when determining turbulence intensity,
especially when using X-wire sensors in a flow characterized by
relatively high turbulence levels, that is, turbulence
intensities above approximately 10%. When used in calculating
velocities and, in conjuction with the correlator, to find the
microscales and integral scales, linearization does not provide
any additional smoothing of the resultant curves.

5. A fourth order polynomial curve fit to the calibration
data points results in a coefficient matrix of only five terms,
which is easily input to any program using that particular
sensor, and materially reduces the computer space and time
required over that necessary if the calibration data is stored
as a "look-up" table.

VII. Recommendations

The following are recommendations for future study:

1. A study making use of the techniques developed by Robinson (Ref 9:24-27) should make use of the data acquisition system to control stepper motors positioning the sensors behind the free jet facility, in addition to collecting data. Addition of position encoders to accurately determine sensor location would then provide a completely automated system for any future investigations.

2. A perforated plate mounted behind the free jet to generate turbulence should be studied. The integral scales of turbulence behind such a plate should be the size of the holes in the plate. This study would prove a further check on the accuracy of both the anemometry and the data acquisition system.

3. A study using this apparatus and heating the flow should be conducted to determine what corrections need to be made to sensor calibrations when the calibration can not be accomplished at the same temperature as the flow field being investigated.

5. A study could be made using a laser velocimeter to determine the interference generated by the sensor and probe support on the flow. This information would be useful in analyzing errors in data collected by hot wire anemometry.

6. Using the techniques developed in this study, a less turbulent flow should be analyzed, again comparing linearized and non-linearized signals to determine differences.

7. A pressure transducer could be used to moniter chamber pressure and, along witn a thermocouple, would provide a continuous check on chamber conditions. A range of allowable temperatures and pressures could be input to the computer, and the automatic data acquisition system could then alert tne operator to any variations outside these limits.

8. The automatic data acquisition system could be configured to control and operate a pressure regulator valve, both for controlling pressure in the calming chamber during calibration, and controlling pressure in the free jet calming chamber during data acquisition.

9. Addition of a seperate computer subroutine to sketch the flow field, test section, and sensor location would provide tne operator with a visual check of the test planes, allowing a more thorough investigation of areas of particular interest.

Bibliography

1. Abramovish, G. N. *The Theory of Turbulent Jets*. Cambridge, Massachusetts: The M.I.T. Press, 1963.

2. Bradshaw, P. *An Introduction to Turbulence and Its Measurement*. Oxford, England: Pergamon Press, Ltd., 1971.

3. Freathy, A. E. *Velocity Measurements and Turbulence Related Parameters in Two-Dimensional Air Stream*. M.S. Thesis. Wright-Patterson Air Force Base, Ohio: Air Force Institute of Technology, December 1973.

4. Hewlett-Packard Company. *Operating Information, Model 3455A Digital Voltmeter*. Loveland, Colorado: Hewlett-Packard Co.

5. Hewlett-Packard Company. *Programming and Service Manual, Model 3495A Scanner*. Loveland, Colorado: Hewlett-Packard Co.

6. Hewlett-Packard Desktop Computer Division. *System 45 Operating and Programming*. Ft. Collins, Colorado: Hewlett-Packard Co.

7. Hinze, J. O. *Turbulence*. New York: McGraw-Hill Book Co., 1959.

8. Osborn, J. F. *An Application of Hot Film Anemometry to a Turbulent Mixing Problem*. Published Thesis Report. Wright-Patterson Air Force Base, Ohio: Air Force Institute of Technology, March 1973.

9. Robinson, S. A. *Computerized Data Acquisition Interface to Measure Turbulent Shear Flow Velocity Profiles Behind a Grid of Parallel Rods*. M.S. Thesis. Wright-Patterson Air Force Base, Ohio: Air Force Institute of Technology, December, 1981.

10. Shepard, W. K. *Turbulence Measurements in a Plane Free Jet at High Subsonic Velocities*. M.S. Thesis. Wright-Patterson Air Force Base, Ohio: Air Force Institute of Technology, December 1974.

11. Thermo-Systems, Inc. *Hot Film and Hot Wire Anemometry, Bulletin TB5*. St. Paul, Minnesota: Thermo-Systems, Inc.

12. Thermo-Systems, Inc. *Instruction Manual for Model 1125 Calibrator*. St. Paul, Minnesota: Thermo-Systems, Inc.

13. Thermo-Systems, Inc. *Operating and Service Manual for 1050 Series Constant Temperature Anemometer and Related Accessories*. St. Paul, Minnesota: Thermo-Systems, Inc.

14. Tibbs, G. B. _Documentation of the Design, Construction, and Operation of the GBT2; An Interface Between a 9845T and a 3721A/3720A_. Wright-Patterson Air Force Base, Ohio; Air Force Propulsion Laboratory, June 1981.

15. Zakanycz, S. _Turbulence and the Mixing of Binary Gases_. Ph. D. Dissertation. Columbus, Ohio: Ohio State University, 1971.

Appendix A

Computerized Calibration of Hot-wire Anemometers

One of the objectives of this study was to develop a
technique for calibrating hot wire and hot film sensors using
the automatic data acquisition system. Previous calibration
techniques tended to be time consuming, as calibration data had
to be either plotted by hand, or manually entered into a
central site computer for calculations. Basic instructions for
sensor calibration are found in the TSI operating manual (Ref.
13:2-7).

Equipment Setup

The calibration points were obtained by exposing the
sensor to a controlled flow field using the TSI Model 1125
Calibrator. The pressures in the calibrator stilling chamber
were determined using two pressure transducers. Voltage output
from each transducer was fed directly through the scanner into
the automatic data acquisition system. Anemometer signals from
the bridge and signals from the linearizer were also sent
directly to the data acquisition system. Figure 9 shows the
equipment setup schematic for sensor calibration.

Calibration

The first step in the calibration program is to determine
the equations for the response of the pressure transducers.
Through many runs, it was determined that the transducer
response was linear and remained constant over long periods.
Because of this linearity, three points for each transducer are
all that are necessary to determine the needed coefficients.

The zero flow point, a pressure of about 2.5 in. of water, and

a point of about 1.2 in. of water were found to work best for

the .5 psi transducer. In this range, air is essentially

incompressible, and Bernoulli's equation is valid, so that

$$V = (2*g*h)^.5 \qquad\qquad (4)$$

where h is the chamber pressure in inches of water. Therefore,

in this area of the calibration curve, small changes in

pressure cause large changes in velocity, and extra care must

be exercised during calibration. This is also the reason for

choosing to use the micromanometer and a second transducer to

measure pressures in this region. For the 25 psi transducer,

inputs of approximately 2.5 in. of water, a pressure near the

pressure required to obtain the highest anticipated velocity,

and a pressure approximately midway between the two, gave the

best results. Typical computer output for the 25 psi transducer

is shown in Fig 10.

   After the transducers are calibrated, the calibration

points for the non-linear sensor calibration can be obtained.

The zero flow point is input first, then points in increasing

velocity to the maximum required. The best results were

obtained by inputing 20 data points at approximately equal

increments of bridge voltage. The calibration points are

plotted by the computer, with hard copy available from the

internal thermal printer. Figure 11 shows the computer output

for a typical hot film sensor. A least squares technique is

41

then used to fit a fourth order polynomial to the calibration
points to determine the equation for the calibration curve,
which solves for velocity given voltages from the anemometer. A
typical curve fit is illustrated in Fig 12 for a hot film
sensor.

The least squares routine provides five coefficients for
the fourth order polynomial curve fit. In general, these
coefficients are too large to be set in the TSI Model 1052
Linearizers. Also, the linearizers have only four adjustable
potentiometers, therefore, the coefficients must be normalized
such that the constant term is approximately zero. This is
accomplished by heavily weighting the zero flow point in the
computer program, and by normalizing the remaining four
coefficients to the bridge voltage at zero flow and to the
maximum flow velocity input during the calibration. The
calibration program handles these problems by incorporating a
BASIC program outlined by TSI to compute the required
normalized coefficients. These coefficients are printed by the
computer's internal printer, along with an analysis of their
accuracy.

The computer then halts the program while the user sets
the coefficients into the linearizer. When set, the program is
continued, and the calibration is run again. This time, the
linearized signals are read and stored, and a linear curve is
fit to the calibration points. This provides a check on the
accuracy of the linearizer, and provides the coefficients for
the linearizer curve to be stored. Typical results are shown in

42

Fig 13. Finally, the voltages and velocities used to obtain both sets of calibration curves, as well as the corresponding coefficients, are printed out. Figure 14 shows the result.
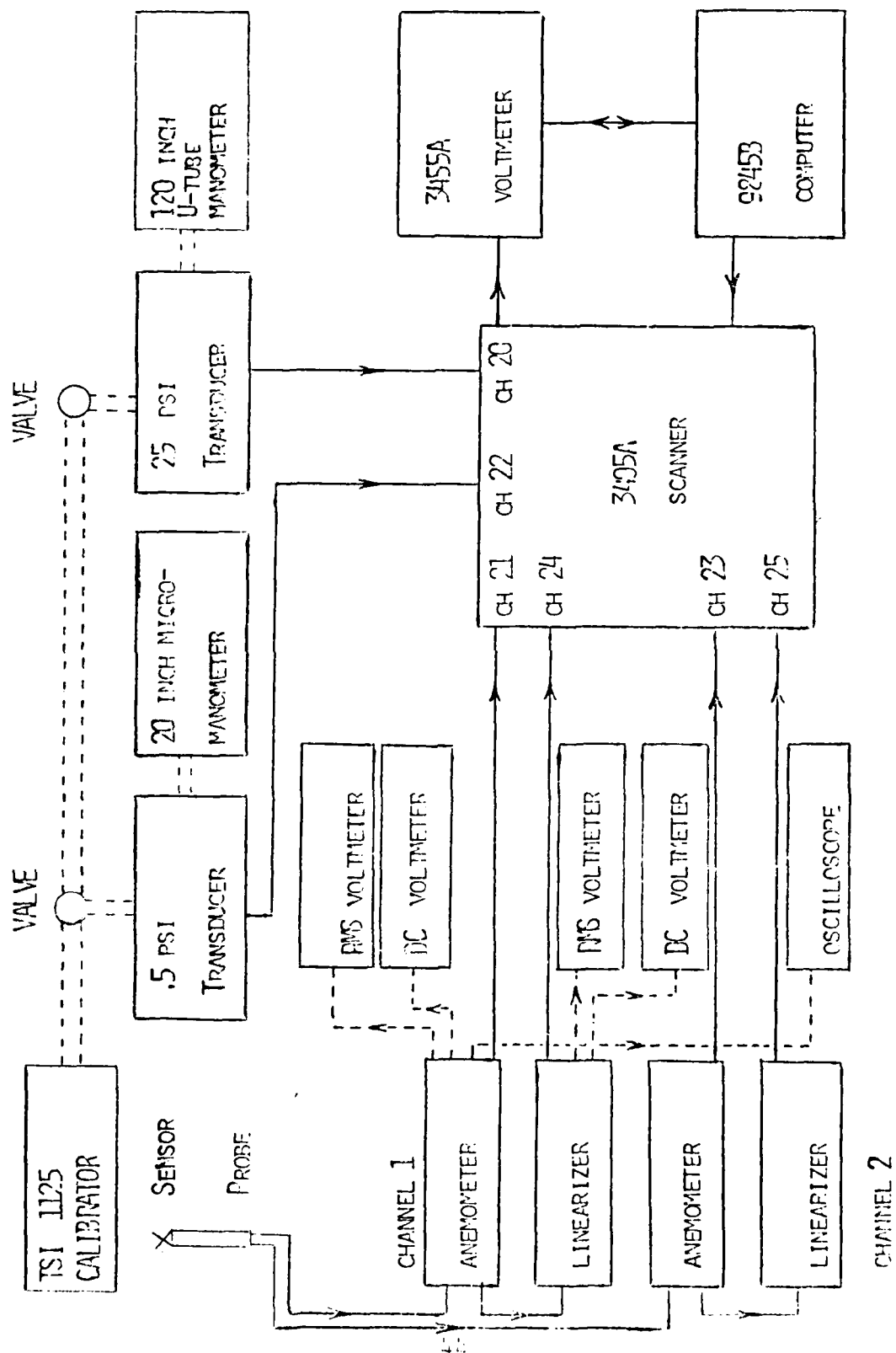
Fig. 9. Calibration Instrumentation Schematic
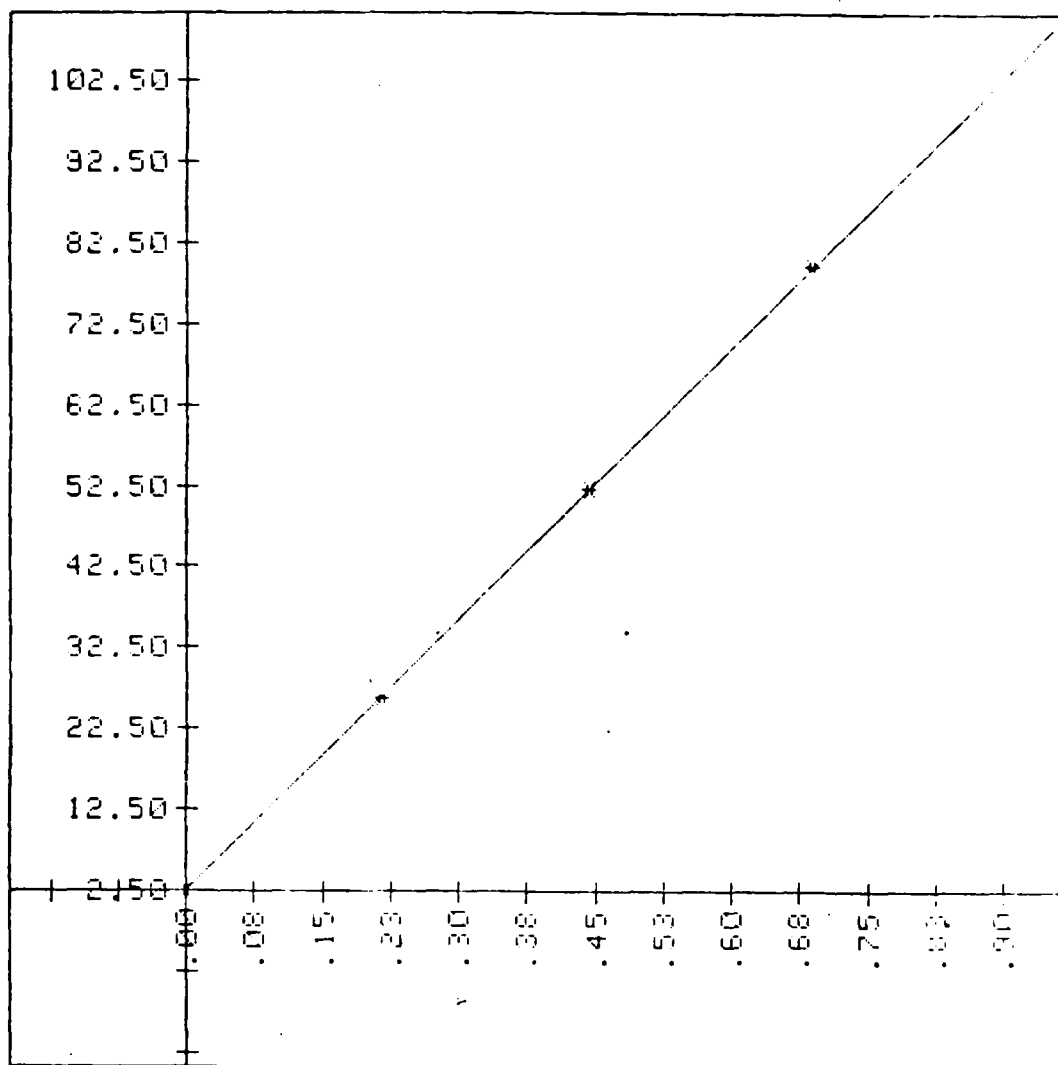
For the 5 psi transducer, volts and inches of water are:
 .00141 .21566 .44424 .68925 .97118

 2.5 26.3 52.1 79.6 110.7

The equation is: InH20= 2.350174134 + 111.74771043 *Vt

Fig. 10. Transducer Calibration

45
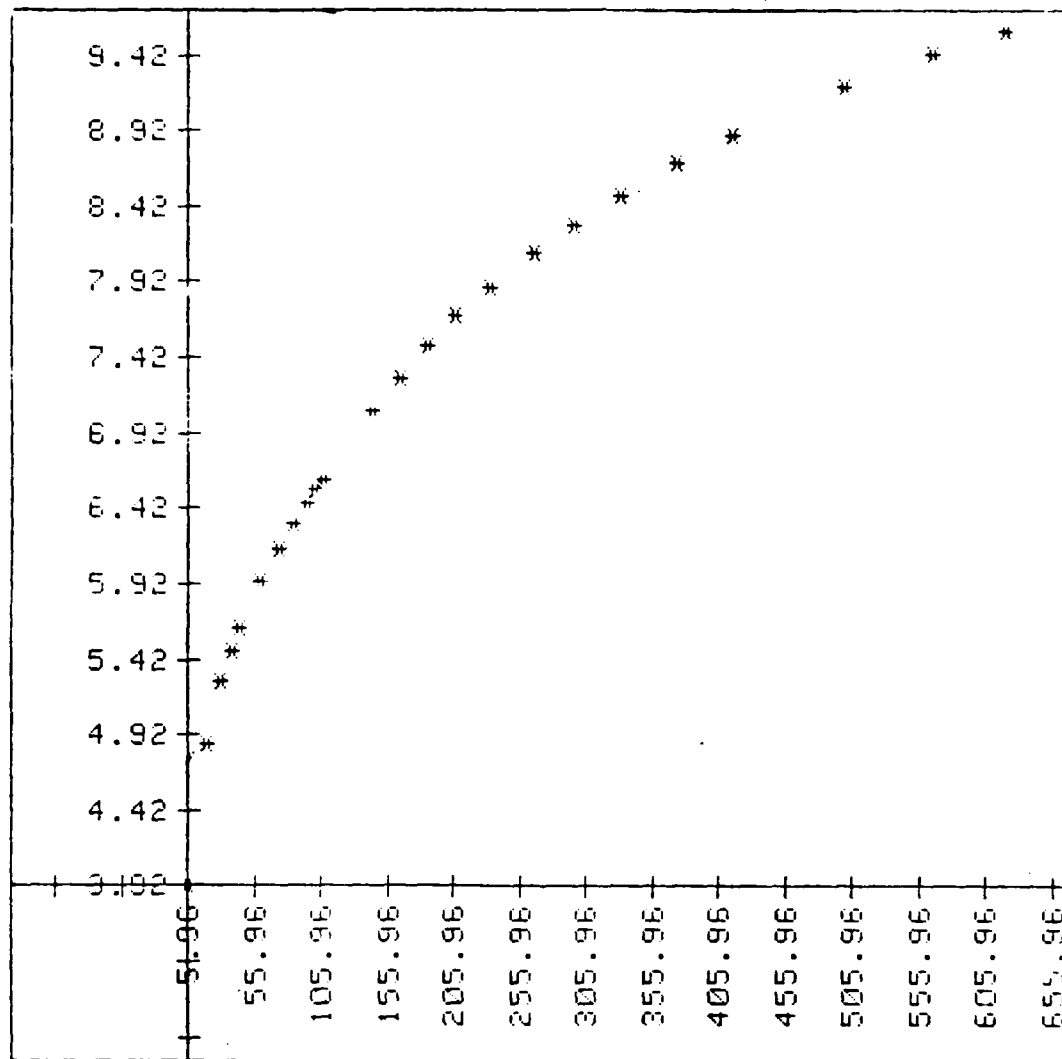
Fig. 11. Calibration Points for a Hot Film Sensor
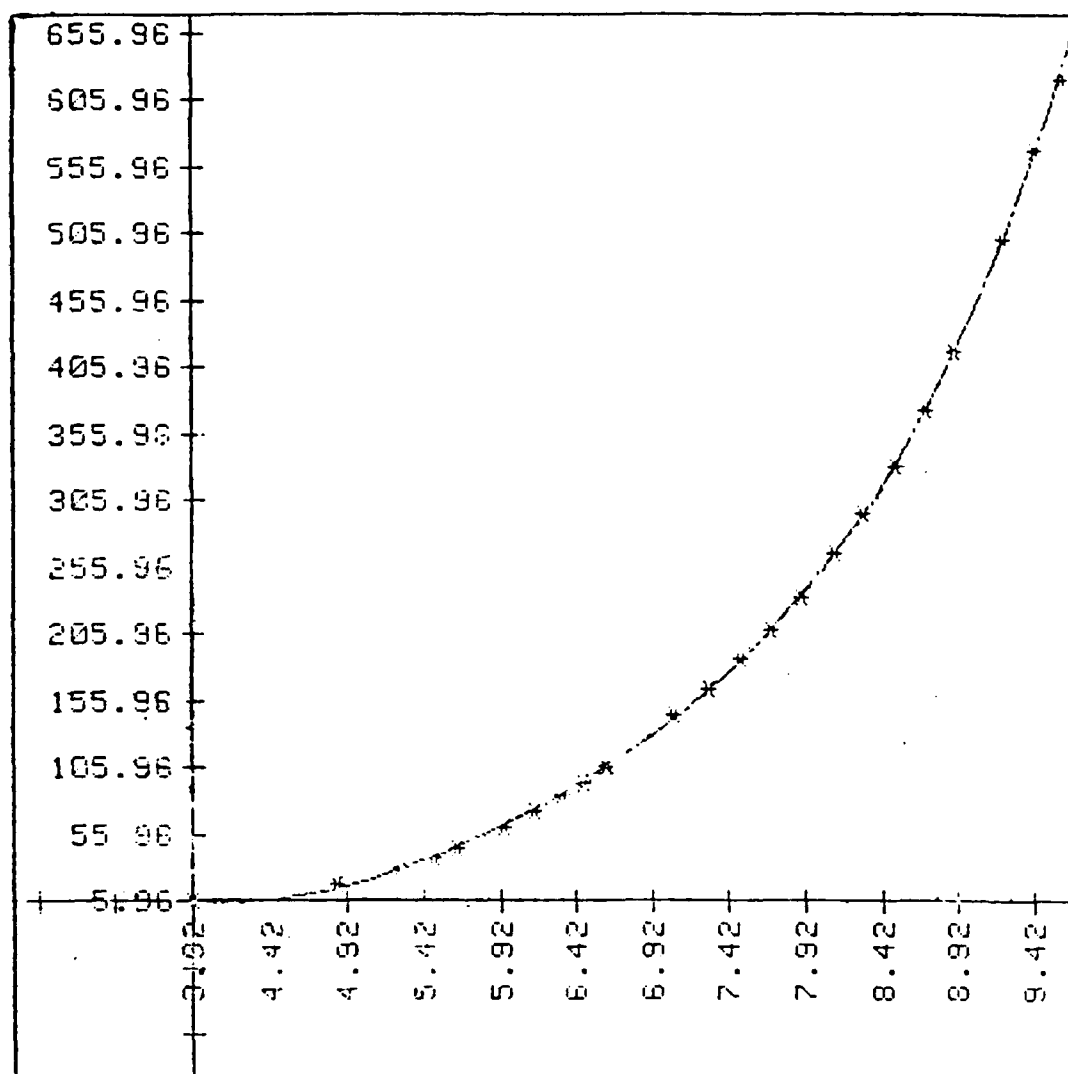
Fig. 12. Calibration Polynomial Curve Fit

47
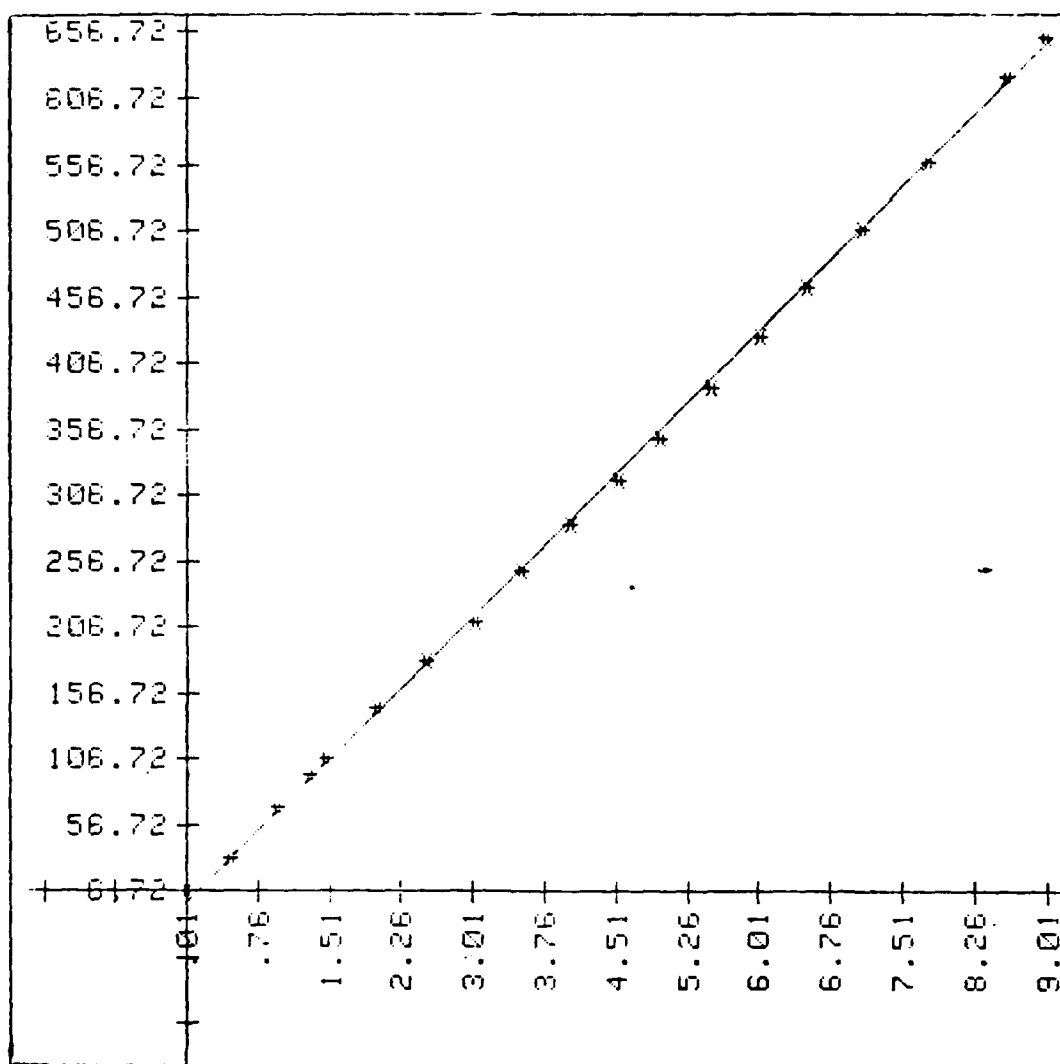
Fig, 13. Linearized Calibration Curve

FOR THE CALIBRATION CURVE:
The hotwire voltages are:
3.921 4.8584 5.2702 5.4777 5.6303 5.9376 6.1424 6.3231 6.4633 6.5486
6.6144 7.0651 7.292 7.4953 7.693 7.8944 8.1058 8.2948 8.5014 8.7083
8.8947 9.2116 9.4318 9.5901 9.7229

The velocities are:
5.96030781649   19.3924639471   30.6151422703   38.2812509759   44.8689399649
60.9555124478   73.3270292787   85.2501004913   94.8365267585   101.161612521
107.233706342   144.273603032   165.172246016   186.393333378   208.082967842
233.172740272   266.49067315   296.002125661   331.002490866   373.17173525
416.776778131   500.46219 3788   566.73 00   620.429564364   669.13513713

The equation to solve for velocity given voltage is:

$$Vel = 1217.01 + -831.9419 \ast Vt + 246.85973 \ast Vt^2 + -22.535213 \ast Vt^3 + .9733367\, Vt^4$$

FOR THE LINEARIZED CALIBRATION CURVE:
The hotwire voltages are:
.006803   .47859   .96588   1.29602
1.1992   2.001   2.5114   3.0232
3.031   4.021   4.5241   4.9785
5.5181   6.0214   6.5196   7.0952
7.7851   8.6054   8.4823   9.2233

The velocities are:
6.7214451189   31.5999583502   69.9383227023   94.4401903974
107.542988418   145.733924478   180.463596322   211.360645646
249.265862639   284.130002884   318.376064131   349.813531267
388.257344?3   425.680491552   463.016477426   506.163857022
558.408779578   622.279207497   652.308664771   669.823459963

The linear equation is:
$$Vel = -1.608901678 + 71.4108856004\, Vt$$

Fig. 14. Calibration Program Output

49

Appendix B

Experimental Data for Jet Exit Velocity of M=0.4
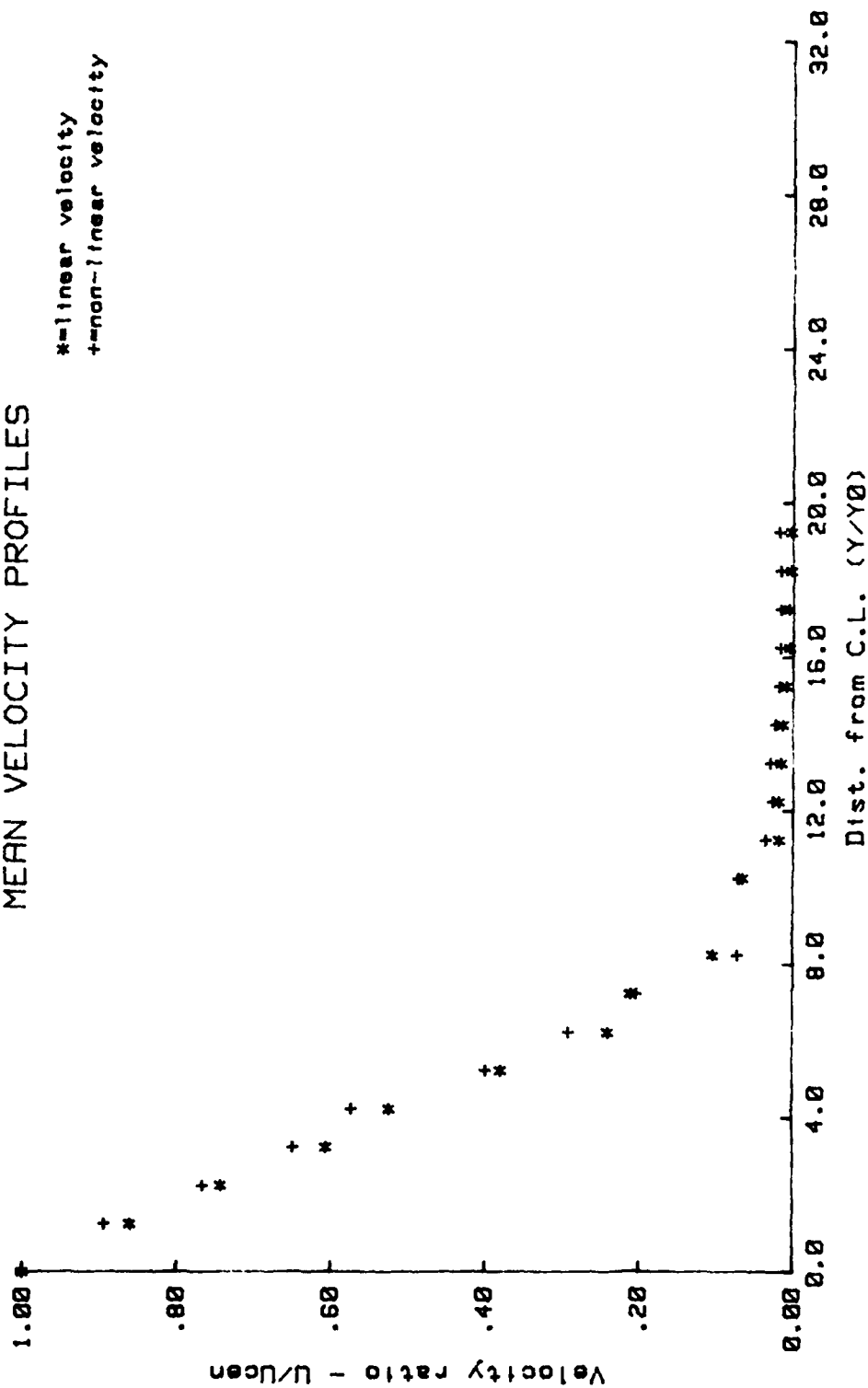
Fig. 15. Mean Velocity at 25 cm, M=0.4

51

TURBULENCE INTENSITY PROFILES
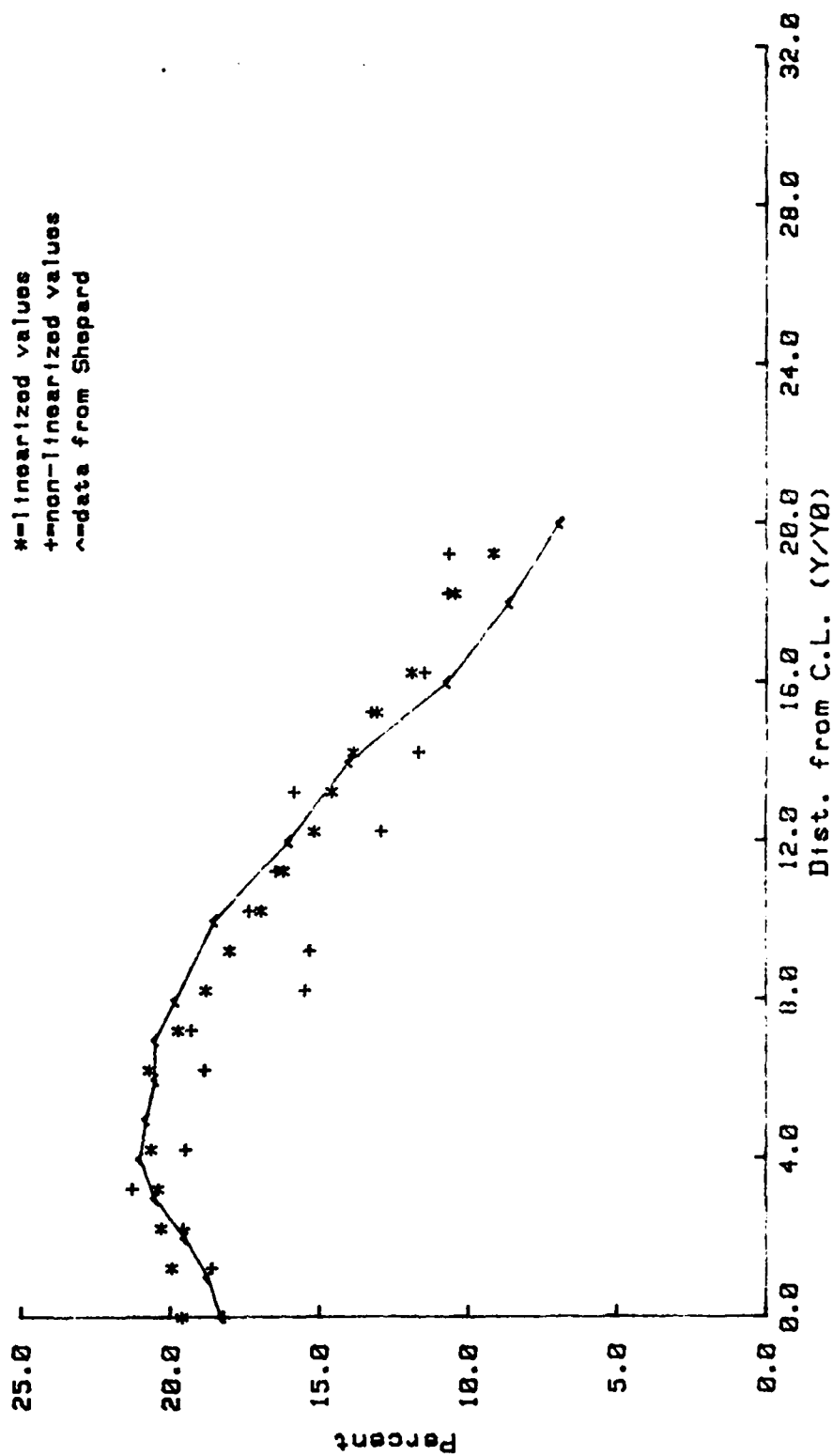
*=linearized values
+=non-linearized values
^=data from Shepard

Fig. 16. Turbulence Intensity at 25 cm, N=0.4

MICROSCALE PROFILES

*=linearized values
+=non-linearized values
^=data from Shepard

2000

1600

1200

800

400

Microscale -sec(E6)

0.0   4.0   8.0   12.0   16.0   20.0   24.0   28.0   32.0
Dist. from C.L. (Y/YØ)
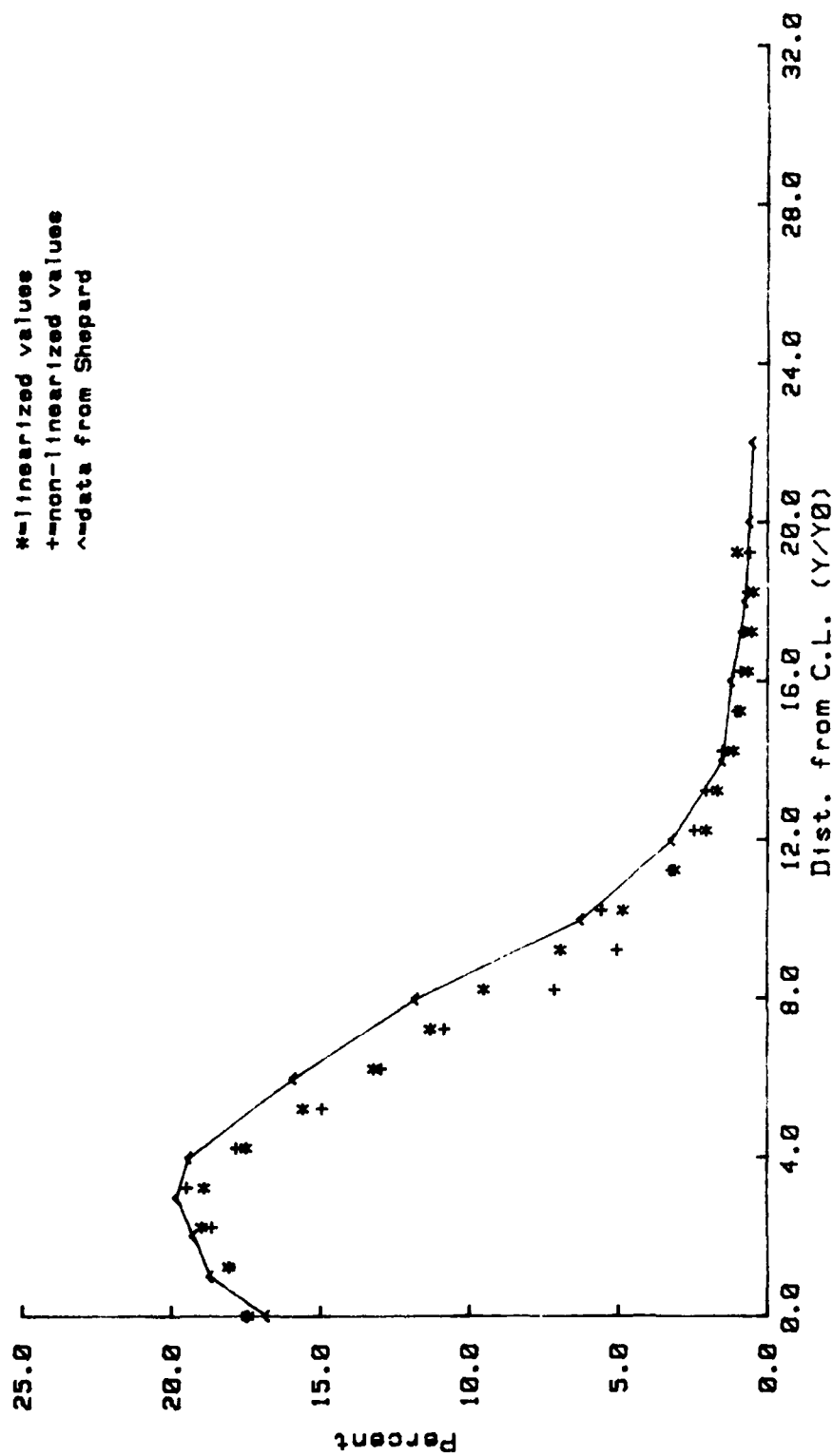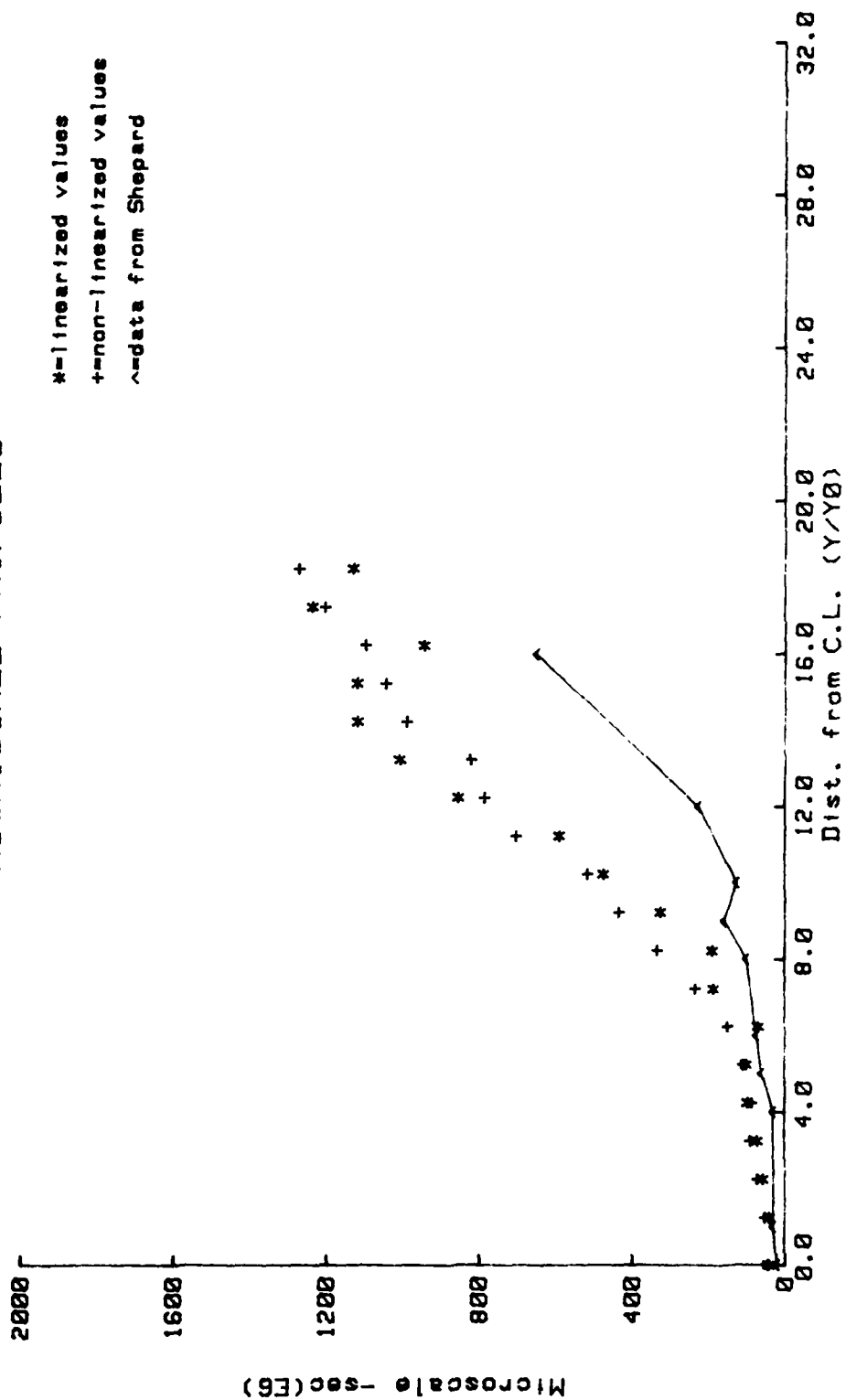
Fig. 17. Time Microscale at 25 cm, M=0.4
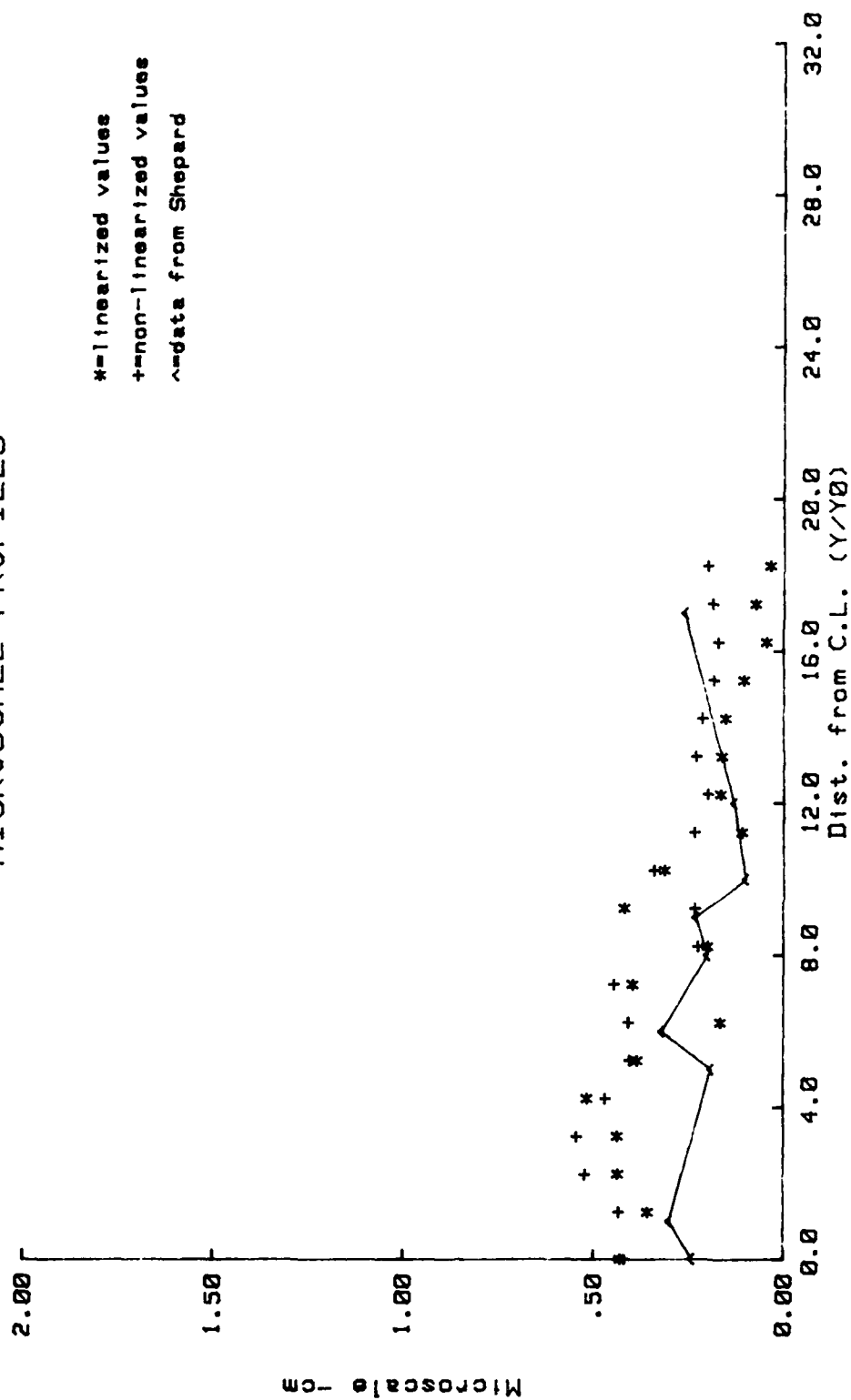
Fig. 18. Spatial Microscale at 25 cm, M=0.4

54

INTEGRAL SCALE PROFILES

*=linearized values

+=non-linearized values

^=data from Shepard
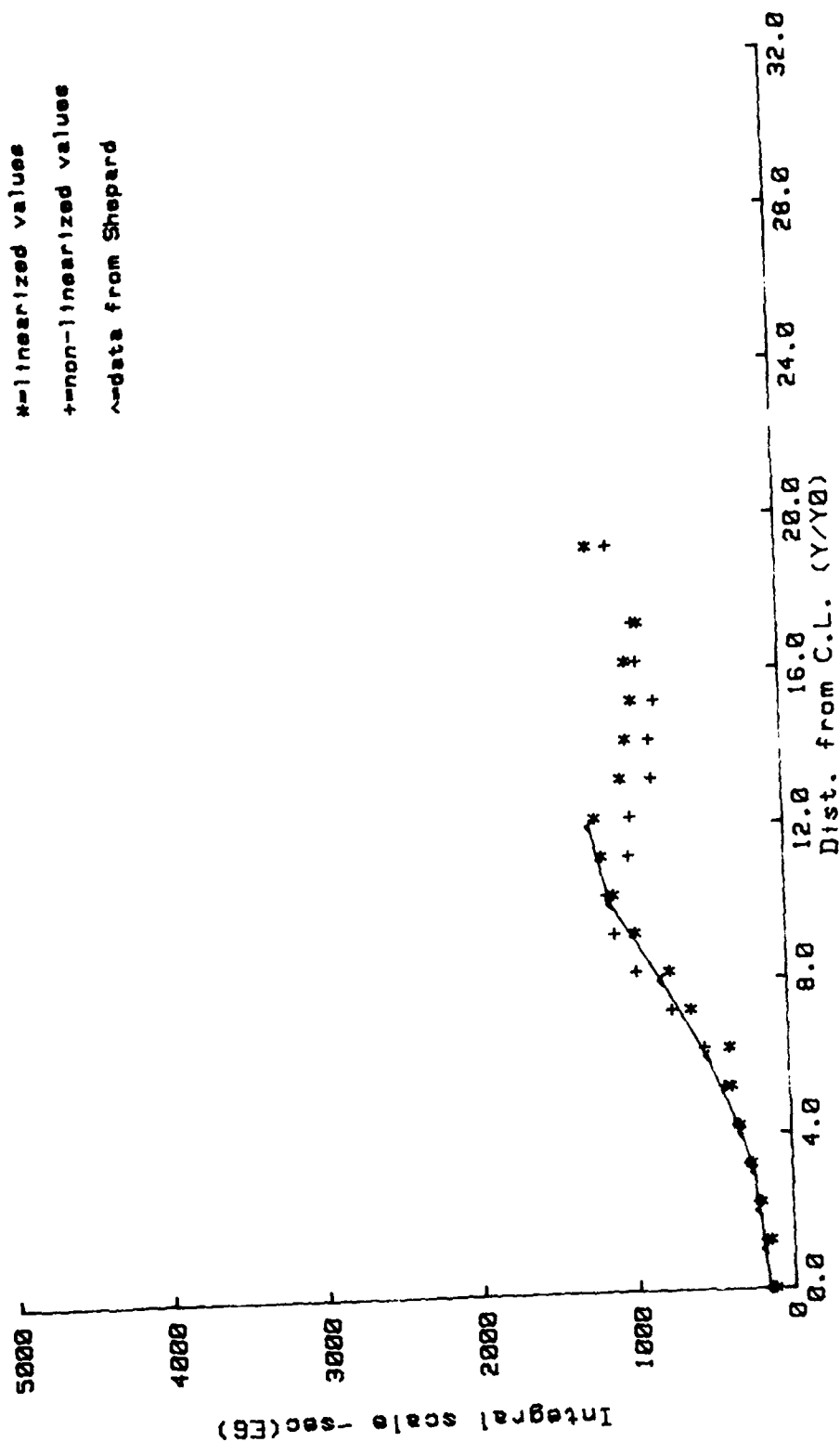
Fig. 10. Time Integral Scale at 25 cm, "=0.4

55
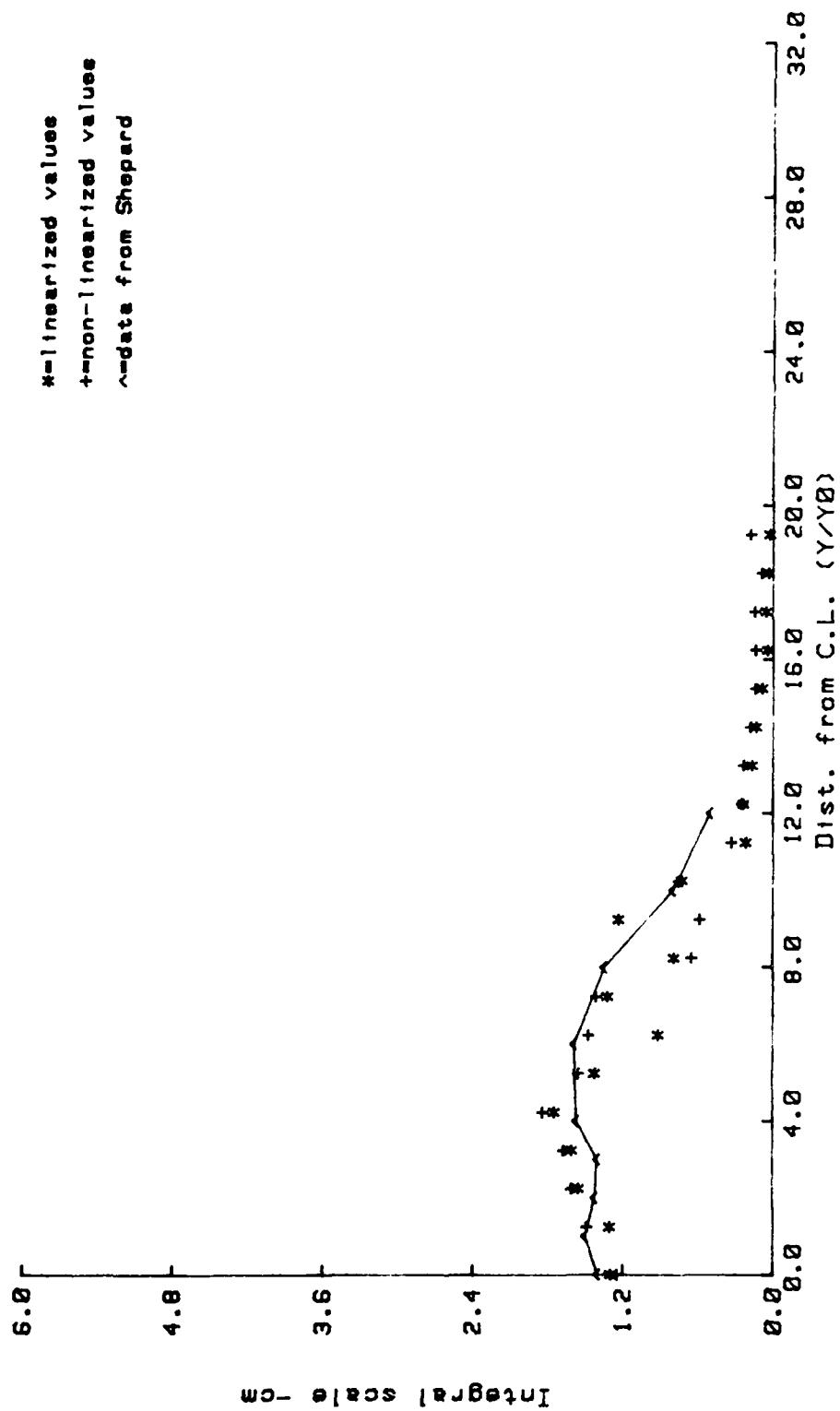
Fig. 20. Spatial Integral Scale at 25 cm, N=0.4

Fig. 21. Hot-wire Time Microscale at 25 cm
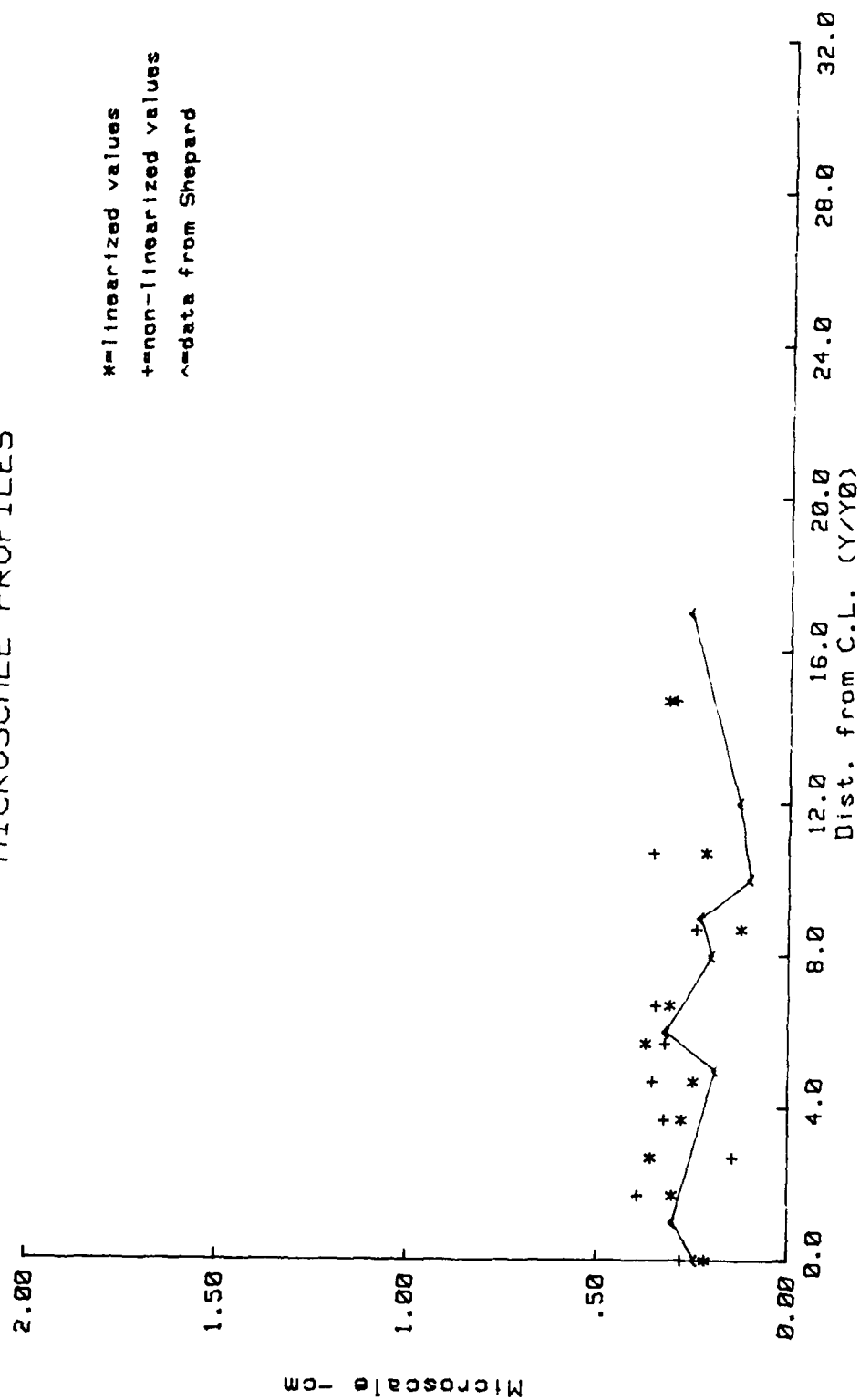
57

MICROSCALE PROFILES

*=linearized values
+=non-linearized values
^=data from Shepard

Microscale -cm

Dist. from C.L. (Y/Y0)

Fig. 22. Hot-wire Spatial Microscale at 25 cm

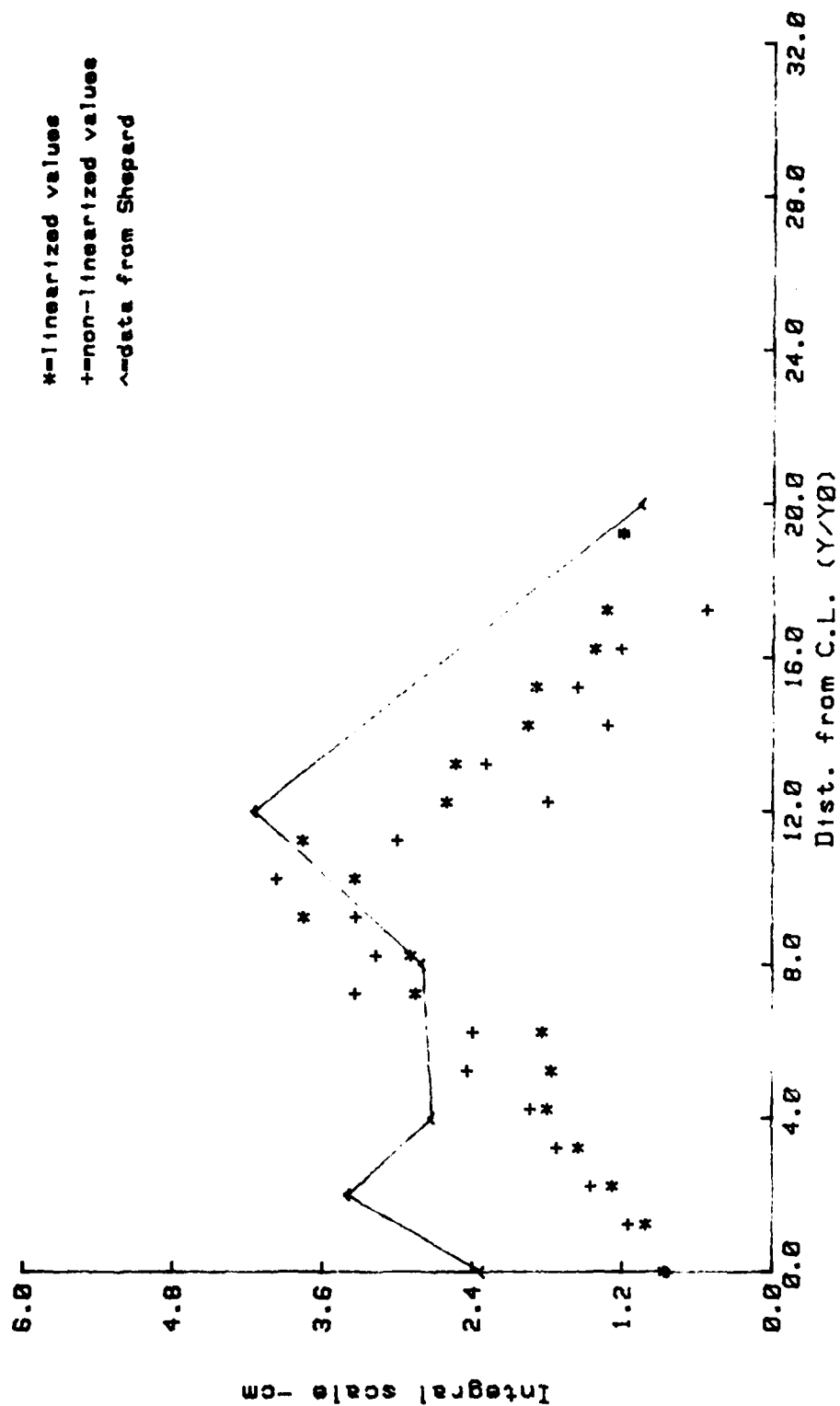Fig. 22. Hot-wire Time Integral Scale at 25 cm

59

INTEGRAL SCALE PROFILES

*=linearized values
+=non-linearized values
^=data from Shepard

Fig. 24. Hot-wire Spatial Integral Scale at 25 cm

Dist. from C.L. (Y/Y0)

Integral scale -cm

TURBULENCE INTENSITY PROFILES

*=linearized values, u'/Ucen
+=non-linearized values, u'/Ucen
&=linearized values, v'/Ucen
@=non-linearized values, v'/Ucen

Percent

25.0
20.0
15.0
10.0
5.0
0.0

0.0   4.0   8.0   12.0   16.0   20.0   24.0   28.0   32.0
Dist. from C.L. (Y/Y0)

Fig. 25. Y-wire Turbulence Intensity at 25 cm

63

MEAN VELOCITY PROFILES

*=linear velocity
+=non-linear velocity

Velocity ratio — U/Ucen

Dist. from C.L. (Y/YØ)
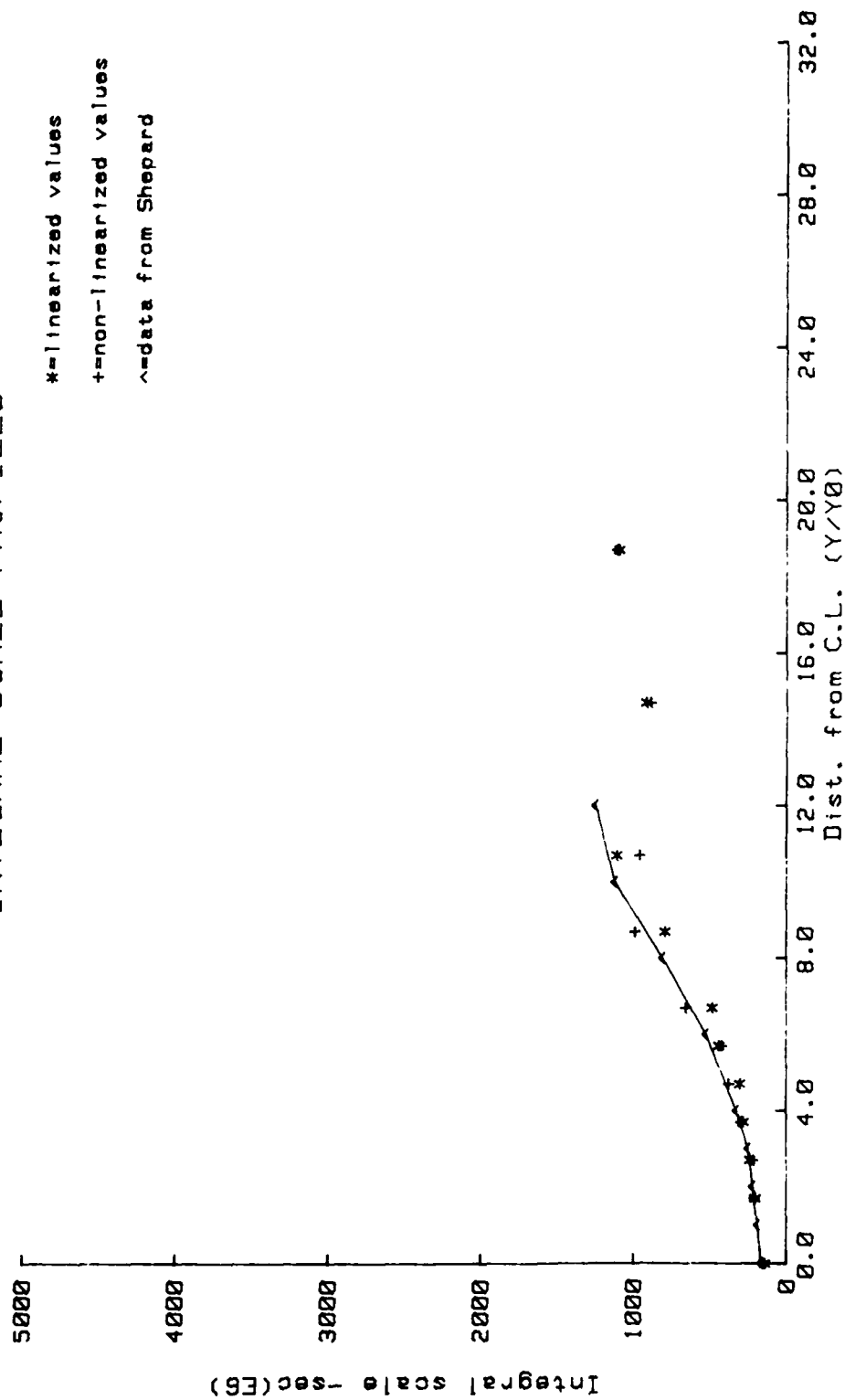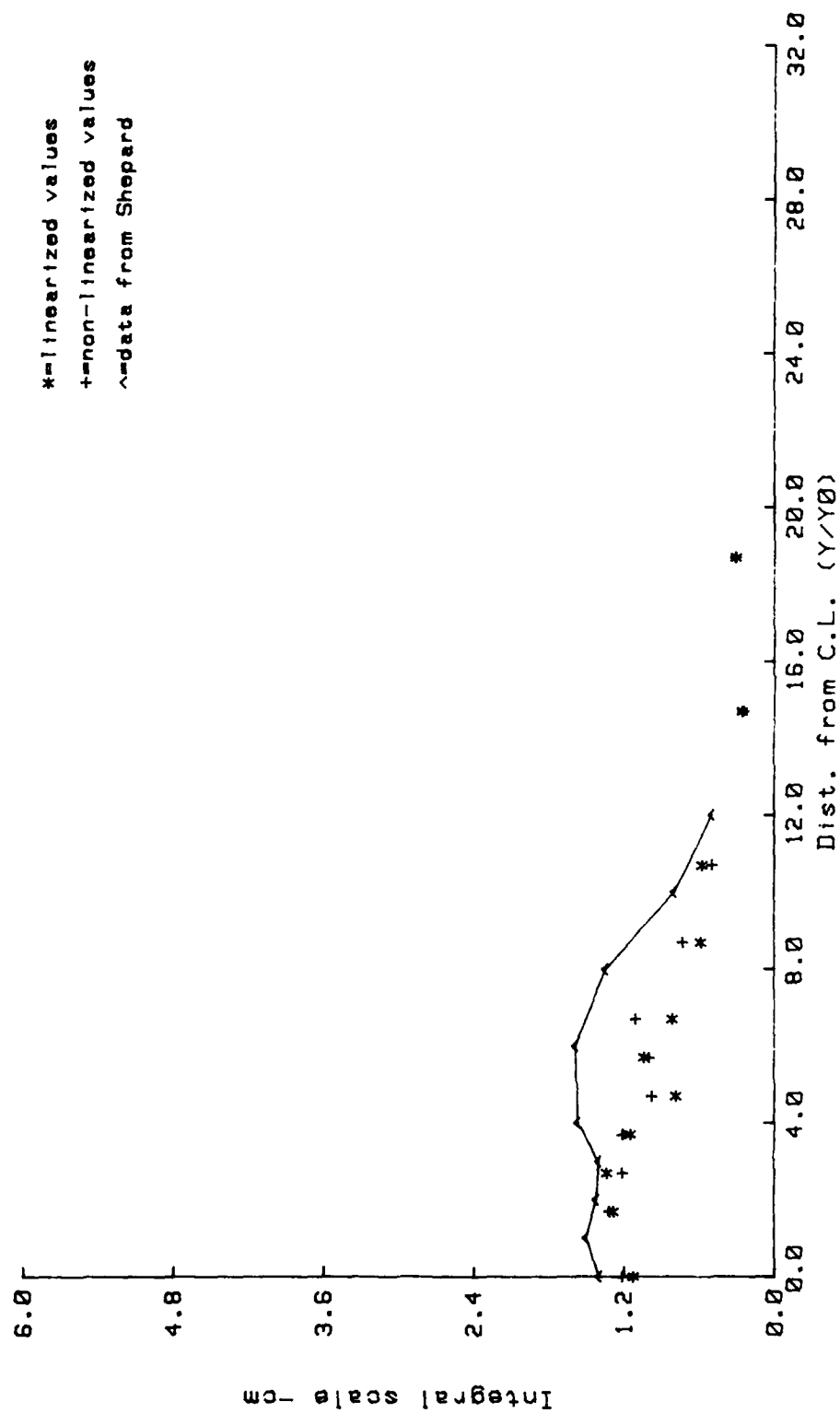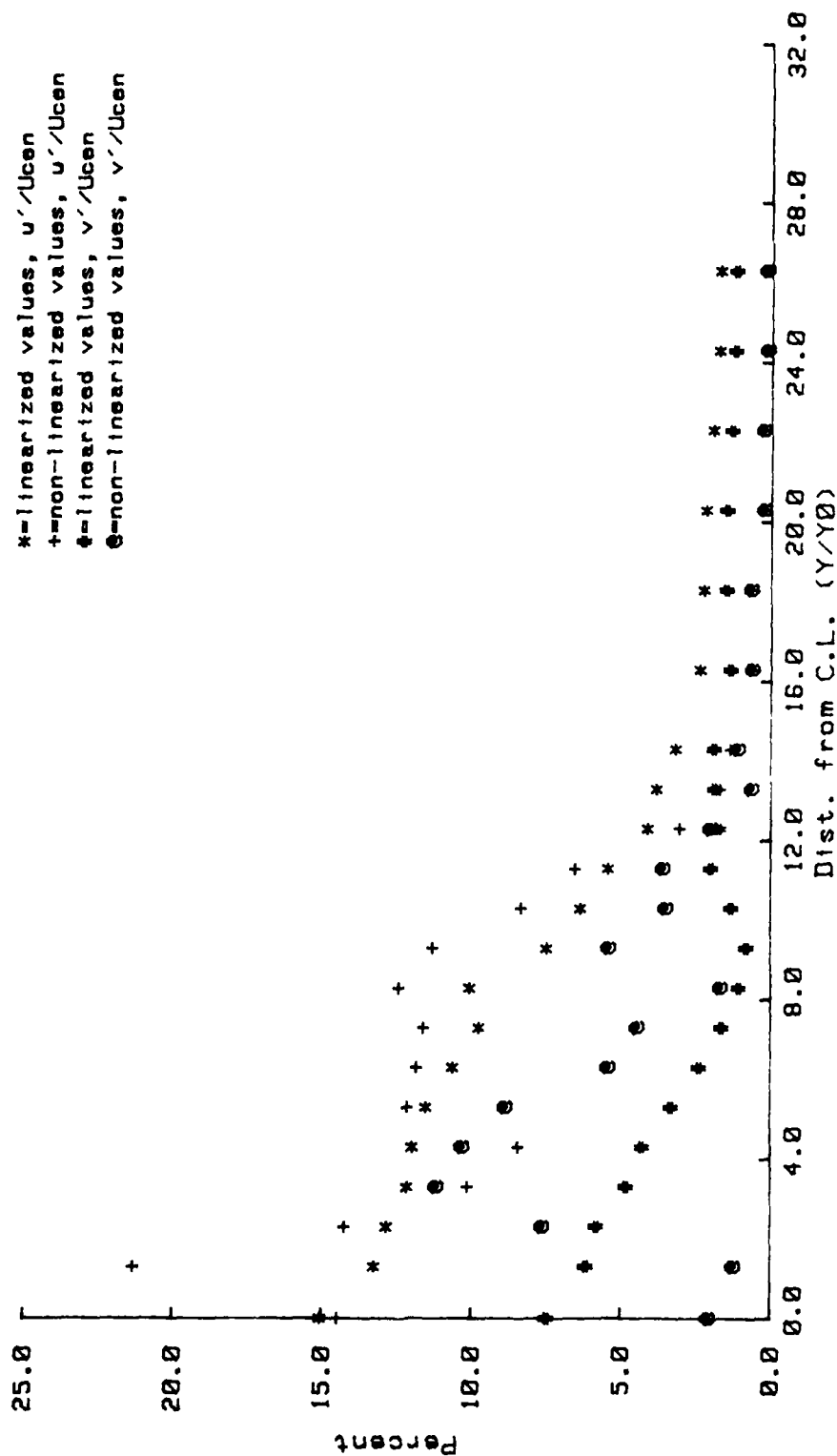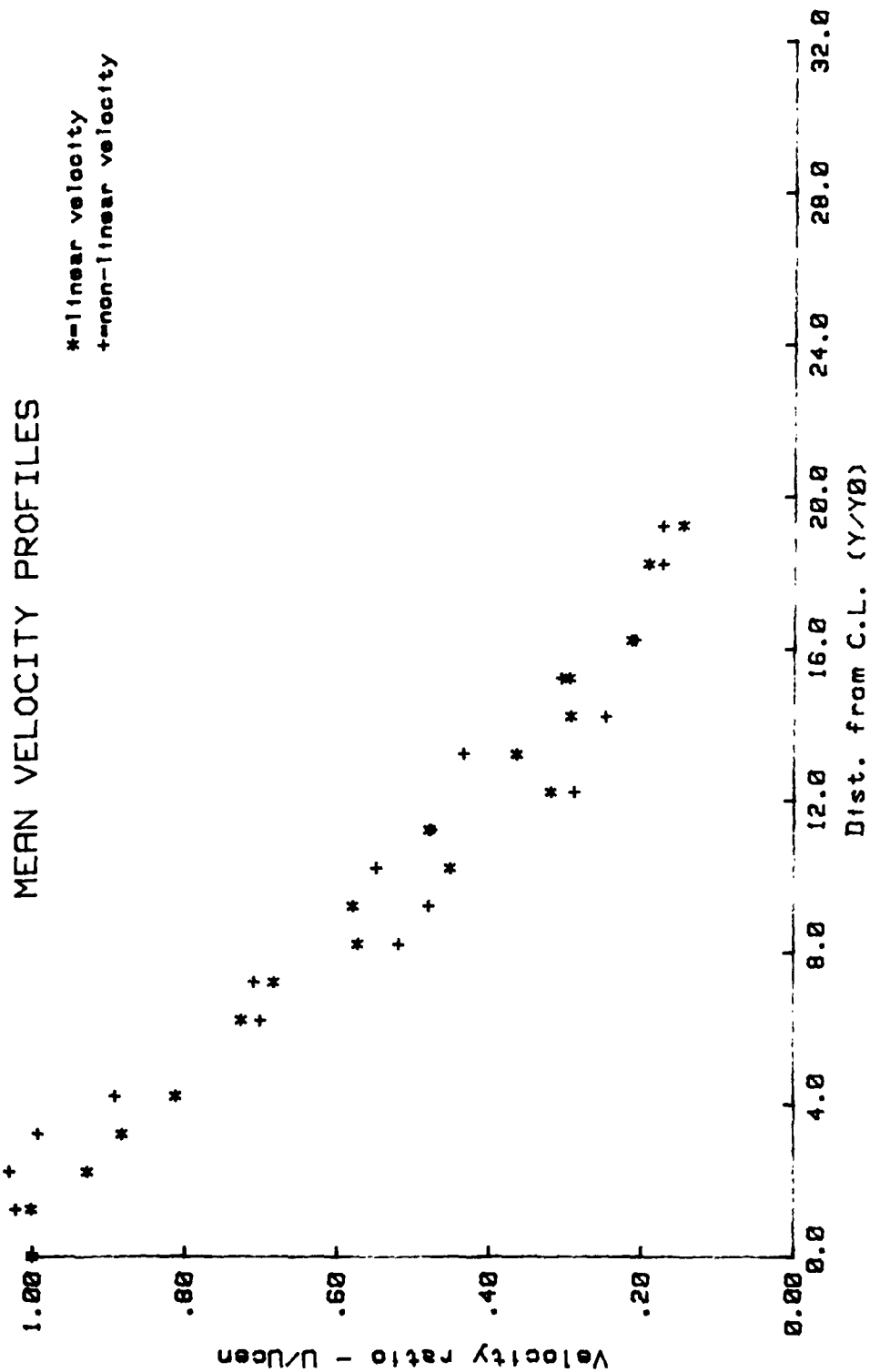
Fig. 26. Mean velocity at 50 cm, M=0.4

TURBULENCE INTENSITY PROFILES

*=linearized values
+=non-linearized values
^=data from Shepard

Fig. 27. Turbulence Intensity at 50 cm, M=0.4

63

MICROSCALE PROFILES

*=linearized values
+=non-linearized values
^=data from Shepard

Microscale -sec(E6)

Dist. from C.L. (Y/Y0)

Fig. 28. Time Microscale at 50 cm, M=0.4

64

Fig. 29. Spatial Microscale at 50 cm, M=0.5

INTEGRAL SCALE PROFILES

*=linearized values
+=non-linearized values
^=data from Shepard

Integral scale -sec(E6)

Dist. from C.L. (Y/YB)

Fig. 30. Time Integral Scale at 50 cm, M=0.4

66

INTEGRAL SCALE PROFILES

*=linearized values
+=non-linearized values
^=data from Shepard

Integral scale -cm

Dist. from C.L. (Y/YØ)
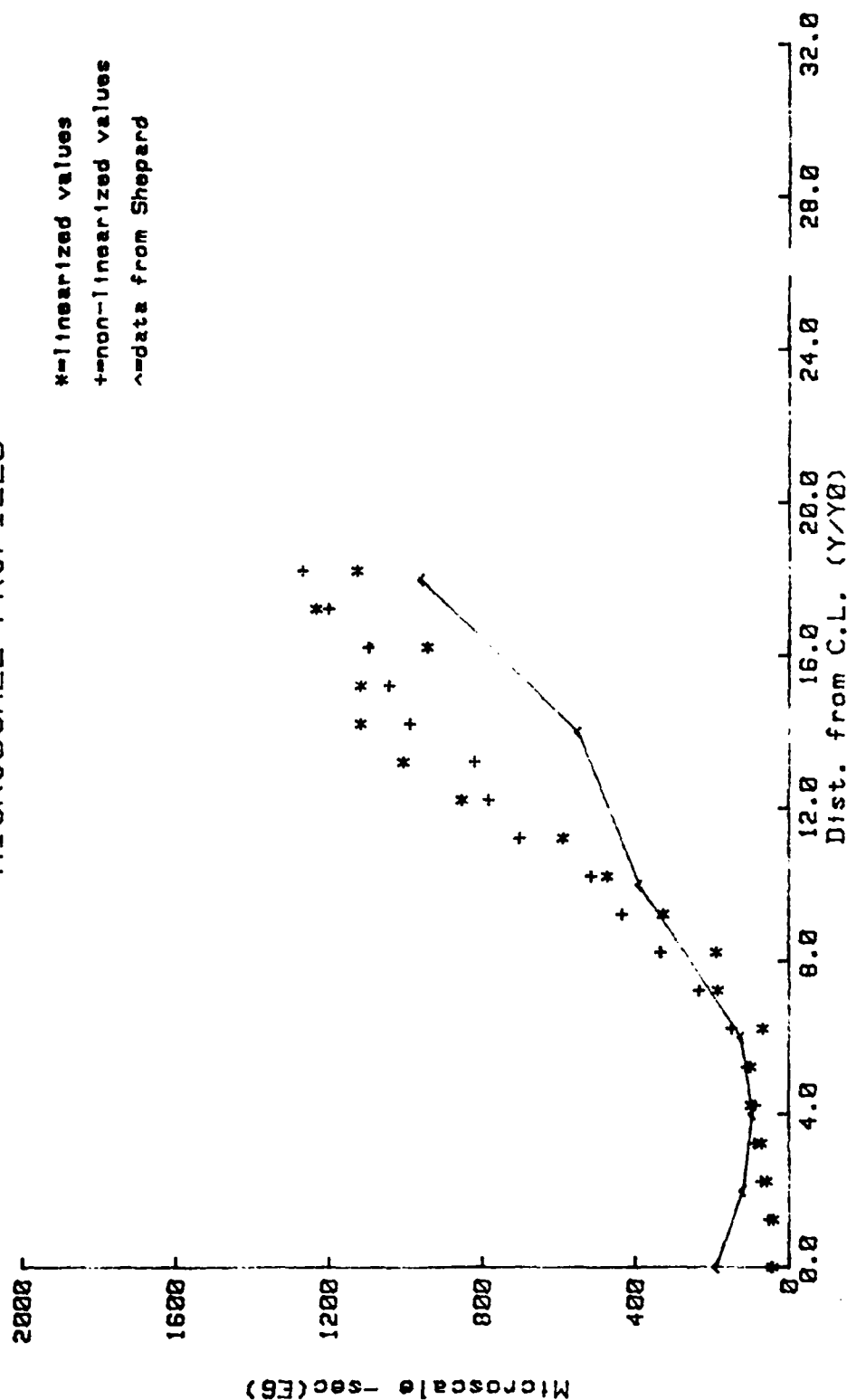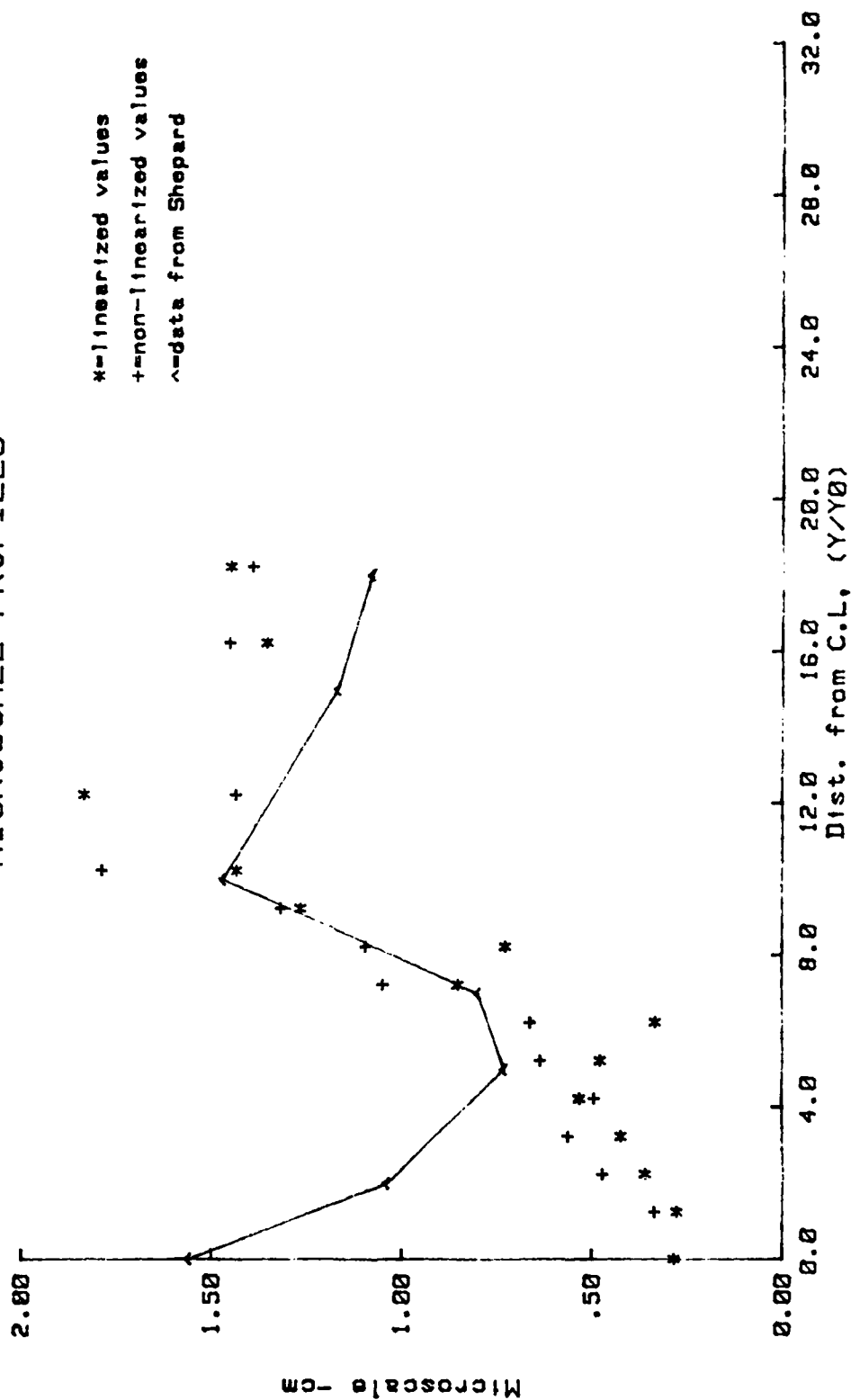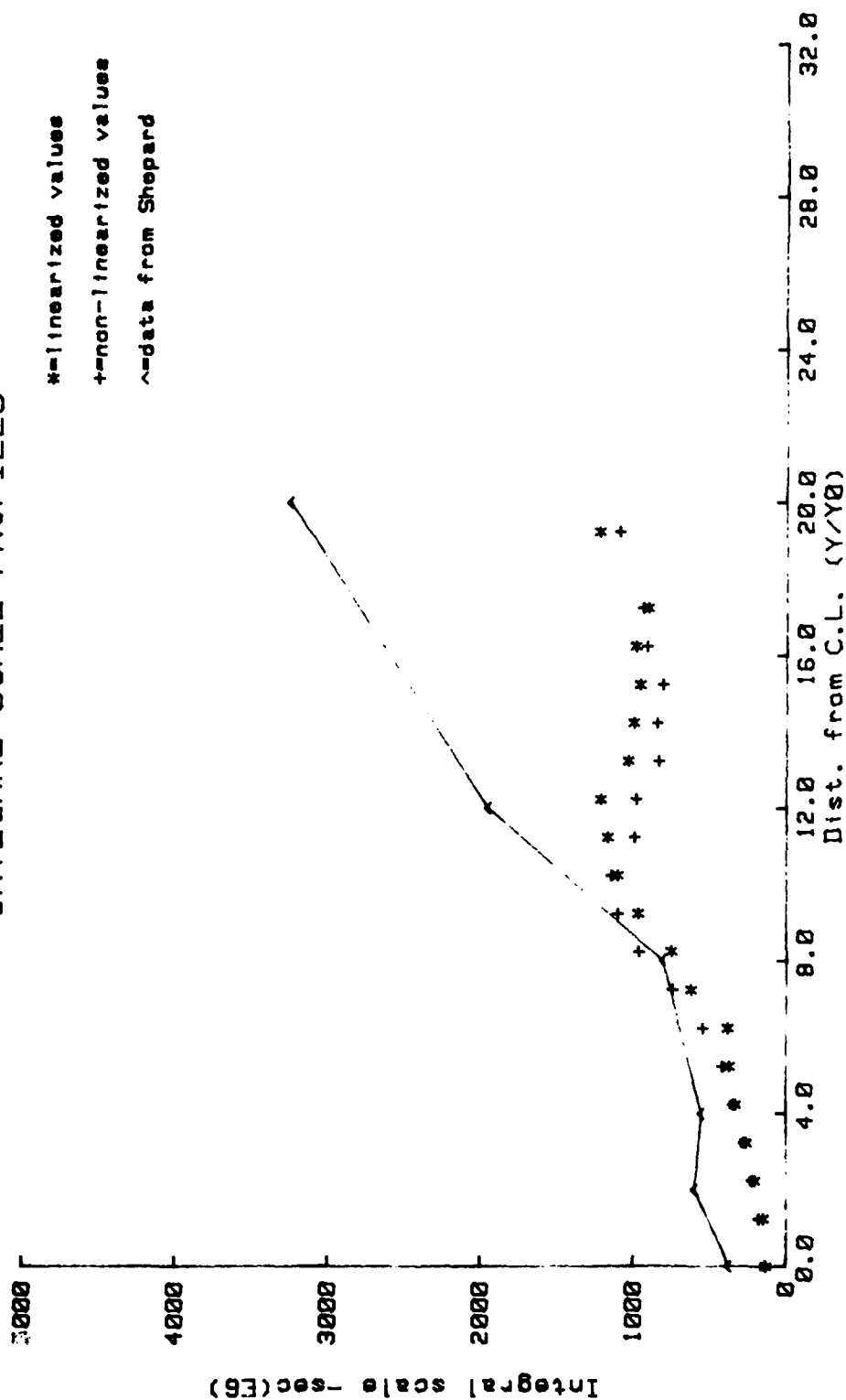
Fig. 31. Spatial Integral Scale at 50 cm, M=0.4

MICROSCALE PROFILES

*=linearized values

+=non-linearized values

^=data from Shepard

Fig. 32. Hot-wire Time Microscale at 50 cm, M=0.4

Microscale -sec(E6)

Dist. from C.L. (Y/Y0)
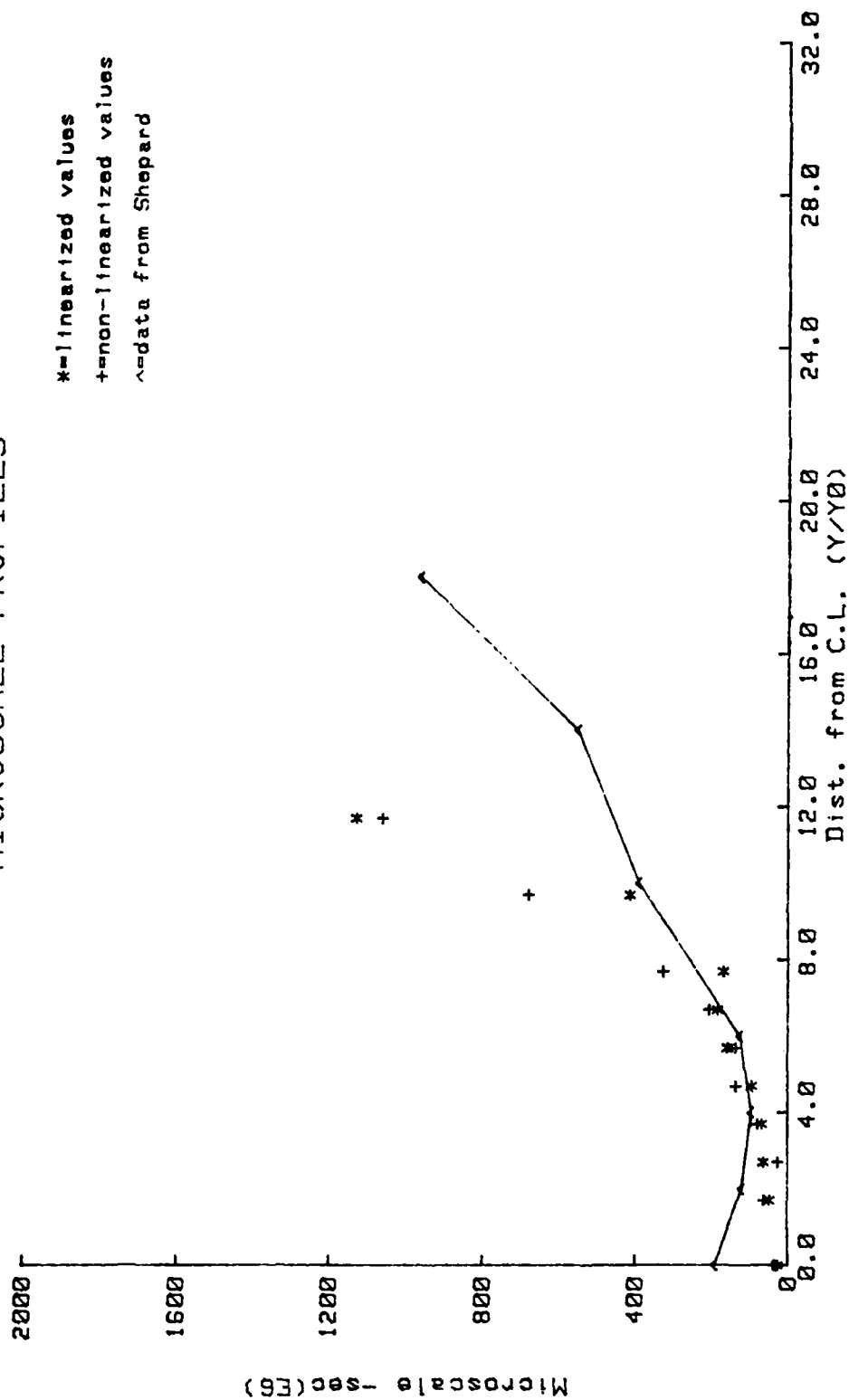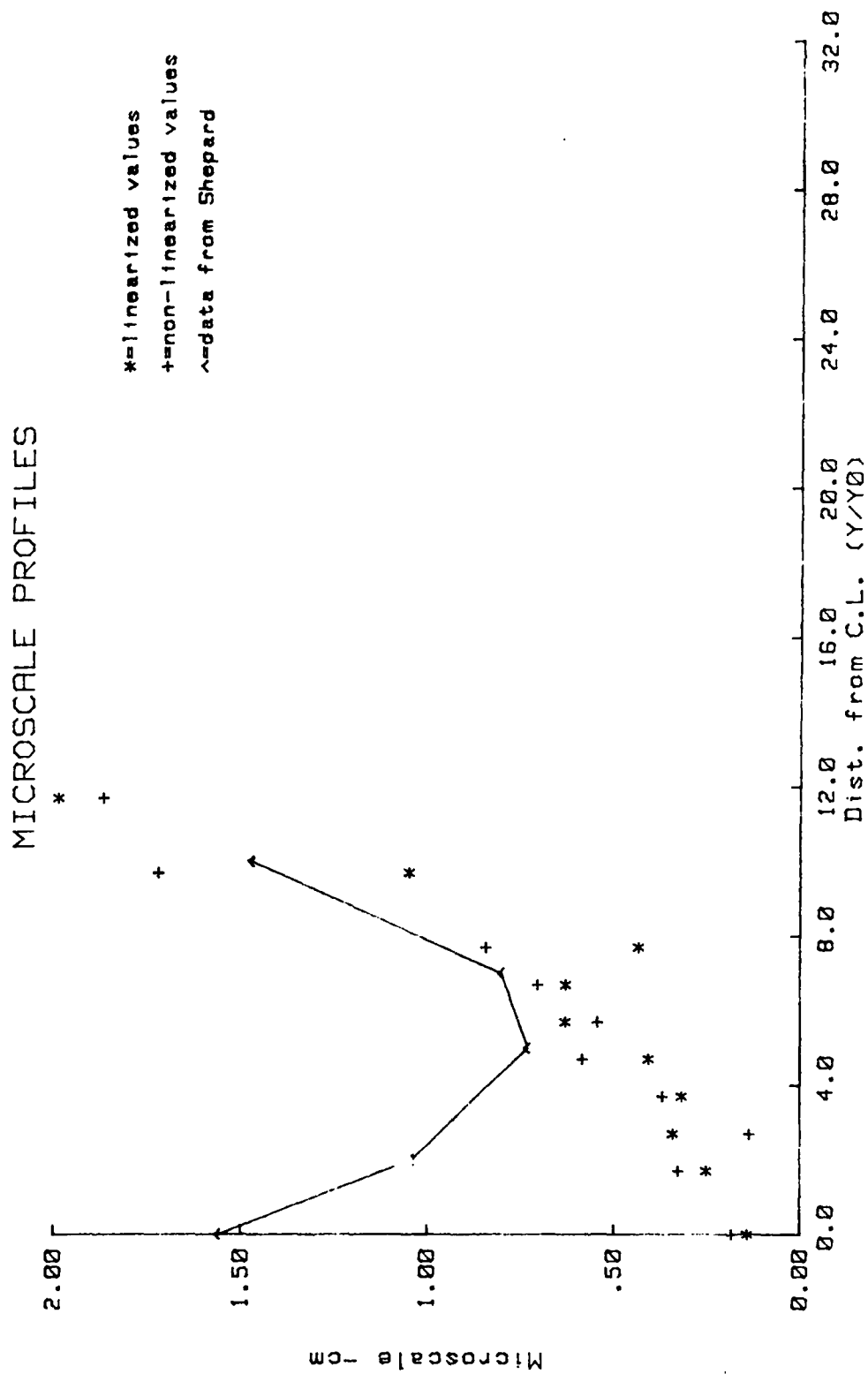
Fig. 33. Hot-wire Spatial Microscale at 50 cm, M=0.4

INTEGRAL SCALE PROFILES

*=linearized values
+=non-linearized values
^=data from Shepard

Integral scale -sec(E6)

Dist. from C.L. (Y/YØ)

Fig. 34. Hot-wire Time Integral Scale at 50 cm, M=0.4

INTEGRAL SCALE PROFILES

*=linearized values
+=non-linearized values
^=data from Shepard

Dist. from C.L. (Y/Y0)

Integral scale -cm

Fig. 35.   Hot-wire Spatial Integral Scale at 50 cm, M=0.4

71

TURBULENCE INTENSITY PROFILES

*=linearized values, u'/Ucen
+=non-linearized values, u'/Ucen
+=linearized values, v'/Ucen
@=non-linearized values, v'/Ucen
o=linearized values, w'/Ucen
&=non-linearized values, w'/Ucen

Fig. 36. X-wire Turbulence Intensity at 50 cm

<u>Appendix C</u>

Experimental Data for Jet Exit Velocity of M=0.6
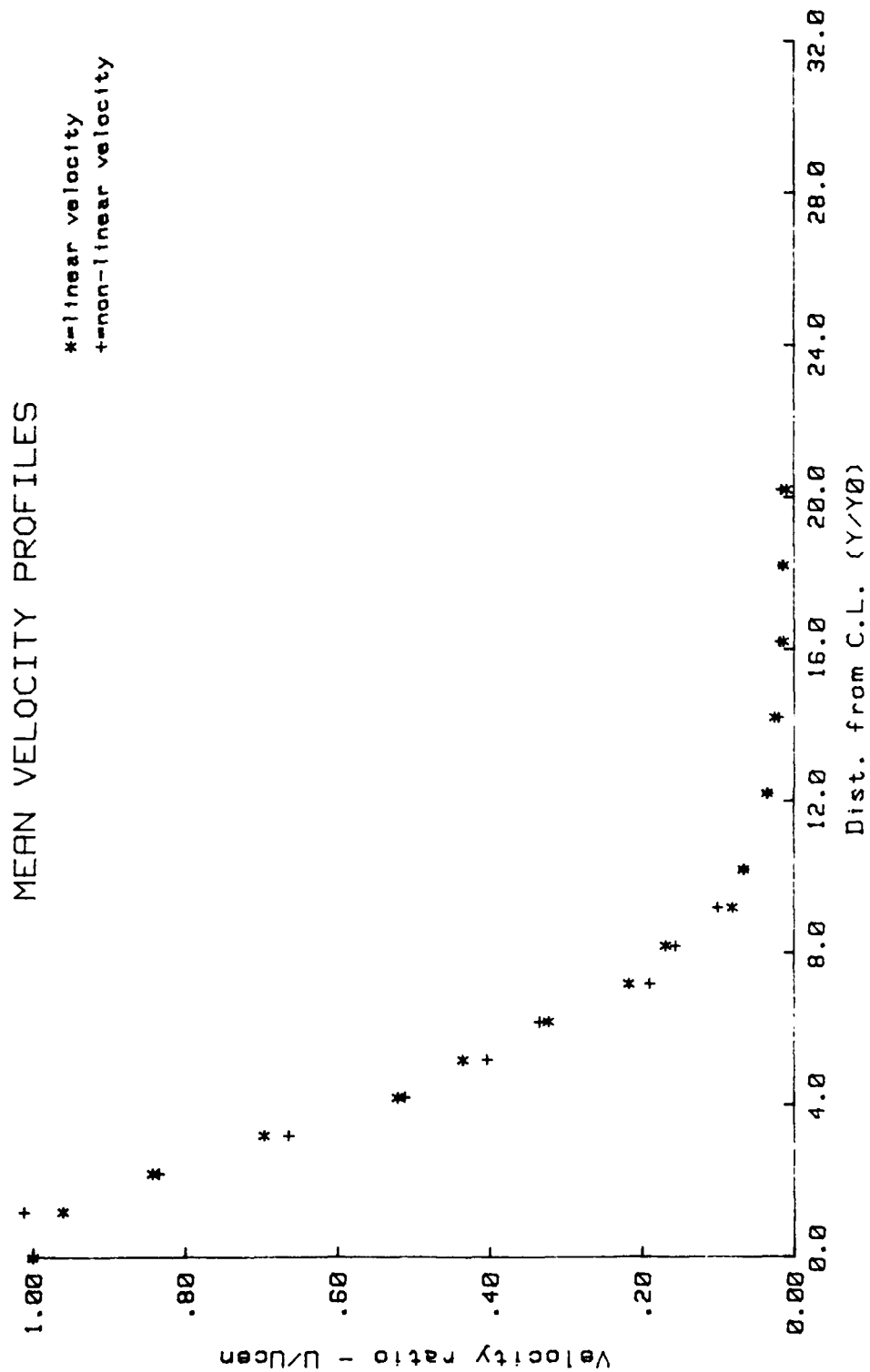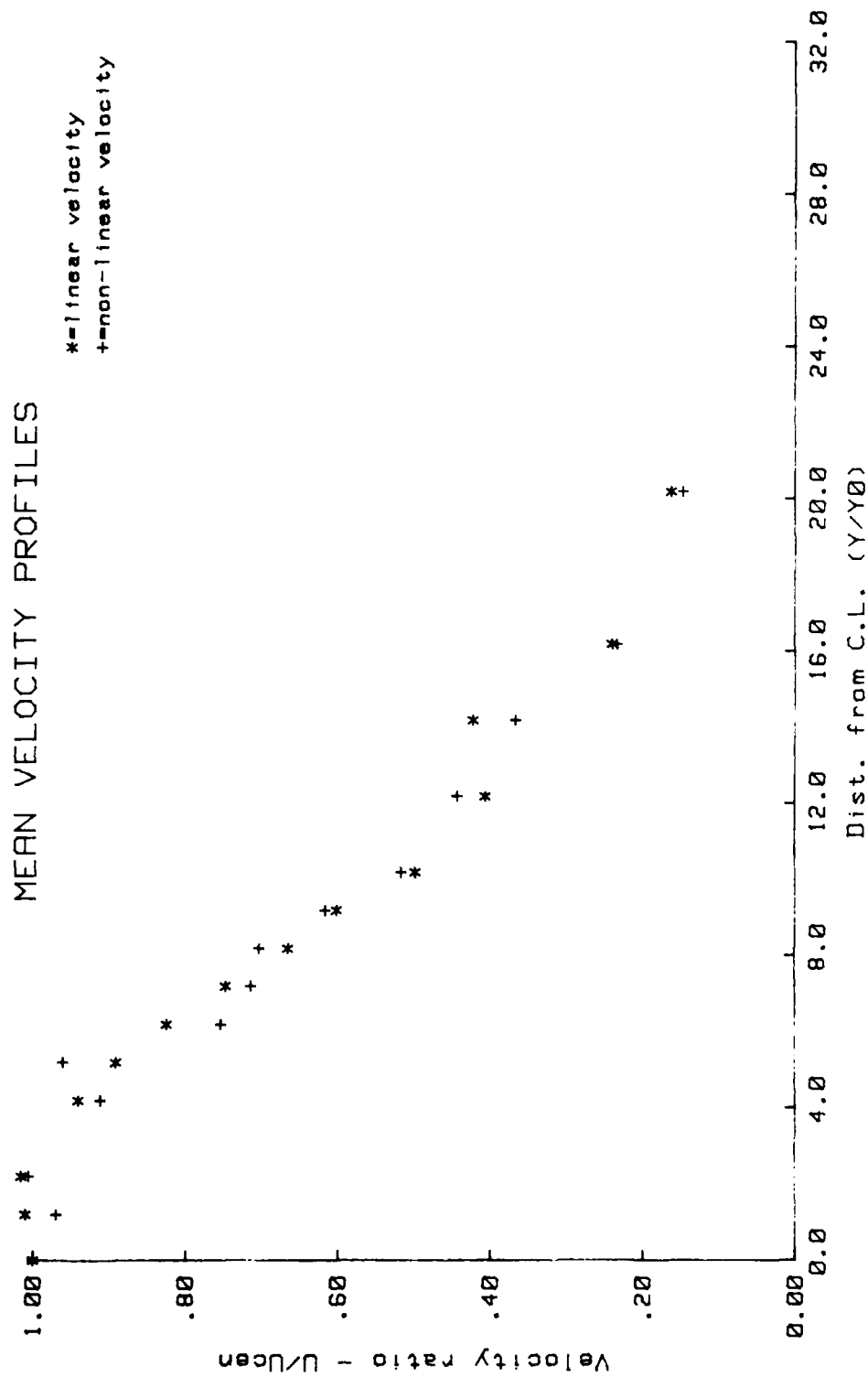
Fig. 37. Mean Velocity at 25 cm, $M=0.6$

TURBULENCE INTENSITY PROFILES

*=linearized values
+=non-linearized values
^=data from Shepard

Percent

Dist. from C.L. (Y/Y0)
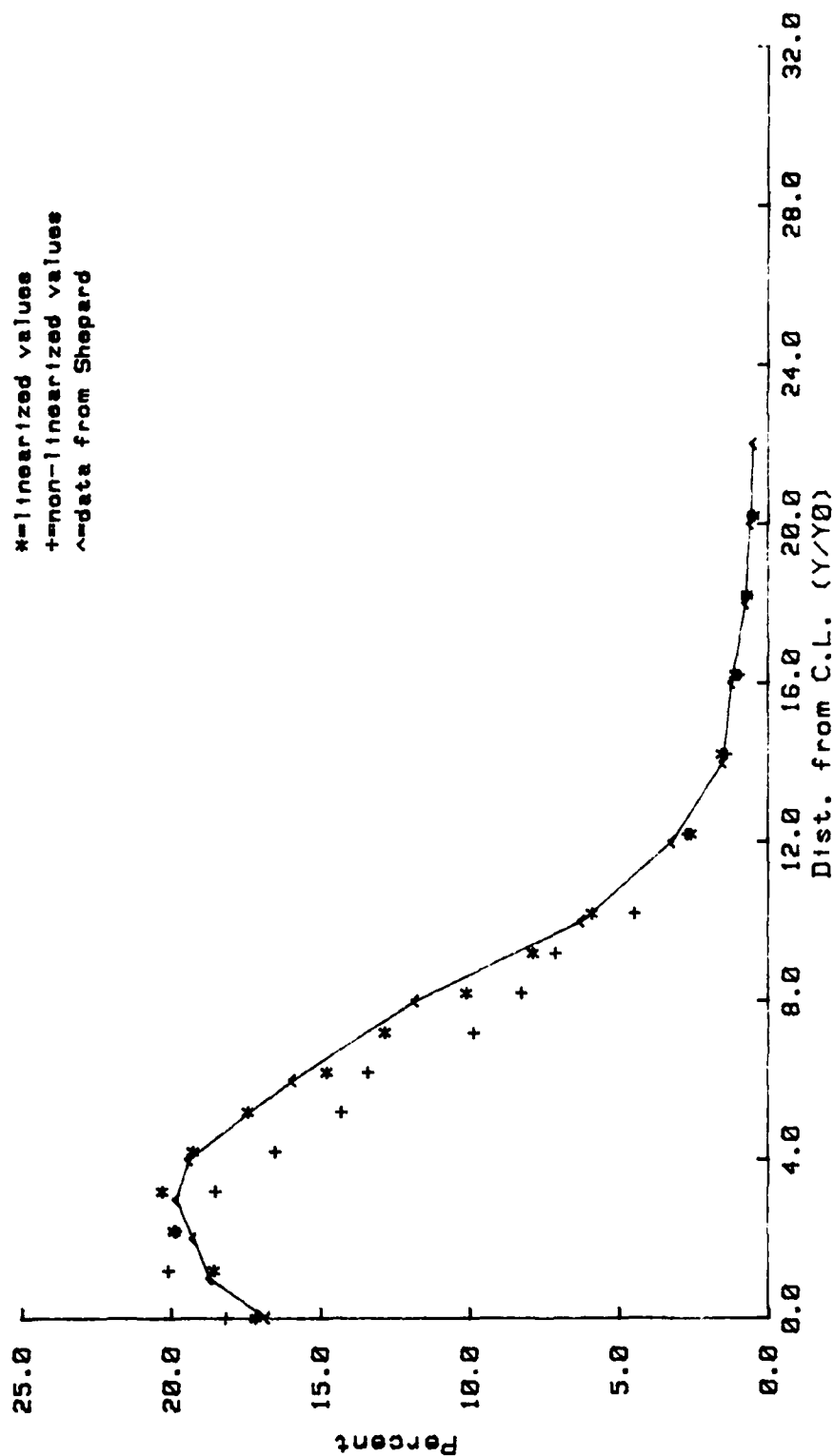
Fig. 38. Turbulence Intensity at 25 cm, M=0.6

MICROSCALE PROFILES
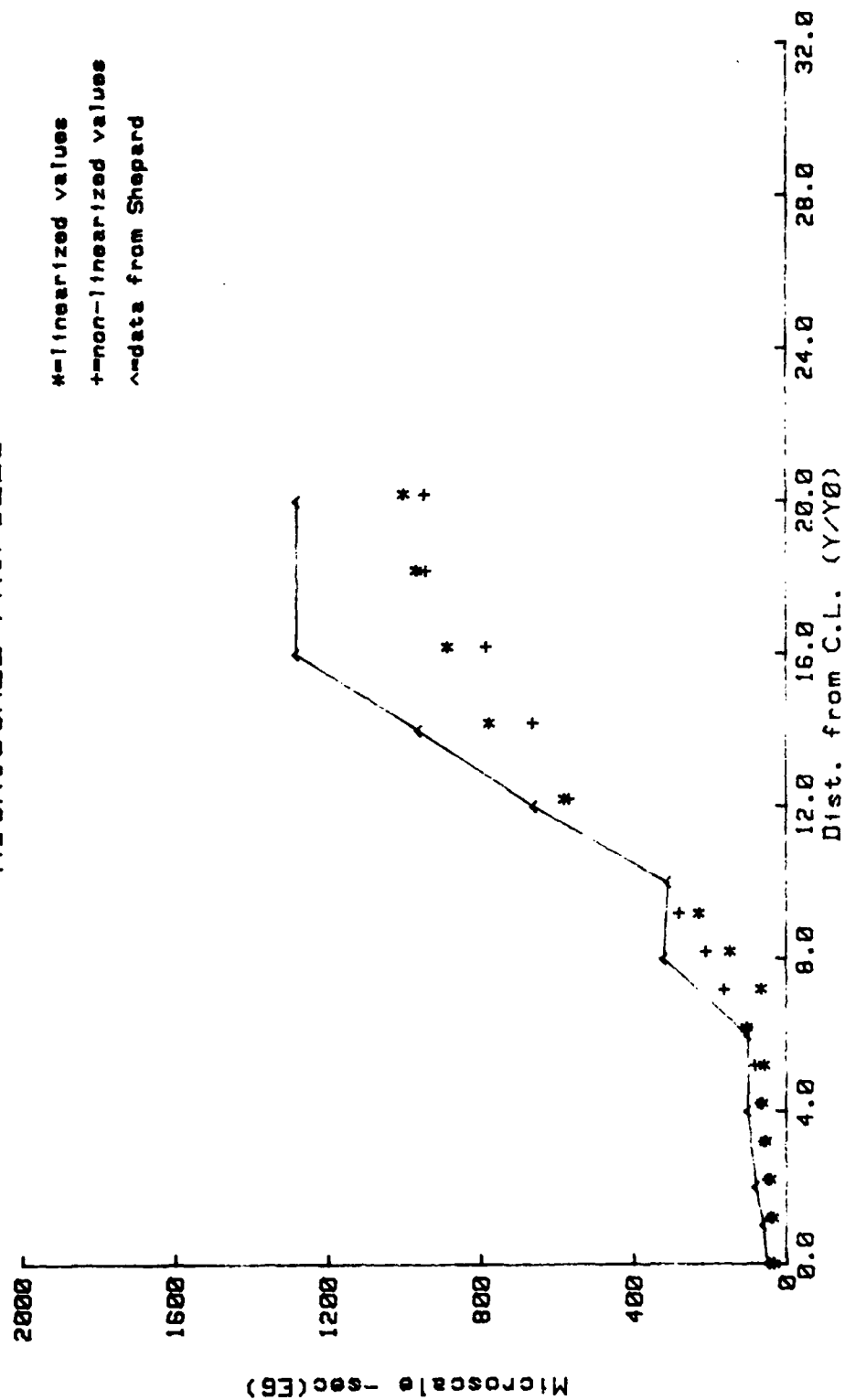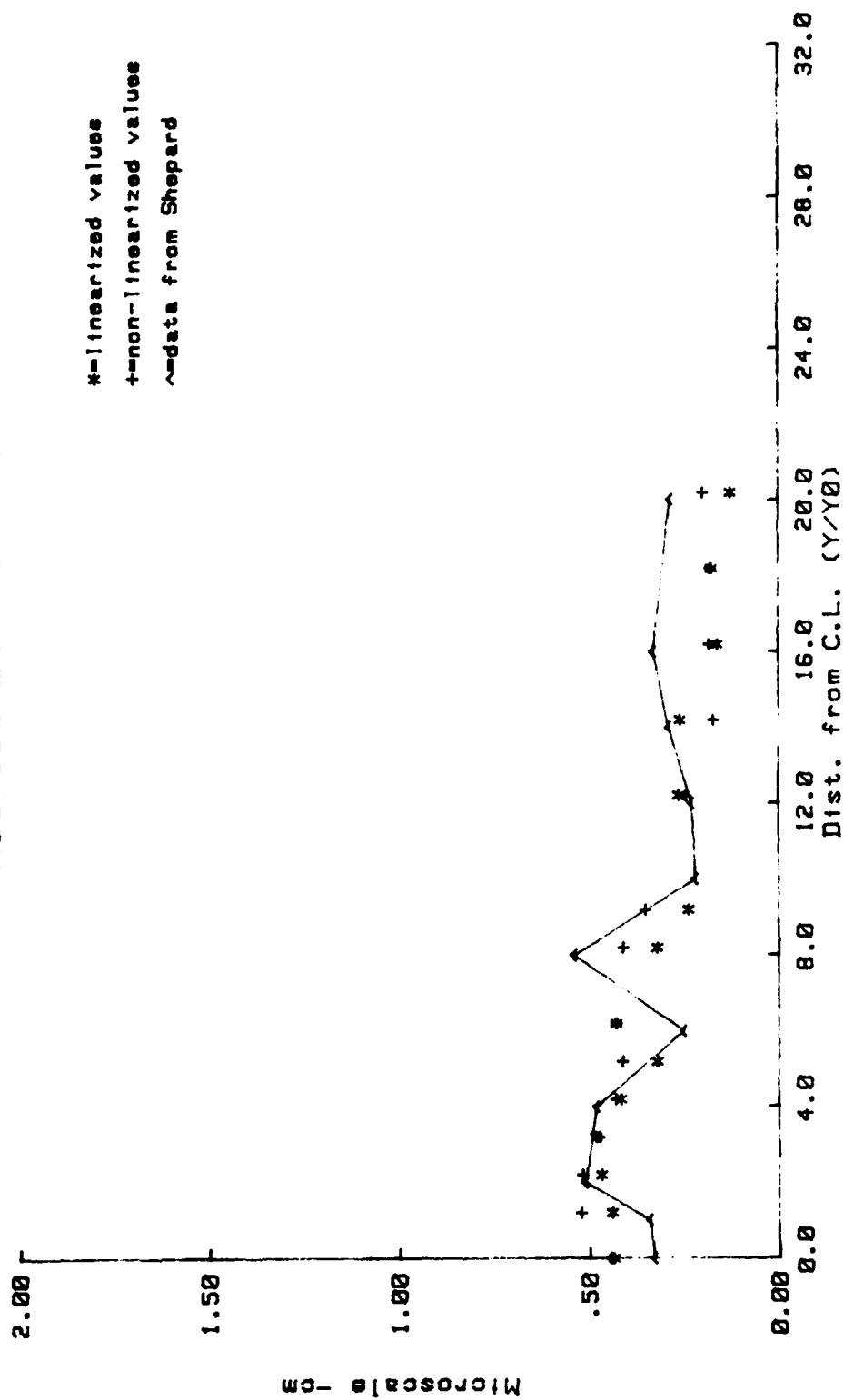
*=linearized values

+=non-linearized values

^=data from Shepard

Fig. 39. Time Microscale at 25 cm, M=0.6

76

MICROSCALE PROFILES

*=linearized values

+=non-linearized values

^=data from Shepard

Microscale -cm

2.00 1.50 1.00 .50 0.00

0.0   4.0   8.0   12.0 16.0 20.0 24.0 28.0 32.0

Dist. from C.L. (Y/Y0)

Fig. 40. Spatial Microscale at 25 cm, M=0.6

7̃
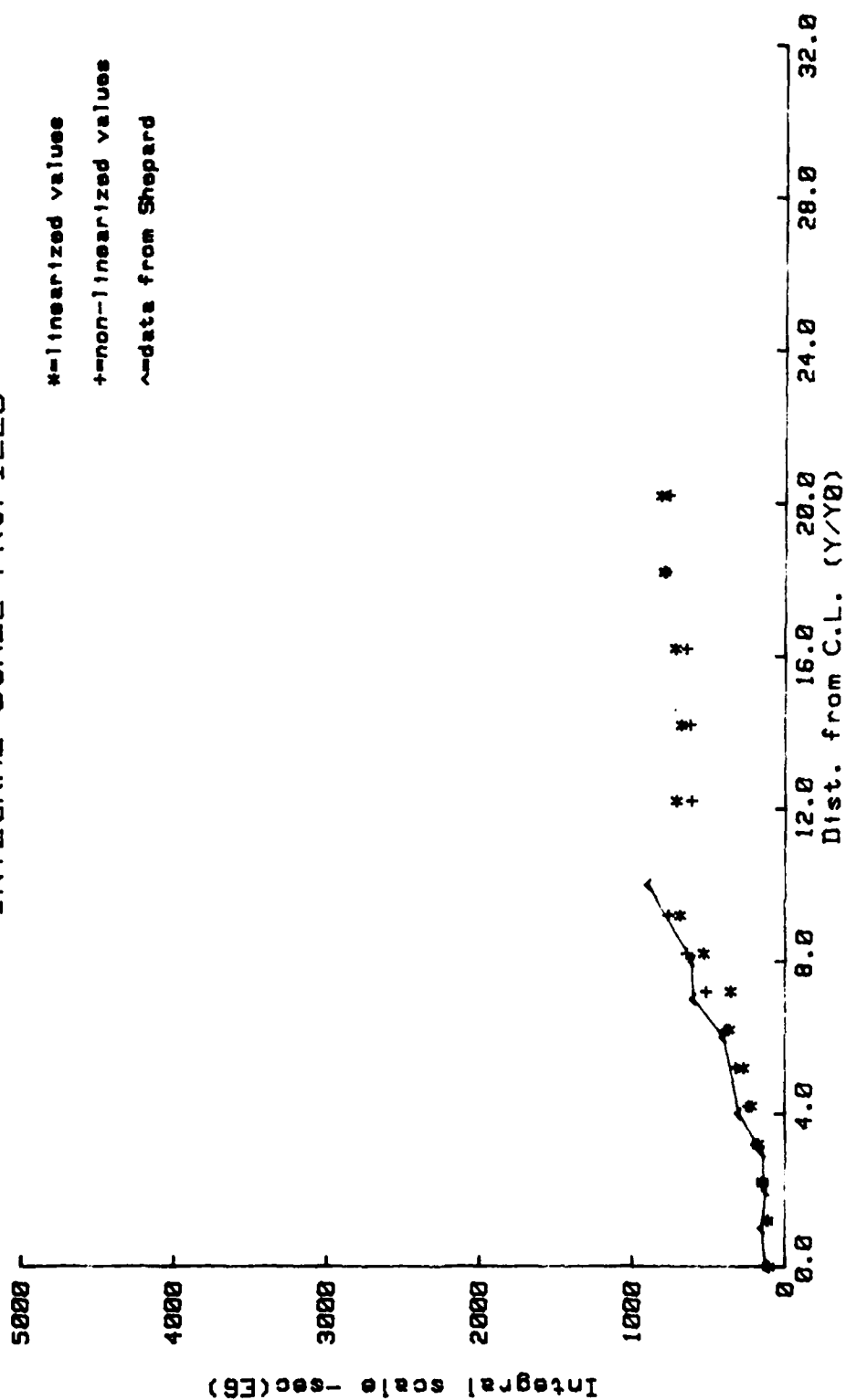
Fig. 41. Time Inegral Scale at 25 cm, M=0.6
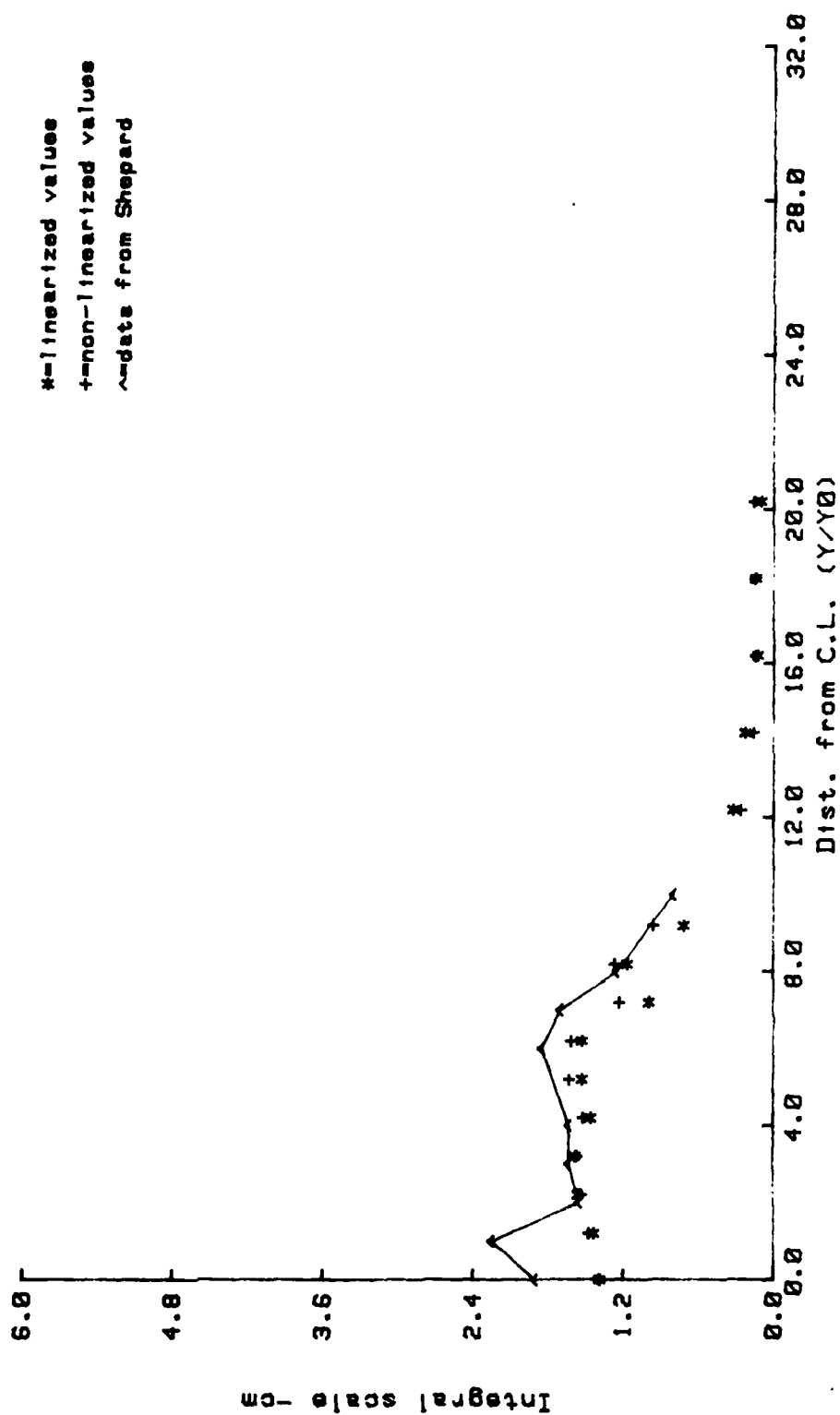
Fig. 42. Spatial Integral Scale at 25 cm, M=0.6

TURBULENCE INTENSITY PROFILES
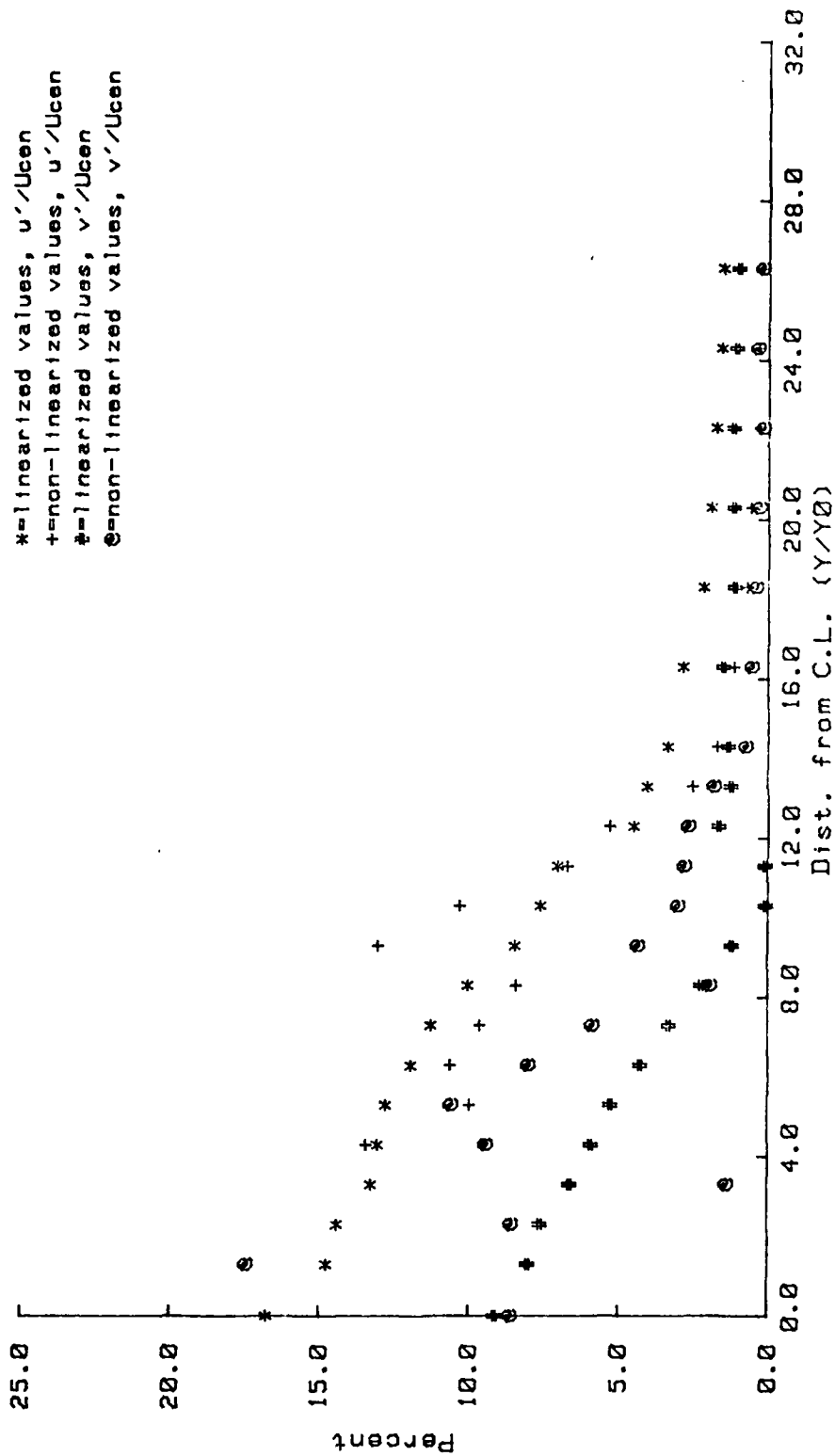
*=linearized values, u'/Ucen
+=non-linearized values, u'/Ucen
#=linearized values, v'/Ucen
@=non-linearized values, v'/Ucen

Fig. 43. Y-wire Turbulence Intensity at 25 cm

MEAN VELOCITY PROFILES

*=linear velocity
+=non-linear velocity

Velocity ratio — U/Ucean

Dist. from C.L. (Y/YØ)

Fig. 44. Mean Velocity at 50 cm, M=0.6
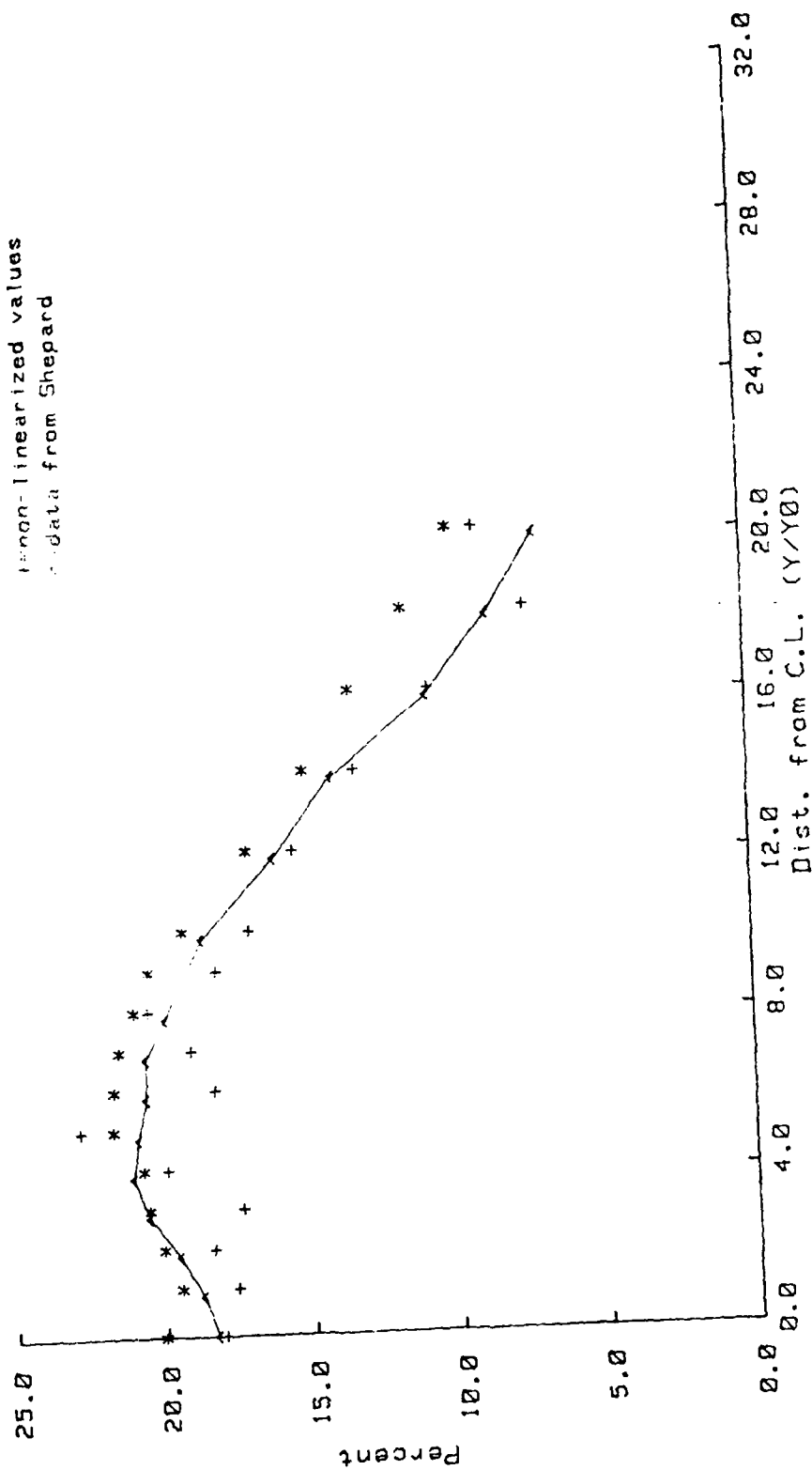
Fig. 45. Turbulence Intensity at 50 cm, M=0.6

MICROSCALE PROFILES

*=linearized values
+=non-linearized values
^=data from Shepard

Microscale -sec(E6)
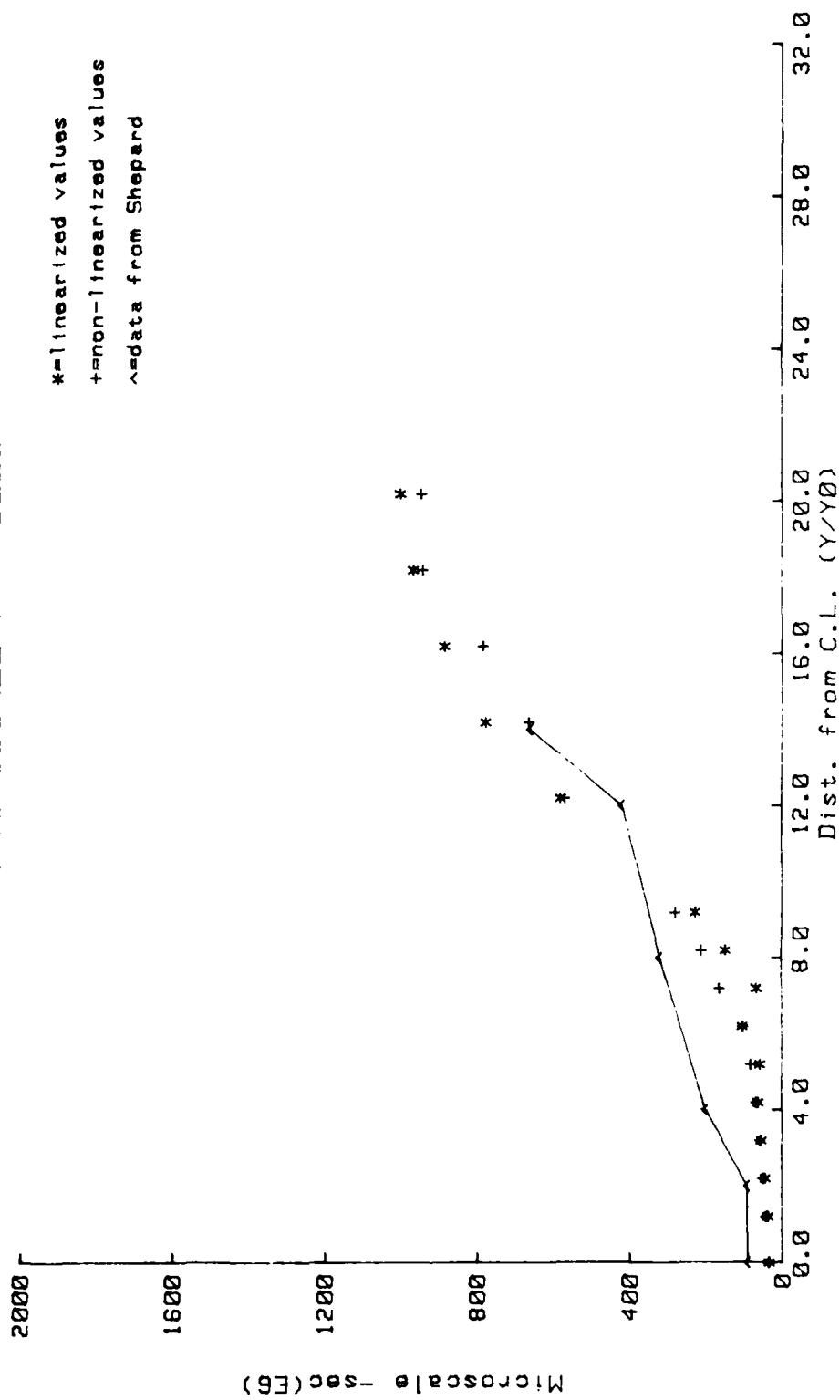
Dist. from C.L. (Y/Y0)

Fig. A6. Time Microscale at 50 cm, M=N.6

83
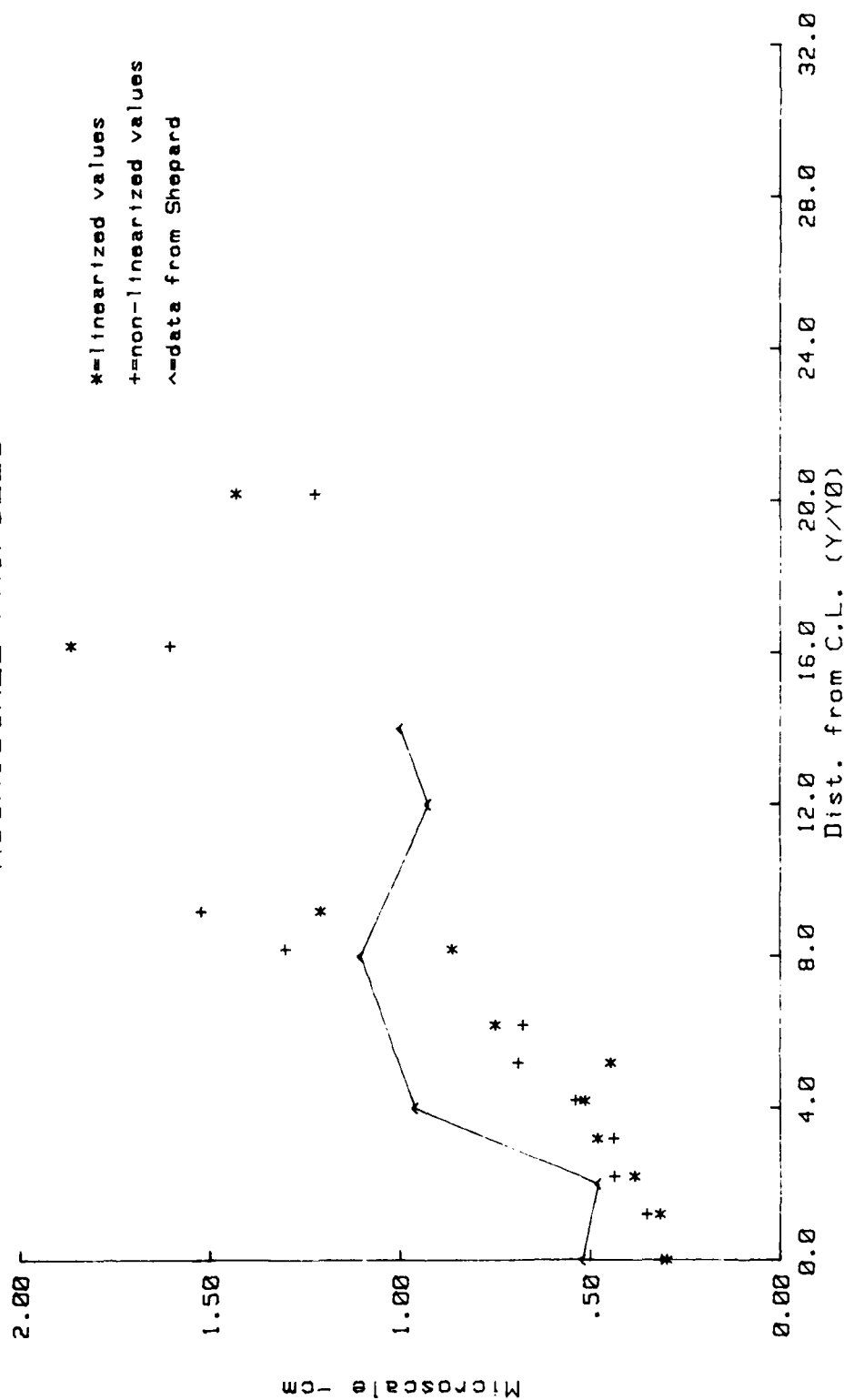
Fig. 47. Spatial Microscale at 50 cm, M=0.6

INTEGRAL SCALE PROFILES
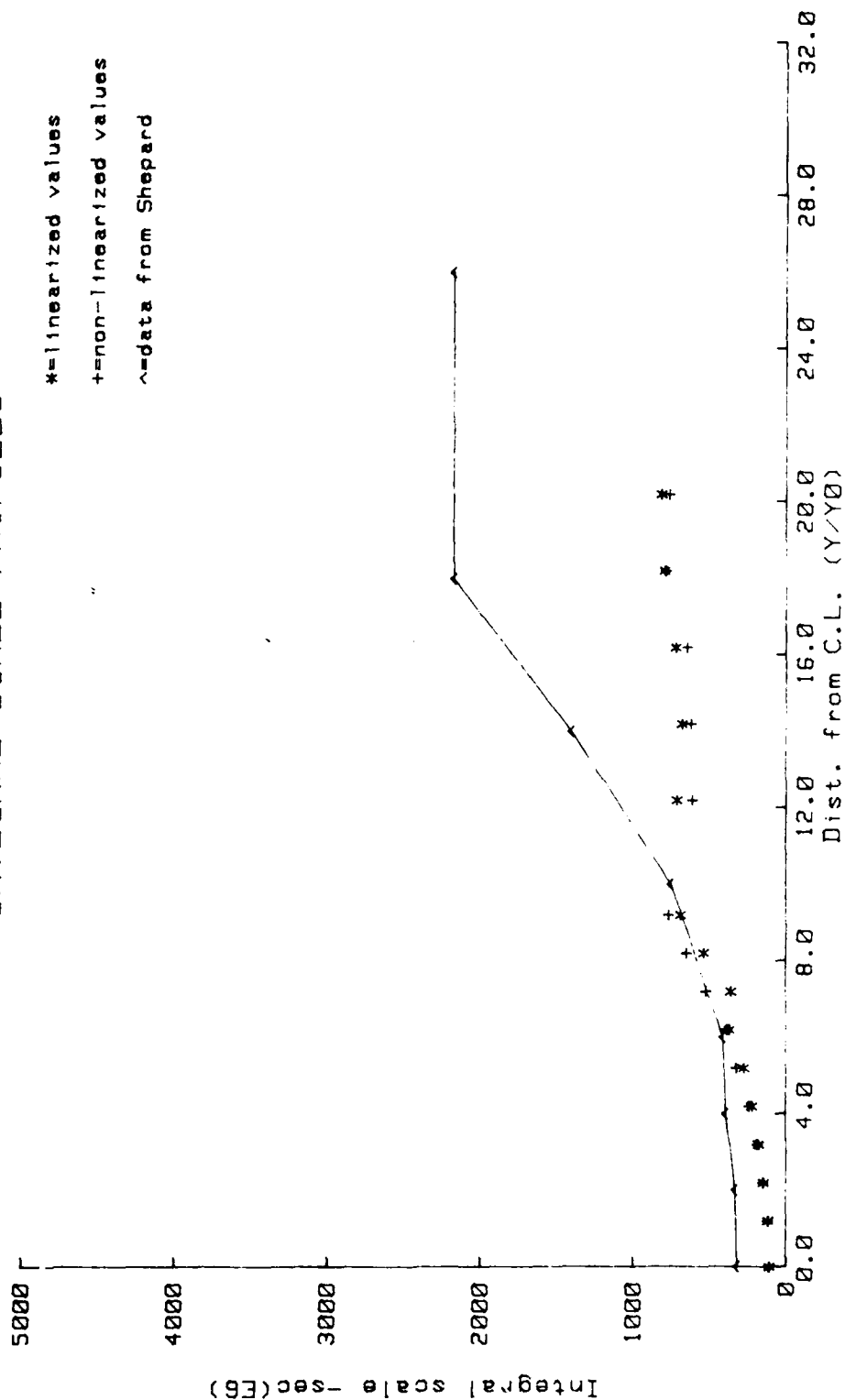
*=linearized values
+=non-linearized values
^=data from Shepard

Fig. 4P. Time Integral Scale at 50 cm, M=0.6

5
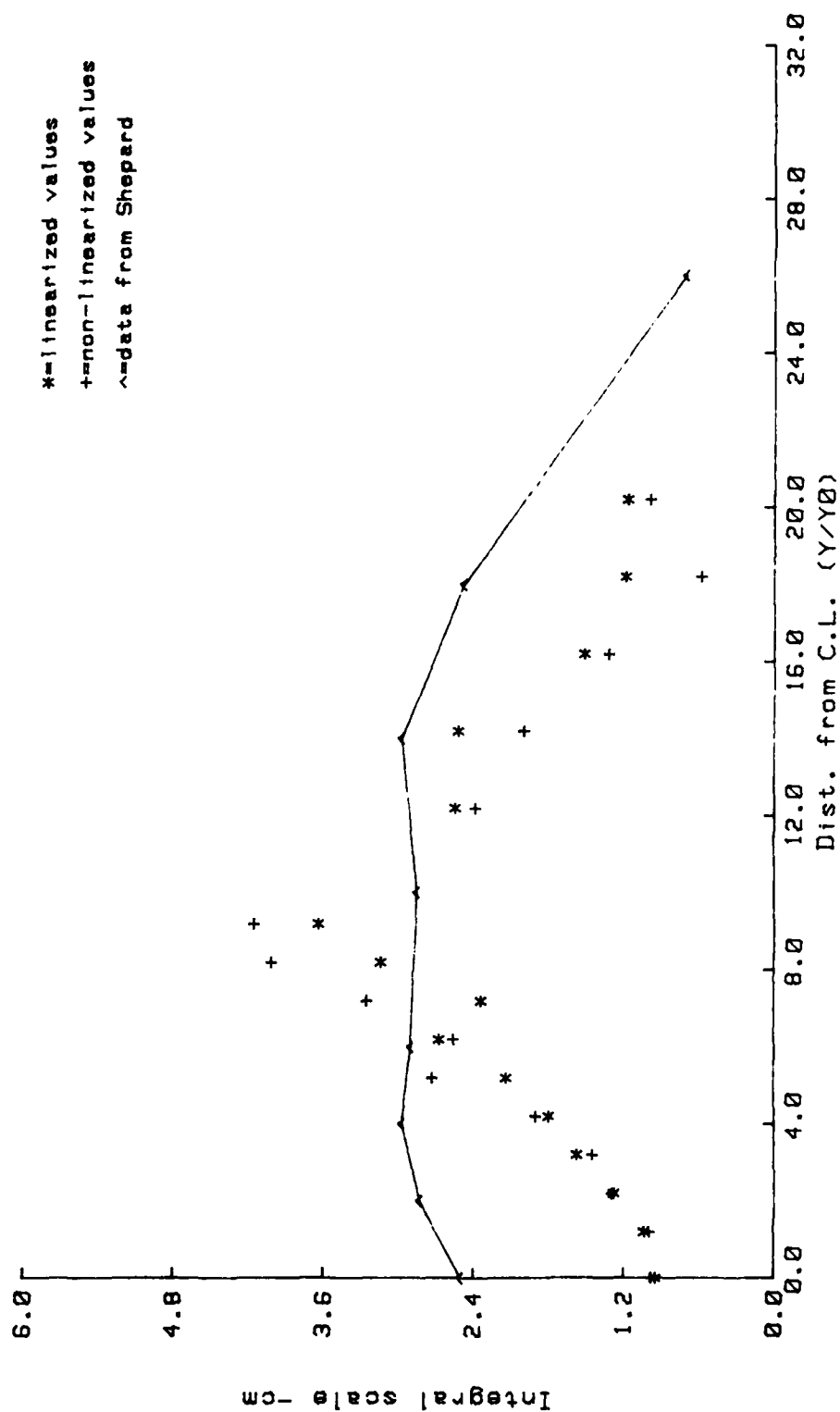
Fig. 49. Spatial Integral Scale at 50 cm, M=0.6

TURBULENCE INTENSITY PROFILES

*=linearized values, u'/Ucen
+=non-linearized values, u'/Ucen
#=linearized values, v'/Ucen
@=non-linearized values, v'/Ucen
o=linearized values, w'/Ucen
&=non-linearized values, w'/Ucen

Percent

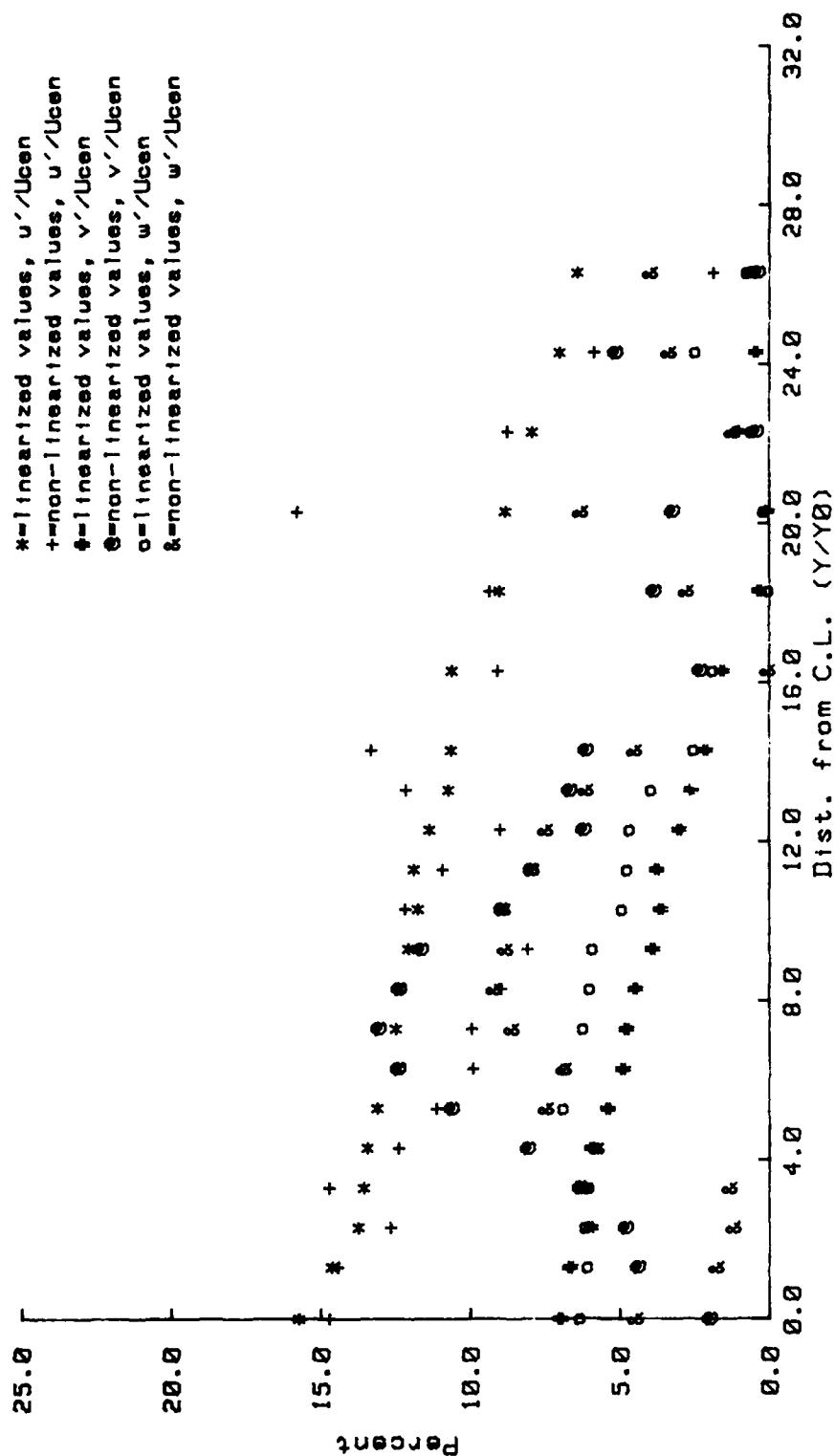Dist. from C.L. (Y/YØ)

Fig. 50. X-wire Turbulence Intensity at 50 cm

<u>Vita</u>

Capt. Michael J. Kirchner was born 13 July 1950 in St. Louis, Missouri. He was graduated from Oak Ridge High School in 1968. He received an appointment to the United States Air Force Academy in 1968. He received his Bachlor of Science Degree, with a major in Aeronautical Engineering, from the Academy in 1972. He attended pilot training and became an instructor pilot in T-38 aircraft in 1973. He served a tour of duty as a B-52 aircraft commander from 1977 to 1980, and entered the Graduate Aeronautical Engineering Program at the Air Force Institute of Technology in June 1980.

Permanent address: Rt. 1 Box 61
Friedheim, Missouri 63747

REPORT DOCUMENTATION PAGE	READ INSTRUCTIONS BEFORE COMPLETING FORM

1. REPORT NUMBER AFIT/GAE/AA/81D-17	2. GOVT ACCESSION NO. AD-A111169	3. RECIPIENT'S CATALOG NUMBER

4. TITLE (and Subtitle) COMPUTER ASSISTED VELOCITY AND TURBULENCE MEASUREMENTS IN A PLANE FREE JET AT HIGH SUBSONIC VELOCITIES	5. TYPE OF REPORT & PERIOD COVERED MS Thesis
	6. PERFORMING ORG. REPORT NUMBER

7. AUTHOR(s) Michael J. Kirchner Capt USAF	8. CONTRACT OR GRANT NUMBER(s)

9. PERFORMING ORGANIZATION NAME AND ADDRESS Air Force Institute of Technology (AFIT/EN) Wright Patterson AFB, Ohio 45433	10. PROGRAM ELEMENT, PROJECT, TASK AREA & WORK UNIT NUMBERS

11. CONTROLLING OFFICE NAME AND ADDRESS	12. REPORT DATE December 1981
	13. NUMBER OF PAGES 99 pages

14. MONITORING AGENCY NAME & ADDRESS(if different from Controlling Office)	15. SECURITY CLASS. (of this report) Unclassified
	15a. DECLASSIFICATION DOWNGRADING SCHEDULE

16. DISTRIBUTION STATEMENT (of this Report)

Approved for public release; distribution unlimited.

17. DISTRIBUTION STATEMENT (of the abstract entered in Block 20, if different from Report)

28 JAN 1982

18. SUPPLEMENTARY NOTES

Approved for public release; IAW 190-17

Fredric C. Lynch, Major, USAF
Director of Public Affairs

19. KEY WORDS (Continue on reverse side if necessary and identify by block number)

Automatic Data Acquisition System
Hot-wire Anemometer
Plane Free Jet
Turbulence

20. ABSTRACT (Continue on reverse side if necessary and identify by block number)

Methods and results of an experimental study of turbulence parameters for a plane free jet at high subsonic velocities, using hot wire anemometer signals outputing directly to an on-line computer controlled data acquistion system are reported. The apparatus studied had a nozzle exit, 1 x 10 cm, designed for two-dimensional flow.

Two measurement planes at 25 and 50 jet widths downstream were chosen to provide measurements to compare with existing data for the facility.

DD FORM 1473 EDITION OF 1 NOV 65 IS OBSOLETE
1 JAN 73

Nozzle velocities of M=0.4 and M=0.6 were chosen for the same reason.

The techniques for employing hot-wire anemometry coupled with computer controlled data acquisition are described. A comparison of data obtained with the computer is made to data previously obtained by more traditional methods. A comparison of linearized and non-linearized anemometer output is made. A new calibration technique, also utilizing the data acquisition system to greatly decrease the sensor calibration time, was also developed.

The turbulence parameters compared are mean velocity, turbulence intensities, micro-scale, and integral scale of turbulence. The computer determined parameters compared favorably in all cases with the already available data.

DATE
FILMED

3-8